2017

Multi-Cellular And Multi-Scale Approaches For Cartilage Repair

Minwook Kim
University of Pennsylvania, kimminw@mail.med.upenn.edu

Multi-Cellular And Multi-Scale Approaches For Cartilage Repair

Abstract
To date, there are no surgical interventions that can fully restore damaged cartilage. While the field of tissue engineering has emerged as a potential solution, there exist numerous shortcomings in existing technologies. This thesis addresses some of these shortcomings by developing multi-cellular and multi-scale approaches to advance technologies for cartilage repair. For instance, co-culture systems have recently been introduced as a novel tissue engineering strategy for cartilage repair. We show here that a small pool of young/healthy chondrocytes (CH) can rejuvenate a larger pool of older/infirm mesenchymal stem cells (MSC), improving matrix deposition while suppressing MSC hypertrophic conversion. This resolves the deficiency of CH supply as well as phenotypic instability and age-related decline in potential of MSCs. Biomimetic design in cartilage tissue engineering is yet another challenge, given the complexity of the native tissue. While articular cartilage is a highly stratified tissue with depth-dependent properties, most cell-laden cartilage constructs described in the literature simply recapitulate bulk functional properties without morphologic recapitulation. Here, we develop a layer-by-layer fabrication strategy to promote depth dependent tissue formation and function. We also introduce a novel method to properly transport nutrients and wastes into/out of engineered constructs. Finally, another equally important aspect in designing engineered cartilage tissue is clinical translation. In this, the simplicity of application, including ease of handling and preparation, and methods for implantation in situ, are required for clinical translation. To address this, we developed a micro-scale co-culture system that can be easily fabricated and delivered into cartilage defects in the context of current clinical cartilage repair procedures. Collectively, the thesis advances our understanding of the chondrogenic capacity of MSCs, introduces various methods to improve MSC chondrogenesis (using chemical and natural factors), and identifies some of the underlying mechanisms regulating this process. Further, this work introduces novel methods to fabricate engineered cartilage to mimic the structure of native tissue as well as clinical relevant methods to couple tissue engineering efforts with current clinical practice. These innovative approaches may aid the many patients who suffer from cartilage disease by enhancing cartilage tissue engineering strategies and reducing them to clinical practice.

Degree Type
Dissertation

Degree Name
Doctor of Philosophy (PhD)

Graduate Group
Bioengineering

First Advisor
Robert L. Mauck

Second Advisor
Jason A. Burdick

Keywords
Cartilage repair, Chondrocytes, Co-culture, Mesenchymal stem cells, Micro-noodles, Tissue engineering

Subject Categories
Biomedical

MULTI-CELLULAR AND MULTI-SCALE APPROACHES FOR CARTILAGE REPAIR

Minwook Kim

A DISSERTATION

in

Bioengineering

Presented to the Faculties of the University of Pennsylvania

in

Partial Fulfillment of the Requirements for the

Degree of Doctor of Philosophy

2017

Supervisor of Dissertation

_____

Dr. Robert L. Mauck
Mary Black Ralston Professor of Orthopaedic Surgery
Professor of Bioengineering
Director, McKay Orthopaedic Research Laboratory
Department of Orthopaedic Surgery
University of Pennsylvania

Graduate Group Chairperson

_____

Dr. Jason A. Burdick
Professor of Bioengineering
University of Pennsylvania

Dissertation Committee

Jason A. Burdick, Professor of Bioengineering, University of Pennsylvania
James L. Carey, Assistant Professor of Orthopaedic Surgery, University of Pennsylvania
Maurizio Pacifici, Professor of Orthopaedic Surgery, The Children's Hospital of Philadelphia
Clark T. Hung, Professor of Biomedical Engineering, Columbia University

MULTI-CELLULAR AND MULTI-SCALE APPROACHES FOR CARTILAGE REPAIR

ACKNOWLEDGMENTS

Firstly, I would like to express my sincere gratitude to my advisor Dr. Robert L. Mauck for the continuous support of my Ph.D study and related research, for his patience, motivation, and immense knowledge. His guidance helped me in all the time of research and writing of this thesis. I could not have imagined having a better advisor and mentor for my Ph.D study.

Besides my advisor, I would also like to thank the rest of my thesis committee: Drs. Jason A. Burdick, James L. Carey, Maurizio Pacifici, and Clark T. Hung, for their insightful comments and encouragement, but also for the critical questions which incented me to widen my research from various perspectives.

My sincere thanks also goes to Drs. Nancy Pleshko, Adele L. Boskey and George R. Dodge, who provided me an opportunity to join their team at the Hospital for Special Surgery and Nemours/Alfred I. DuPont Hospital for Children. Without their precious support it would not be possible to start and continue my science career. Special thanks to Dr. David Steinberg and Mitchell R. Jones for both scientific and funding support.

I would like to thank Rani Roy, Xiaohong Bi, Xu Yang, Yukiji Fujimoto, Joan Pugarelli, Diane Preske, Alice H. Huang, Isaac E. Erickson, and Arlene Adair for their contributions to my work, along with my the rest of the Mauck lab, Megan J. Farrell, Sean T. Garrity, Marwa Choudhury, Mac Sennett, Blair Ashley, Brendan Stoeckl, Bhavana Mohanraj, Brian Cosgrove, Feini (Sylvia) Qu, Sonia Bansal, Tonia Tsinman, Beth Ashinsky, Eric Dai, Sarah Gullbrand, Donghwa Kim, Spencer Szczensny, Suchin Heo, Eddie Bonnevie,

James M. Friedman, Alexander L. Neuwirth, Vishal Saxena, Elizabeth Henning and Breanna Seiber.

I would like to thank Rev. Byungkyu Kim and his wife, Mrs. Dongsun Lee for their prayers and kind regards and my best friend, Henry Hyun Song.

My parents Deokil Kim and Kyungja Ha have given me a lifetime of love and support. They have sacrificed so much for me. I thank them for their example of diligent hard work that permeated the fibers of our family and has had a profound impact on my life. Special thanks to my parents-in-law Soonshin Kwon and Youngsook Lee, for their prayers and support.

Most importantly, I must acknowledge my wife Yongran Kwon for her prayer, love and support. Without her sacrifice, I would not have accomplished anything. I thank my lovely children Chanwoo (Joshua), Yunwoo (Rachel) and Geonwoo (Isaac) for being my son and daughter, who are the lifetime resource of joy and happiness.

Last but not least, I would like to thank Father God, who is the wonderful counsellor and the purpose of life. I dedicate this small piece of work to you with all of my heart.

SOLI DEO GLORIA!

ABSTRACT

MULTI-CELLULAR AND MULTI-SCALE APPROACHES FOR CARTILAGE REPAIR

Minwook Kim

Robert L. Mauck

To date, there are no surgical interventions that can fully restore damaged cartilage. While the field of tissue engineering has emerged as a potential solution, there exist numerous shortcomings in existing technologies. This thesis addresses some of these shortcomings by developing multi-cellular and multi-scale approaches to advance technologies for cartilage repair. For instance, co-culture systems have recently been introduced as a novel tissue engineering strategy for cartilage repair. We show here that a small pool of young/healthy chondrocytes (CH) can rejuvenate a larger pool of older/infirm mesenchymal stem cells (MSC), improving matrix deposition while suppressing MSC hypertrophic conversion. This resolves the deficiency of CH supply as well as phenotypic instability and age-related decline in potential of MSCs. Biomimetic design in cartilage tissue engineering is yet another challenge, given the complexity of the native tissue. While articular cartilage is a highly stratified tissue with depth-dependent properties, most cell-laden cartilage constructs described in the literature simply recapitulate bulk functional properties without morphologic recapitulation. Here, we develop a layer-by-layer fabrication strategy to promote depth dependent tissue formation and function. We also introduce a novel method to properly transport nutrients and wastes into/out of engineered constructs. Finally, another equally important aspect in designing engineered cartilage tissue is clinical translation. In this, the simplicity of application, including ease of handling and preparation, and methods for implantation in

situ, are required for clinical translation. To address this, we developed a micro-scale co-culture system that can be easily fabricated and delivered into cartilage defects in the context of current clinical cartilage repair procedures. Collectively, the thesis advances our understanding of the chondrogenic capacity of MSCs, introduces various methods to improve MSC chondrogenesis (using chemical and natural factors), and identifies some of the underlying mechanisms regulating this process. Further, this work introduces novel methods to fabricate engineered cartilage to mimic the structure of native tissue as well as clinical relevant methods to couple tissue engineering efforts with current clinical practice. These innovative approaches may aid the many patients who suffer from cartilage disease by enhancing cartilage tissue engineering strategies and reducing them to clinical practice.

TABLE OF CONTENTS

LIST OF TABLES

LIST OF ILLUSTRATIONS

Figure 6-1: Impact of zonal-CH co-culture with MSCs of juvenile and adult origin. (A) MSCs and CHs were isolated from bone marrow and articular cartilage. Zonal CHs were isolated from the superficial (S), middle (M), and deep zone (D) of juvenile cartilage. Isolated cells were expanded and labeled with CellTracker (MSC: green and CH: red). Juvenile (J) MSCs and Adult (A) MSCs were mixed with zonal CH subpopulations (mixture ratio = CH:MSC = 1:4) at 60 million cells per mL of 1% HA. Constructs (Ø4 x 2.25mm) were cultured in CM+. (B) Mixed cell populations in all groups (S-M, M-M and D-M) were well distributed within the constructs after 56 days of culture (JMSC:JCH (Left) and AMSC:JCH (Right)). Quantification of CH and MSC sub-populations over time showed that by 8 weeks, 25~30% of cells were CH and 70~75% were MSCs. (C) Equilibrium modulus (E_Y; kPa) of juvenile MSC/juvenile CH co-cultures (JMSC:JCH, Top) and adult MSC/juvenile CH co-cultures (AMSC:JCH, Bottom) where zonal origin is indicated by S, M, or D. Additional groups included zonal CH alone (S, M, and D, Left-most groups) and MSC alone (MSC, Right-most group). Constructs formed from JMSCs grew well on their own, while those formed from AMSCs failed to mature. No synergistic effect of co-culture was observed for JCH/JMSC groups, whereas AMSCs co-cultured with JCHs exceeded expectations based on individual cultures (Lighter bars = Day 28, Darker bars = Day 56; N=4/group; $p<0.05$). (D) To assess the efficacy of co-culture, actual ($E_{Y\ Actual}$; Y-axis) and expected E_Y ($E_{Y\ Expected}$; X-axis) values for S-M, M-M and D-M co-cultures were plotted. Expected E_Y was calculated based on the rule of mixtures, equating to the sum of 20% of $E_{Y\ zonal\ CH}$ and 80% of $E_{Y\ MSC}$ ($E_{Y\ Expected\ Mixed} = 0.2 * E_{Y\ Actual\ CH} + 0.8 * E_{Y\ Actual\ MSC}$). Slopes (◢; dotted line) in each group indicate the growth rate between 4 and 8 weeks. JMSC:JCH co-cultures showed mainly negative or independent effects of co-culture while AMSC:JCH co-cultures showed a positive effect of co-culture,

CHAPTER 1: Introduction

Articular cartilage is a dense connective tissue that provides a smooth and lubricated surface for articulation. Due to its avascular nature, cartilage has a limited self-healing capacity. When cartilage damage is initiated, the degradation progress is irreversible and often results in widespread and permanent degeneration, a condition termed osteoarthritis (OA). To intervene in this process, surgical repair strategies are often necessary, depending on the size of defect, age of patients and/or disease status. However, no surgical interventions have been fully successful for cartilage repair, and this raises an urgent demand for novel strategies using tissue engineering principles.

In cell-based cartilage tissue engineering, chondrocytes (CHs) are a primary source for cartilage tissue engineering and have been found to be superior to mesenchymal stem cells (MSCs) in matrix production and stability of phenotype. However, CH are in limited supply and donor site morbidity generally limits their use. Thus, MSCs are an attractive alternative cell source, as they are readily expandable, easy to obtain, and can undergo chondrogenesis. Given these characteristics, the use of MSCs in engineering cartilage tissue has been considered as a promising alternative. Indeed, these cells can generate cartilage-like repair cartilage tissue when placed in combination with a variety of 3D platforms. Our own data show that healthy, young MSCs seeded in 3D hydrogels can produce robust extracellular matrix with comparable mechanical properties and biochemical content to native cartilage.

However, one limitation of MSC-based tissue engineering is that the chondrogenic capacity of MSCs is attenuated with aging. Further, there exists a noted donor-to-donor variability, which may hinder reliable functional outcomes and will need to be further

investigated using multiple donors when considering clinical applications. MSCs are also multi-potent, and so are susceptible to changing their phenotype in response to changes in their microenvironment (e.g., chemical factors and mechanical stimulation). These cells are therefore most often cultured in a chemically defined media condition (MSC-friendly). However, for clinical application, these same MSCs need to be viable, maintain a stable phenotype, and accumulate robust matrix in the joint space, where anabolic and catabolic signals are mixed. Thus, the chondrogenic capacity of MSCs needs to be optimized under both defined conditions as well as in environments that mimic native growth conditions (e.g., serum containing media). Since people suffering from OA are mostly the aged populations, restoring chondrogenic capacity of adult MSCs is critical.

Despite the current endeavors and accomplishments, one remaining challenge is to recapitulate the native structure of cartilage, including its cellular organization, distribution of extracellular matrix proteins (e.g., collagen and proteoglycan), and depth-dependent functional properties that will be crucial for successful integration under the dynamic loading condition. Since the choice of surgical procedure depends on the size of the cartilage defect, fabrication of engineered constructs also needs to address the varying size, repair depths, and locations of defects. Recently, several studies have demonstrated the growth of larger/thicker constructs, with some being anatomically shaped. However, one critical challenge is to improve nutrient transport to the cells in these larger constructs during in vitro cultivation. This is particularly critical for constructs based on MSCs, which are more susceptible to cell death in response to challenging nutrient environments.

Finally, another equally important aspect in engineering cartilage tissue is to make these new technologies relevant for clinical application. To make tissue engineering

approaches readily applicable, novel designs may need to be somewhat simplified, while at the same time addressing limitations that are experienced with current clinical procedures (e.g., microfracture or ACI) while combining novel concepts in basic science with clinical practice.

Given these limitations and challenges, the overall objectives of this thesis was to first understand the chondrogenic capacity of MSCs in 3D hydrogels, to optimize functional maturation of MSC-laden constructs by understanding nutrient components that are responsible for anabolic and catabolic activities by MSCs, especially in conditions mimicking the in vivo environment, develop tissue engineered constructs that recapitulate native structure and function by mimicking structural complexity, and finally fabricate engineered constructs that are rather simple but readily applicable and most suitable for clinical application in combination with current clinical procedures.

Chapter 2 will provide a brief background on the basic science of articular cartilage, cartilage pathology, and current approaches in cartilage tissue engineering.

In **Chapter 3**, to investigate chondrogenic capacity of MSCs, we derived human MSCs (hMSCs) from eight donors, spanning a range of ages and disease conditions, and evaluated their ability to undergo chondrogenesis in pellet culture and in HA hydrogels. Based on findings from initial studies, we next evaluated the impact of variation in cell and HA macromer concentration on functional outcomes. Finally, given our observation of overt gel contraction for some donors, we reduced cytoskeletal tension during chondrogenesis to stabilize construct dimensions while preserving functional outcomes.

In **Chapter 4**, given the donor variability of human populations and inferiority in matrix accumulation, we changed cell sources to young/healthy bovine MSCs and explored the optimal delivery of TGF-β3 to promote functional outcomes of MSC-laden constructs. We specifically explored short term exposure at very high doses (10, 50 and 100 ng/mL) and durations (3, 7, 21 and 63 days) to determine the most optimal timing and dose to deliver to promote tissue formation.

While TGF-β3 is a known factor in MSC chondrogenesis, **Chapter 5** investigates the maturation of mesenchymal stem cell (MSC)-laden HA constructs with various combinations of chemically defined media (CM) components, and determines the impact of dexamethasone and serum on construct properties. For this, constructs were cultured in CM+ (chemically defined media (CM) supplemented w/ TGF-β3), CM in the absence of dexamethasone (DEX-) or a serum substitute (ITS/BSA/LA-), or in serum containing media (Serum+). Next, constructs were cultured in CM+ or DEX- for 4 weeks, and continuously maintained or transferred to CM+ or DEX- for the following 4 weeks. Finally, constructs were cultured for 4 weeks in CM+ and maintained in CM+ or transferred to Serum+ with or without dexamethasone for the following 4 weeks.

In addition to synthetic factors in culture media, we investigated the effect of natural molecular factors secreted from primary cells on MSCs. In **Chapter 6**, we investigated the influence of co-culture of zonal CHs on MSC chondrogenesis and explored the age-dependence of this phenomenon. Next, we identified the distance over which the molecular factors can act to induce the co-culture effect and determined how these factors are transferred between signaling and target cells. Zonal CHs and MSCs were isolated from bovine cartilage or bone marrow, expanded in a serum containing basal medium (BM) during 2D expansion (TCP) and cultured in a chemically defined medium

(CM) with TGF (CM+; 10 ng/mL) during 3D culture (HA hydrogel). To track cell populations, each cell type was labeled with a fluorescent dye and analyzed by confocal microscopy and fluorescent activated cells sorting (FACS). Finally, to identify delivery mechanisms, we manipulated cellular communication between subpopulations using inhibitors of vesicular production, release, and binding.

Based on the findings on the importance of intercellular mechanisms in the functional maturation of cell-laden hydrogels from Chapter 6, In **Chapter 7**, we fabricated tri-layered constructs that recapitulated the depth-dependent cellular organization and functional properties of native tissue, using zonally derived chondrocytes co-cultured with MSCs. We also introduced porous hollow fibers (HFs) and HFs/cotton threads to enhance nutrient transport.

To develop engineered cartilage with clinical relevance, in **Chapter 8**, we developed a CH-laden micro-scale noodle-shaped construct (i.e., micro-noodle) that can be readily implemented in the context of microfracture, allowing endogenous MSCs from the underlying bone marrow to migrate into the defect and percolate into a micro-noodle fiber weave. We report on the chondrogenic capacity of adult porcine CHs and MSCs, design and fabricate micro-noodles, demonstrate their chondro-inductive capacity in an environment mimicking microfracture (MSC-laden fibrin gel), and evaluate the retention of micro-noodles in an in vivo large animal model of cartilage repair.

Finally, **Chapter 9** contains a summary of the major findings from this work and a discussion of its implications for the field of cartilage therapeutics and regenerative medicine as well as future research directions.

CHAPTER 2: Background

2.1 Articular Cartilage

2.1.1 Function and composition

Articular cartilage is a connective tissue covering the ends of long bones. In humans, cartilage ranges from 4-7 mm thick (Ateshian, Soslowsky et al. 1991, Eckstein, Gavazzeni et al. 1996, O'Connell, Lima et al. 2012). Articular cartilage gives rise to a nearly friction-free surface that has great load-bearing properties responsible for resisting compressive forces and distributing loads (Nieminen, Toyras et al. 2000, Rieppo, Toyras et al. 2003). The compressive modulus of cartilage is approximately 0.1-0.2 MPa (unloaded), 4-5 MPa (walking) and 10-20 MPa (standing), respectively (Chen, Falcovitz et al. 2001). The tensile modulus is 5-50 MPa and is derived from the collagen content and network (Akizuki, Mow et al. 1986).

Articular cartilage is composed of water, chondrocytes and extracellular matrix (Muir 1970, Korhonen, Laasanen et al. 2003). Water is the most abundant component, representing 65-80% (Wet Weight; WW) of the tissue (Maroudas and Bullough 1968, Maroudas, Bullough et al. 1968). Chondrocytes (~1% of the total tissue volume) are the primary cell type that produces and regulates extracellular matrix proteins and maintains cartilage homeostasis (Broom and Marra 1986, Huber, Trattnig et al. 2000). The size, shape and number of chondrocytes depend on the maturity and location in cartilage matrix. Cartilage extracellular matrix (ECM) includes collagens and proteoglycans (PGs) (Maroudas, Bullough et al. 1968, Korhonen, Laasanen et al. 2003). The ECM can be classified into pericellular, territorial, and interterritorial matrices, depending on the location the cells.

Collagen (10-20% WW) is a fibrous protein, and type II collagen (80-90% of total collagen) is the most abundant (Huber, Trattnig et al. 2000). Type VI, IX and XI collagens are also present in cartilage, and are cross-linked between type II collagens to stabilize and strengthen the collagen networks (Eyre 2002). A primary function of the collagen mesh is to prevent the proteoglycan molecules from swelling beyond their volumetric range (Eyre 2002). The tensile forces of the collagen network thus enable the maintenance of balance between the osmotic swelling pressure from proteoglycans (PGs) and the resistance to compressive forces (Bayliss, Osborne et al. 1999, Nieminen, Toyras et al. 2000).

Proteoglycans such as aggrecan, decorin, biglycan and fibromodulin (Ueda, Baba et al. 2001) are macromolecules that impart creep and stress-relaxation function to the cartilage (Korhonen, Laasanen et al. 2003), and aggrecan aggregate (4-7%WW) is the most abundant (90% of total PG mass) (Bayliss, Osborne et al. 1999, Huber, Trattnig et al. 2000, Theocharis, Tsara et al. 2001).

2.1.2 Structure

Cartilage structure varies not only in its molecular composition but also in the distribution and organization of components from the articular surface to the bottom of the tissue. The layers are termed superficial zone, middle (or transitional zone), deep (or radial zone) and the calcified zone located in between the tidemark and subchondral bone (Bhosale and Richardson 2008, Sophia Fox, Bedi et al. 2009). The superficial (or tangential) zone is the thinnest zone and accounts for 10-20% of the entire thickness in articular cartilage. It contains a low proteoglycan content, oval-shaped chondrocytes and densely packed collagen fibers, with both cells and fibers being parallel to articular surface (Huber, Trattnig et al. 2000, Sophia Fox, Bedi et al. 2009). The middle

(transitional or intermediate) zone comprises 40-60% of the cartilage height. Chondrocytes are spherically shaped and collagen fibers are thicker and randomly oriented. Water content becomes decreased and proteoglycan content is increased. The deep (radial) zone includes 30% of cartilage thickness from the bottom and a lower content for both water and collagen. Chondrocytes are perpendicularly arranged to the articular surface and proteoglycan content is the highest.

2.1.3 Pathology

Articular cartilage is also characterized as being hypocellular, aneural, alymphatic and avascular (Buckwalter, Mankin et al. 2005). These characteristics result in a limited capability to repair after injury often leading to a progressive disease called osteoarthritis (OA) (Pritzker, Gay et al. 2006). OA is a musculoskeletal disorder characterized by progressive deterioration of articular cartilage, which is accompanied by pain, stiffness and limited joint motion. In 1994, the Center for Disease Control and Prevention (CDCP) reported that by the year 2020, arthritis would be the most prevalent disease of new patients in the United States. Approximately 20% of Americans (about 60 million people) are at risk and more than 80% of people older than 75 years develop the symptoms of OA. An annual loss for individuals in direct traditional medical costs and indirect economic and wage loss from the disease has been reported in excess of $65 billion (Jackson, Simon et al. 2001).

Articular cartilage can be degraded by continual loads, which lead to wear, tear and fissure of the tissue (Martel-Pelletier 1998, Goldring 2012). Collagen network breakdown and proteoglycan degradation are typical signs of cartilage degeneration leading to OA, which result in decreased tensile strength in collagen fibers, increased water content and proteoglycan loss (Rieppo, Toyras et al. 2003). The superficial zone is involved in the

early stage of cartilage degradation and eventually progresses to the subchondral bone (Rieppo, Toyras et al. 2003). These structural and compositional changes impair normal joint function (Korhonen, Laasanen et al. 2003). OA is usually found in the hand, knee, hip, foot, spine and other joints such as elbows, shoulders and toes. The risk factors for the disease are generally thought to be aging, obesity, lower bone density, genetic factors, trauma and repetitive stresses. Pain is attributed to joint movement and is soothed by rest in the early stages of OA, but the pain becomes severe even at rest as the disease progresses (Buckwalter, Mankin et al. 2005). Physical therapy, drug therapy and surgery are currently used clinically to treat the disease, but with limited success. A significant complication in the treatment of OA is the inability to diagnose the disease process at an early stage, and the lack of methods to evaluate the tissue response to therapeutic and tissue engineering interventions.

2.2 Differential regenerative potentials of zonal chondrocytes

The metabolic and matrix forming capacity of chondrocytes is different depending on their original anatomic location through the depth. Previous studies have shown that superficial zone (SZC) and deep zone chondrocytes (DZC) have distinct phenotypic characteristics in monolayer (Aydelotte, Greenhill et al. 1988, Aydelotte and Kuettner 1988, Darling and Athanasiou 2005, Darling and Athanasiou 2005, Cheng, Conte et al. 2007, Jiang, Leong et al. 2008, Ng, Ateshian et al. 2009), pellet culture (Cheng, Conte et al. 2007) and 3D hydrogels (Ng, Ateshian et al. 2009). DZC show greater PG accumulation associated with larger cell diameters and high gene expression of runt-related transcription factor-2 (RUNX2) as an indicator of a hypertrophic phenotype, in comparison to SZC (Cheng, Conte et al. 2007). Further, Middle/DZC-laden 3D hydrogels produced greater mechanical and biochemical (PG and collagen) properties than SZC-laden hydrogels (Ng, Ateshian et al. 2009). These results confirm that articular zonal

chondrocytes cultured in vitro retain differential matrix forming capacity, which indicates that there may be intrinsic differences in zonal articular chondrocytes.

2.3 Chondrogenesis of MSCs and CHs in co-culture

Over the past decade, numerous studies have investigated the effect of MSCs and CHs in co-culture in various comparison groups, including species of cell sources (i.e., human, bovine, porcine or rabbit), proximity (i.e., direct- or non-contact), culture platform (i.e., TCP, 2D scaffold [PCL], 3D pellet, beads or hydrogel) and cross-species conditions (i.e., auto-, allo-, or xenogenic). With such a variety of experimental conditions, the reported results have also been diverse. Fisher et al., and other groups have shown that CHs promote MSC chondrogenesis (COL II, SOX 9) and functional properties, while suppressing MSC hypertrophy (COL X, IHH) (Fischer, Dickhut et al. 2010, Aung, Gupta et al. 2011, Bian, Zhai et al. 2011, Lai, Kajiyama et al. 2013, Sabatino, Santoro et al. 2015, Zhang, Su et al. 2015). Conversely, Xu et al., and others have reported that there is no synergistic effect with co-culture in the absence of contact in both 2D (Transwell) (Acharya, Adesida et al. 2012, Xu, Wang et al. 2013) and 3D (alginate bead) culture (Xu, Wang et al. 2013) while Levorson et al., reported a synergistic effect in co-culture without contact (2D PCL scaffold or 3D agarose gel) (Yang, Lee et al. 2012, Levorson, Santoro et al. 2014). Interestingly, several groups have reported that there is a reciprocal effect, where CHs and MSCs influence one another (Acharya, Adesida et al. 2012, Diao, Yeung et al. 2013, Wu, Cai et al. 2013). Although these conclusions are somewhat at variance with each other, one of the most consistent findings is that a direct cell-cell contact or very close proximity is required to induce synergistic effects while the direction of chondro-induction between MSCs and CHs as signaling and receiving cells (vice versa) remains controversial (i.e., trophic effect) (Meretoja, Dahlin et al. 2012, Wu, Post et al. 2015).

2.4 Fabrication of multi-layered constructs to recapitulate zonal organization

Biomimetic design in cartilage tissue engineering is a challenge given the complexity of native tissues (Buckwalter and Mankin 1998). Differences in matrix accumulation in zonal CHs have motivated the novel cell-based strategies in cartilage tissue engineering. Indeed, several studies have created multi-layered constructs, where respective zonal CHs-laden hydrogel sublayers are combined in a “layer-by-layer” scheme, to mimic a tissue morphology, cellular organization and depth-dependent heterogeneity of native tissue (Kim, Sharma et al. 2003, Moutos, Freed et al. 2007, Klein, Rizzi et al. 2009, Ng, Ateshian et al. 2009, Nguyen, Kudva et al. 2011, Schuurman, Klein et al. 2015). These layered constructs exhibit cellular organization and depth-dependent functional properties similar to native cartilage.

2.5 Methods to Improve Nutrient Transport in Cell-Laden Tissue Engineered Cartilage Constructs

Another challenge in cartilage tissue engineering, particularly for hydrogel-based constructs, is to improve nutrient transport. Due to the lack of nutrient and waste transport into and out of the core of the construct, the distribution of matrix accumulation in cell-laden hydrogels is usually inhomogeneous. It has been noted that greater and stiffer matrix production is observed near the peripheral region while less and softer matrix production occurs deep inside of the construct (O'Connell, Lima et al. 2012). To improve nutrient transport and functional properties, several studies have reported on the introduction of macro/micro channels (Bian, Angione et al. 2009, Buckley, Thorpe et al. 2009) into the construct to create improved paths for nutrient diffusion as well as dynamic loading (Kelly, Ng et al. 2006, Vaughan, Galie et al. 2013) to stimulate the fluid movement into and out of the construct (Bian, Angione et al. 2009, Cigan, Nims et al. 2014). However, relatively early in culture channels can become filled with newly formed

matrix blocking nutrient transport. Further, dynamic loading promotes the greatest fluid exchange at the peripheral region, which further increases heterogeneity of matrix properties (Kelly, Ng et al. 2006).

CHAPTER 3: Donor-to-Donor Variability in Functional Chondrogenesis by Human Mesenchymal Stem Cells in Hyaluronic Acid Hydrogels

3.1 Introduction

Cartilage tissue engineering aims to develop functional constructs to replace damaged or degenerated tissues (Langer and Vacanti 1993). Although human chondrocytes have been utilized as primary sources for cartilage repair, their availability and quality is somewhat limited, especially when derived from arthritic donors (Dore, Pelletier et al. 1994, Yang, Saris et al. 2006, Cravero, Carlson et al. 2009). Given this, mesenchymal stem cells (MSCs) have arisen as an attractive cell type for cartilage tissue engineering as they are nearly unlimited in supply and can under chondrogenesis in a variety of 3D platforms (Caplan 1991, Johnstone, Hering et al. 1998, Mackay, Beck et al. 1998, Pittenger, Mackay et al. 1999). To date, there has been considerable progress towards optimizing MSC chondrogenesis in 3D culture; however, much of this work has relied on the use of MSCs from animal sources (Buckley, Thorpe et al. 2009, Erickson, Huang et al. 2009, Huang, Farrell et al. 2010, Nakagawa, Muneta et al. 2016, Tangtrongsup and Kisiday 2016).

From a clinical perspective, effective repair will depend on successful translation of these findings to human MSCs (hMSCs), preferably those derived from an autologous source. However, some have noted species-to-species variation in chondrogenic potential, which may depend on the 3D microenvironment. For example, hMSCs encapsulated within hydrogels lacking adhesion moieties show a marked loss in viability with time, in contrast to bovine MSCs (Salinas, Cole et al. 2007). In addition, as osteoarthritis (OA) and cartilage degeneration primarily affect the aged population (Murphy, Dixon et al. 2002), optimization strategies must consider both the effect of age

as well as the disease status of the donor cells. Studies suggest that the chondrogenic potential of hMSCs cultured in pellet form may be independent of age, but that their potential decreases with the onset of OA (Murphy, Dixon et al. 2002, Payne, Didiano et al. 2010). The impact of age and disease on chondrogenesis in 3D culture has not yet been well studied. In one recent study, we showed that healthy juvenile hMSCs in photocrosslinkable hyaluronic acid (HA) hydrogels accrue functional properties with time in culture (Chung, Beecham et al. 2009). HA hydrogels are a biologically relevant material with easily tunable properties (Burdick, Chung et al. 2005, Sahoo, Chung et al. 2008, Chung and Burdick 2009). HA is a non-sulfated glycosaminoglycan (GAG) and one of the major components of articular cartilage and consists of repeating disaccharides of D-glucuronic acid and N-acetyl-D-glucosamine (Burdick, Chung et al. 2005, Fakhari and Berkland 2013). Studies have shown that HA provides a native like microenvironment to MSCs (i.e., through the cell adhesion receptor, CD44) and can enhance functional chondrogenesis compared to other synthetic hydrogels such as poly(ethylene glycol) (PEG) (Knudson and Loeser 2002, Chung and Burdick 2009, Fakhari and Berkland 2013). Our group has likewise shown that juvenile bovine MSCs (jbMSCs) ecapuslated in HA of varying macromer density showed different levels maturation (Erickson, Huang et al. 2009). While higher macromer densities (2 and 5%) started out with superior properties, after 42 days of culture, 1% HA constructs matured to the greatest extent.

Building from these studies, and to better elucidate the consistency of construct maturation using hMSC donors and HA hydrogels, our first objective was to assess the effects of age and disease status on functional chondrogenesis. Human MSCs derived from seven different donors were cultured in HA hydrogels, and their functional maturation was evaluated over time. In a subsequent study, and based on the marked

contraction observed in some donors, our second objective was to determine whether inhibition of cytoskeletal tension could block this contraction while promoting chondrogenesis. In a final study, we sought to optimize donor-specific MSC chondrogenesis by manipulating cell and macromer density. Our findings demonstrate marked donor-to-donor variability by hMSCs in terms of their functional chondrogenesis in HA hydrogels, and show that variation in cell and macromer density might be employed to promote patient-specific cartilage repair.

3.2 Materials and Methods

3.2.1 Isolation and expansion of human MSCs

Human MSCs (hMSC) were obtained from several different sources **(Table 3-1)**. Three young/healthy donors were obtained either from a commercial vendor (Lonza, Wakersville, MD) (18F, 21M, and 22F) or were sourced locally from a patient undergoing treatment for osteochondritis dissecans (OCD). MSCs from five aged/OA donors were obtained from bone marrow aspirates of patients undergoing total hip or knee replacement. These patients ranged in age from 42 to 62. All locally sourced human material was obtained with patient consent and under the auspices of an approved IRB protocol at the University of Pennsylvania. MSCs were cultured and expanded to passage 3-4 in basal media (BM) in order to obtain sufficient cell numbers for both hydrogel encapsulation and pellet formation. BM consist of high glucose DMEM with 10% fetal bovine serum (Thermo Scientific, Grand Island, NY) and 1% penicillin/streptomycin/Fungizone (PSF) (Thermo Scientific, Grand Island, NY).

Table 3-1: Details on human MSC donors and sourcing. (Y = young donor, O = old donor; M = male, F = female; OCD = patient with osteochondritis dissecans; OA = patient undergoing joint replacement surgery as a consequence of hip or knee OA)

Donor	Age/Gender	Source
Y1	18M	Patient (OCD)
Y2	22F	Lonza
Y3	21M	Lonza
O1	62M	Patient (OA)
O2	42F	Patient (OA)
O3	57M	Patient (OA)
O4	46F	Patient (OA)
O5	61F	Patient (OA)

3.2.2 MeHA synthesis

Synthesis of methacrylated hyaluronic acid (MeHA) was as previously described (Burdick, Chung et al. 2005, Erickson, Huang et al. 2009). Briefly, methacrylic anhydride (Sigma-Aldrich, St. Louis, MO) was reacted with 1 wt% HA (65 kDa MW; Lifecore, Chaska, MN) dissolved in deionized water on ice while continuously maintaining pH at 8.0 via dropwise addition 5N NaOH (Sigma-Aldrich, St. Louis, MO) for 6 hours. After the reaction was completed, the macromer solution was purified via dialysis (MW cutoff 6-8 k) against distilled water for one week, with changes to fresh water twice daily. The This MeHA solution was then lyophilized, and the degree of modification was assessed by NMR spectroscopy. Next, the lyophilized MeHA was dissolved in PBS with 0.05% w/v of the photoinitiator I2959 (2-methyl-1-[4-(hydroxyethoxy)phenyl]-2-methyl-1-propanone, Ciba-Geigy, Tarrytwon, NY) to enable UV-mediated photo-polymerization.

3.2.3 MSC encapsulation

Evaluation of donor-to-donor variability

To investigate how MSC chondrogenic capacity varied amongst different human donors, hMSCs were cultured in both pellet and HA hydrogel format. To culture in the pellet format, 250,000 hMSCs from each donor were placed in a 96 well round-bottom polypropylene plate (Nunc, Paperville, IL) and centrifuged at 300xg for 5 minutes. These cell pellets aggregated over the first 24 hours, and were cultured in 200 µL/pellet a chemically defined media (CM) for 2 and 4 weeks. CM consisted of high glucose DMEM with 1x PSF; 0.1µM dexamethasone; 50 µg/mL ascorbate 2-phosphate; 40 µg/mL L-proline; 100 µg/mL sodium pyruvate; and 6.25 µg/mL insulin, 6.25 µg/mL transferrin, 6.25 ng/mL selenious acid, 1.25 mg/mL bovine serum albumin (BSA), and 5.35 µg/mL linoleic acid. CM was supplemented with 10 ng/mL TGF-ß3 (CM+, R&D Systems, Minneapolis, MN) to induce chondrogenesis, and media was changed twice weekly. For HA hydrogel culture, hMSCs were suspended in MeHA solutions at 20 million cells/mL, and MSC-laden MeHA suspensions were then cast in a gel casting device (spacers of 2.25mm) and photo-polymerized by UV exposure using a 365 nm Blak Ray UV lamp (UVL-56, San Gabriel, CA) for 10 minutes (Erickson, Huang et al. 2009). Cylindrical constructs (Ø4 mm × 2.25 mm) were cored from the gel and cultured in CM for 4 and 8 weeks, with media changed twice weekly.

Modulation of cell contractility in HA hydrogels

Because some donors tended to contract the HA hydrogel, a final study was performed to determine whether inhibiting cytoskeletal tension in hMSCs in HA would prevent self-aggregation and promote a more even distribution of formed matrix. For this, hMSCs were seeded in 1% HA hydrogel at 20 million cells/mL and cultured for 4 weeks in CM+ supplemented with Y27632 (10 µM; EMD Millipore, Darmstadt, Germany), a selective inhibitor of the Rho-associated protein kinase/ROCK pathway. Media were changed twice weekly, with fresh Y27632 added at each media change.

Optimization of cell and macromer density

In a subsequent study, to explore whether manipulating cell and macromer density could stabilize construct geometry while promoting functional chondrogenesis, one young/healthy donor (Y2) was utilized. Cells from this donor were cast in HA hydrogels at different cell (20 and 60 million cell/mL) and macromer (1, 1.5 and 2% MeHA) densities and cultured in CM+ for 8 weeks. Media were changed twice weekly.

3.2.4 Mechanical testing

Unconfined compression testing was carried out to determine compressive equilibrium (E_Y) and dynamic (|G*|) moduli of constructs as in (Mauck, Soltz et al. 2000). Compressive modulus was determined via stress-relaxation applied at 0.05%/sec to 10% strain following a creep deformation to 0.02 N applied over 5 min. After gels reached equilibrium, a 1% strain amplitude sinusoidal deformation was applied at 1.0 Hz (Park, Hung et al. 2004). Prior to mechanical testing, the top and bottom surfaces of constructs were carefully trimmed using a freezing stage microtome to ensure an even contact surface. Equilibrium moduli were calculated from the stress relaxation test and sample geometry, while the dynamic modulus was estimated from the dynamic compression test and sample geometry, as outlined in (Soltz and Ateshian 1998).

3.2.5 Biochemical analysis

After mechanical testing, construct wet weight was measured followed by papain digestion (1mL/construct, 0.56U/mL in 0.1M sodium acetate, 10M cysteine hydrochloric acid, 0.05M ethylenediaminetetraacetic acid, pH 6.0) at 60°C for 16 hours. Sulfated glycosaminoglycan (s-GAG) content was assessed using the 1,9-dimethylmethylene blue (DMMB) assay (Farndale, Buttle et al. 1986). Collagen content was measured via

reaction with chloramine T and diaminobenzaldehyde (Stegemann and Stalder 1967). Collagen content was extrapolated from OHP content using a 1:7.14 ratio of OHP:collagen (Neuman and Logan 1950). Given variations in contractility and chondrogenic capacity of MSC donors, GAG and collagen contents from the first experiment were normalized to the number of cells for the donor variation experiment, while the other studies were normalized to the construct wet weight (%WW).

3.2.6 Histological analysis and cell viability

Constructs for histological processing were fixed in 4% paraformaldehyde for 24 hours and embedded in paraffin. Sections (8 μm) were deparaffinized in a graded series of ethanol and stained with Alcian Blue (pH 1.0) and Picrosirius Red (0.1% w/v in saturated picric acid) for proteoglycans (PG) and collagens, respectively. Immunohistochemistry was carried out to visualize type I and type II collagen and chondroitin sulfate (CS). Primary antibodies for type I collagen (MAB3391; Millipore, Billerica, MA), type II collagen (II-II6B3; DSHB, Iowa City, IA), and chondroitin sulfate (CS; C8035, Sigma-Aldrich, St. Louis, MO) were used for immunostaining. On separate constructs, cell viability was evaluated via LIVE/DEAD staining, per the manufacturers' instruction (Molecular Probes, Eugene, OR).

3.2.7 Statistical analysis

Statistical analysis was performed using the SYSTAT software (v10.2, SYSTAT software Inc., San Jose, CA). Significance was determined by one-way ANOVA with Tukey's post hoc testing ($p<0.05$).

3.3 Results

3.3.1 Donor-to-donor variation in hMSC chondrogenesis

A total of 8 human donors, ranging in age from 18-62 provided MSCs for this study, including four males and four females **(Table 3-1)**. These human MSCs were viable when encapsulated in HA hydrogels. Consistent with previous findings (Erickson, Huang et al. 2009), all constructs contracted to some extent over the first few days of culture **(Figure 3-1)**. Of the 8 donors, 2 young/healthy donors (Y1 and Y2) and 1 old/aged donor (O1) maintained their original cylindrical shape **(Figure 3-1A)**. Several of the older/aged donors (O2 and O3) deformed significantly and took on a pellet-like in appearance **(Figure 3-1B)**, while others (O4 and O5) failed to maintain structural integrity and dissolved within a few days **(Figure 3-1C)**.

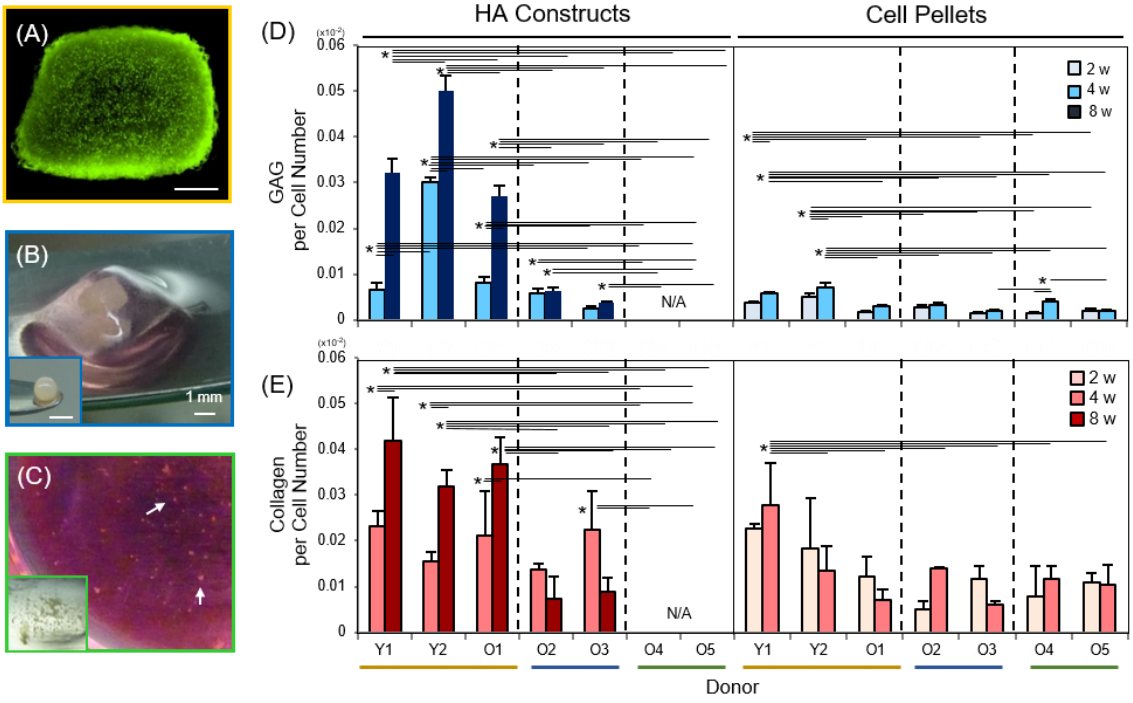

Figure 3-1: Donor-to-donor variation in hMSC chondrogenesis in pellets and HA hydrogels. (A) Some hMSC donors laden in 3D hydrogel maintained a cylindrical morphology (Calcein AM; 8w), (B) while others resulted in severely contracted constructs (1w; inset: cell compaction-induced pellet formation), or (C) simply disintegrated early in

culture (1w; inset: disintegrated hydrogel). (D) GAG and (E) collagen content of hMSC-laden HA hydrogels at 4 and 8 weeks (Left) and cell pellets at 2 and 4 weeks (Right) normalized to their respective starting cell number. (20 million cells/mL in 1% HA, n = 4 (HA hydrogel), n = 3 (Pellet), Scale bar = 1 mm; Lighter bars = 2w, Medium bars = 4w, Darker bars = 8w)

Given this lack of dimensional stability, biochemical content of constructs is reported on a per cell basis. Data for each donor hMSC-laden HA construct as well as donor-matched pellets are shown in **Figure 3-1D and E**. While GAG and collagen content in constructs formed from the least contractile donors (Y1, Y2 and O1) increased with time, the biochemical content of pellets from these same donors generally plateaued by week 2. Notably, the biochemical content of constructs that had contracted (O2 and O3) were lower than these donors (Y1, Y2 and O1).

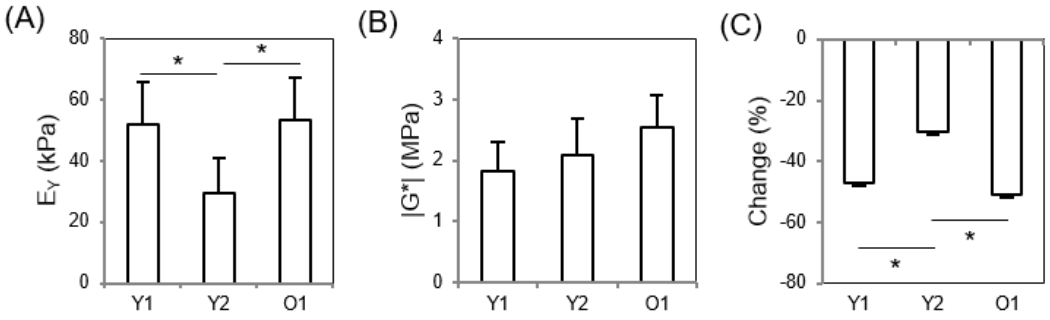

Figure 3-2: Mechanical and morphological properties of hMSC-laden HA constructs at 8 weeks of culture. (A) Equilibrium modulus (kPa), (B) Dynamic modulus (MPa), and (C) Change in volume (% change) for constructs formed from those donors that retained a cylindrical morphology. (n=4/group; *p<0.05)

Mechanical properties of constructs formed from the Y1, Y2 and O1 donors increased with time in culture, reaching equilibrium (and dynamic) modulus of 30-53 kPa (and 1.8-2.5 MPa) by 8 weeks **(Figure 3-2A and B)**. While these three donors retained a

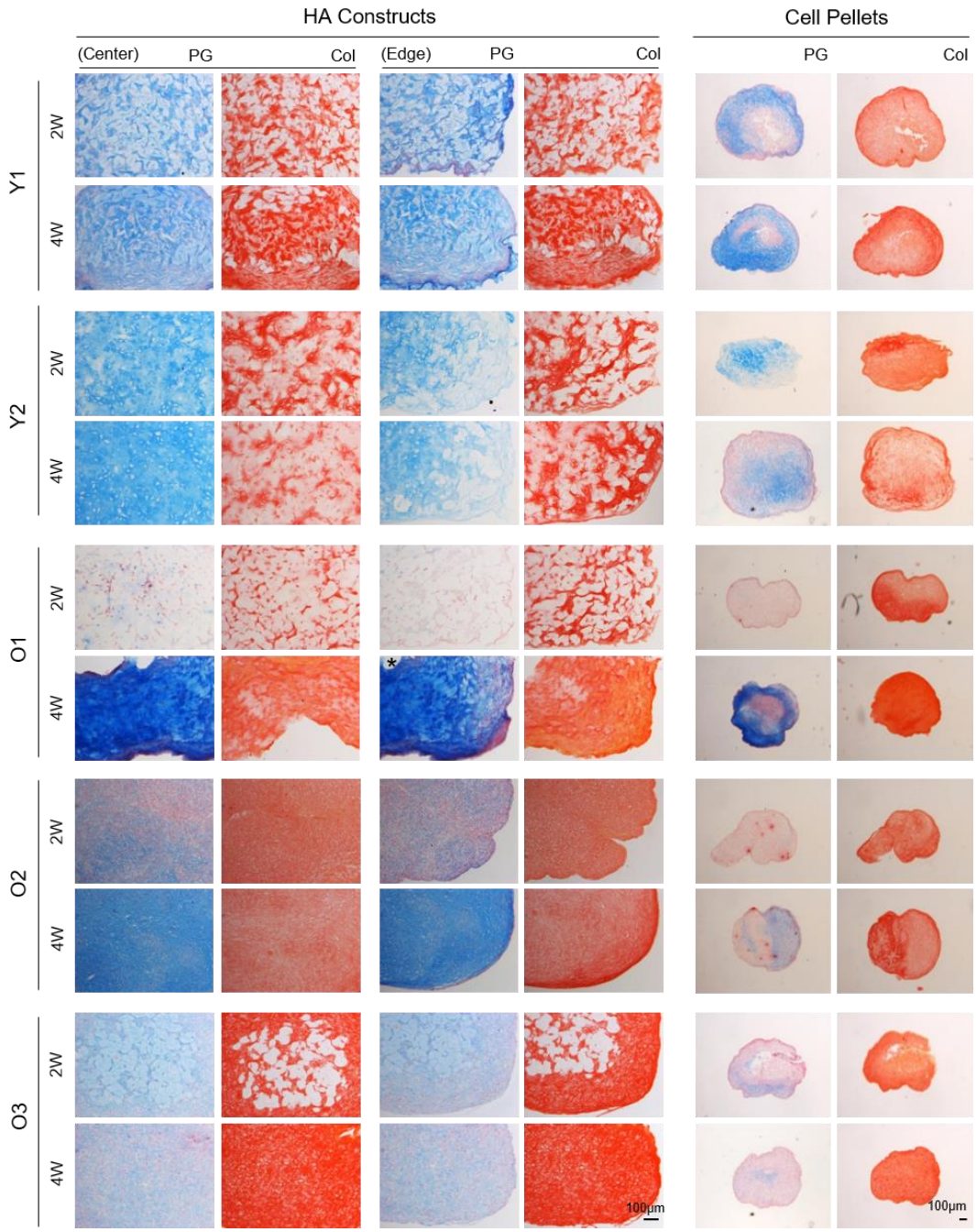

Figure 3-3: Histological evaluation of hMSC-laden HA constructs and pellets. Alcian blue (PG) and Picrosirius red (collagen) stained sections from hMSC-laden HA constructs (Left) and cell pellets (Right) derived from two young/healthy donors (Y1 and Y2) and three old/aged donors (O1, O2 and O3) at 2 and 4 weeks. For HA constructs, images of both center and edge regions are shown. (Scale bar = 100 μm)

cylindrical shape, significant volumetric changes were observed, with decreases on the order of ~30-50% **(Figure 3-2C)**. Histological evaluation for those donors that remained intact showed a dense matrix of proteoglycan (PG) and collagen by week 2 in the young/healthy donors with even distribution of matrix. Conversely, 2 out of 3 of the older/aged donors contracted early in culture and of these, only one produced matrix at the later time point (O2) in hydrogel culture. Staining confirmed that the biochemical content of pellets generally plateaued by 2 weeks **(Figure 3-3)**. Interestingly, the first three donors (Y1, Y2, and O1) all showed abundant proteoglycan in the pellet by week 4, while the remaining two donors assayed did not (O2 and O3). All pellets were rich in collagen as evidenced by the dark Picrosirius red staining.

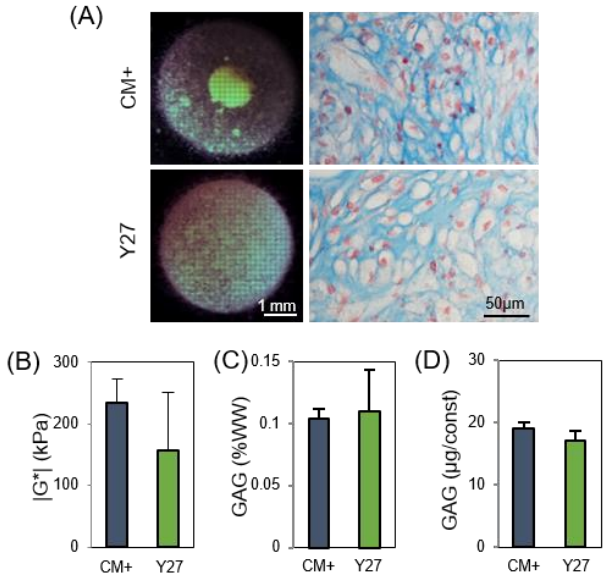

Figure 3-4: Inhibition of cytoskeletal tension preserves cell distributions in hMSC-laden HA constructs. (A) Macroscopic views of hMSC-laden HA hydrogels in control (CM+, Top) and Y27 (Bottom) conditions and Alcian blue staining (Right) at 4 weeks, (B) Dynamic modulus (|G|; kPa), (C and D) GAG content (%WW and µg/construct) (Constructs formed from donor Y3 at 20M cells/mL in 1% HA; n=3/group; Scale bar = 1mm (macroscopic images) and 50 µm (histological stains))

3.3.2 Effect of blockade of cell contractility on construct maturation

Given the contraction observed previously, we next tested whether inhibition of cytoskeletal tension in hMSCs would limit cell aggregation of cells and contraction, and how this might influence matrix production. Constructs treated with the Rho kinase inhibitor Y27632 at each media change maintained an even cell distribution, while control groups showed marked self-aggregation of cells (**Figure 3-4A**). While contraction was minimized, the dynamic modulus of control constructs was 50% higher (233 kPa) than those treated with Y27632 (156 kPa) (**Figure 3-4B**), and both conditions showed similar proteoglycan content (**Figure 3-4C-D**).

3.3.3 Alterations in cell and macromer density impact functional chondrogenesis in 3D culture

Given that blockade of contractility adversely impacted tissue formation, we next evaluated how changes in cell and gel density might impact contraction. We assayed cell densities of 20 or 60 million cells per milliliter and HA densities of 1, 1.5, and 2%. These changes in cell and gel concentration influenced volumetric changes and construct mechanical and biochemical properties (**Figure 3-5**). Specifically, macroscopic imaging of constructs showed central hMSC aggregation at 20 million cells/mL concentration in 1% HA hydrogels by 2 weeks. This resulted in a cell dense core region and a relatively cell-free fringe surrounding this core. With an increase in macromer density to 1.5% or 2% HA, cells did not self-aggregate and construct dimensions were maintained (**Figure 3-5**).

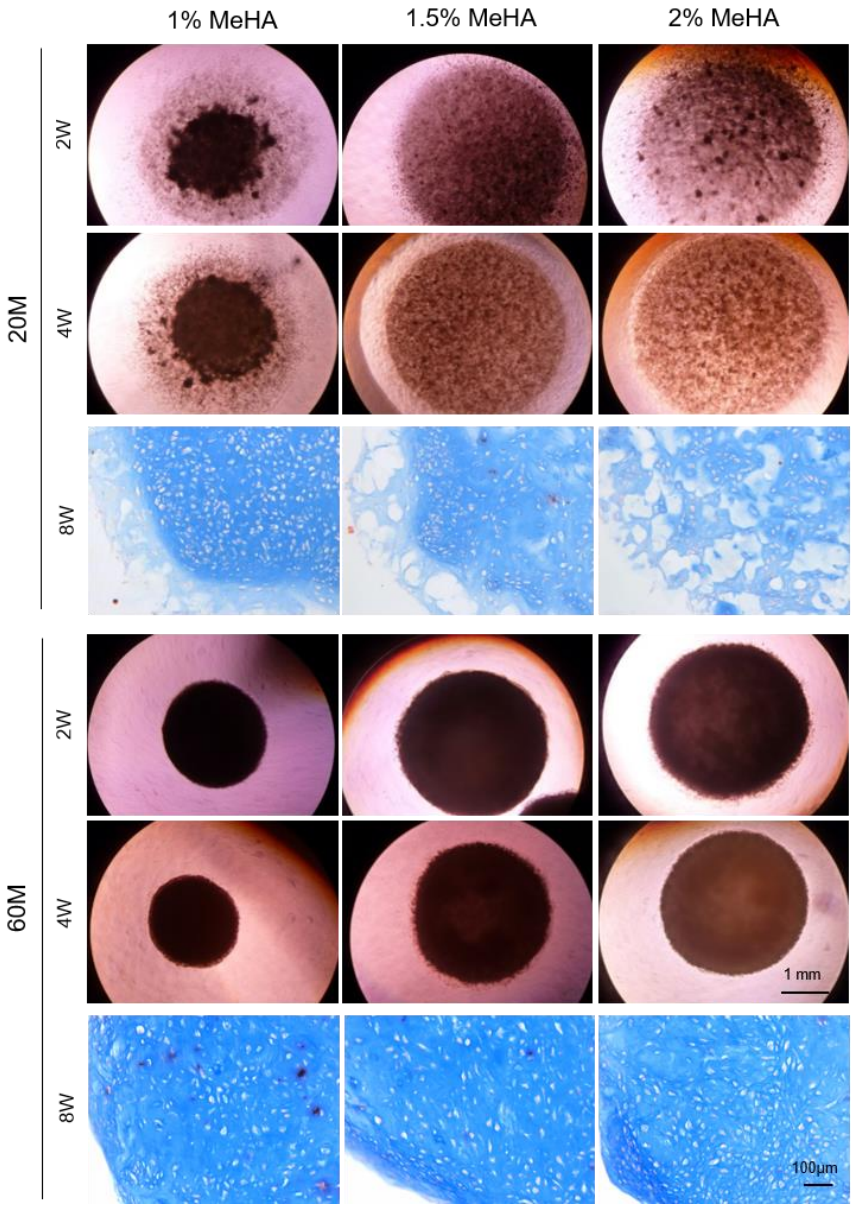

Figure 3-5: Impact of cell and macromer density on hMSC-seeded construct maturation. hMSCs were encapsulated in HA hydrogels at varying cell and macromer densities. 20 million cells/mL (Top panel) and 60million cells/mL (Bottom panel) at either 1% HA (Left column), 1.5% HA (Middle column) and 2% HA (Right column). Macroscopic images demonstrate volumetric contraction at 2 and 4 weeks, and Alcian blue staining at 8 weeks shows variation in proteoglycan staining intensity and distribution. (Scale bar = 1 mm (Macroscopic images) and 100 µm (Histological stains))

Alcian Blue staining of these constructs at 8 weeks showed that matrix staining intensity and distribution matched that of the distribution of cells. That is, proteoglycan distribution in 1% HA constructs was dense and compact in the core region whereas in 2% HA constructs proteoglycans showed dense non-contiguous foci that were distributed across the entire cross-section. When cell density was increased by a factor of three, to 60 million cells per milliliter, we noted an increase in construct compaction in 1% HA hydrogels. Conversely, construct dimensions were maintained in 2% HA, even at this higher cell density (**Figure 3-5**).

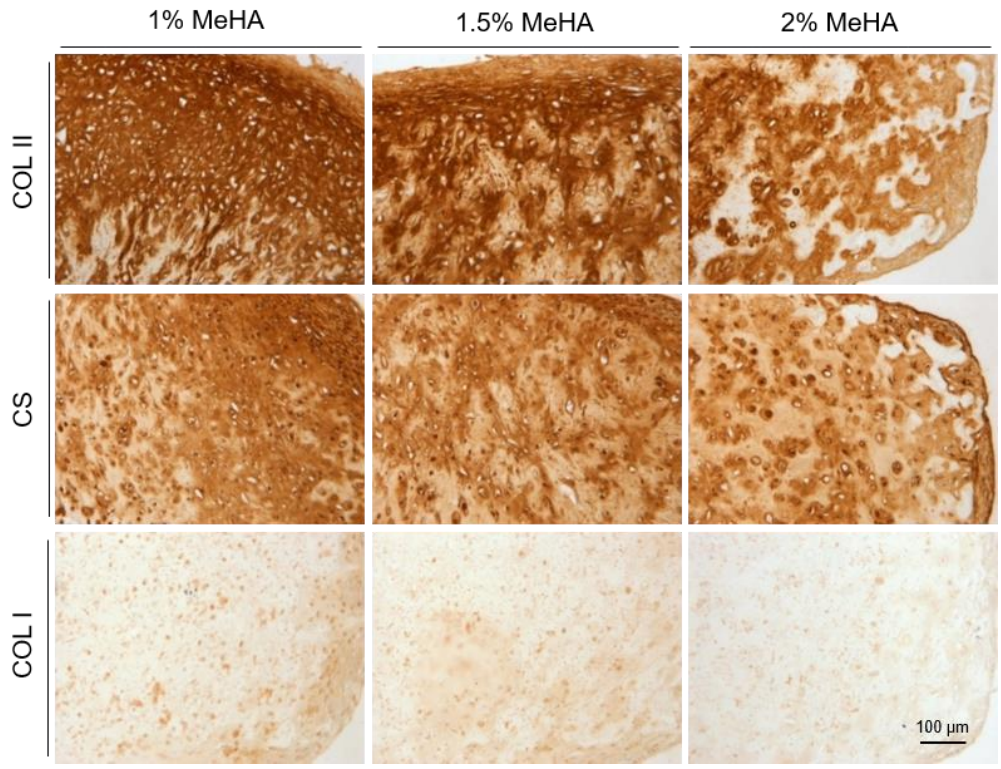

Figure 3-6: Immunohistochemistry of hMSC-laden HA construct formed at varying macromer densities. Type II collagen (COL II; Top), chondroitin sulfate (CS; Middle) and type I collagen (COL I; Bottom) stained sections from 1% HA (Left), 1.5% HA (Middle) and 2% HA (Right) constructs at 8 weeks (60 million cells/mL; Scale bar = 100 µm)

Likewise, proteoglycan staining intensity was high throughout the construct at 8 weeks for all macromere densities. Immunohistochemistry of high density constructs showed that type II collagen and chondroitin sulfate appeared highly concentrated in 1% HA constructs, but staining density and connectivity of these foci decreased with increasing macromer concentration. Overall, there was little type I collagen produced under any condition (**Figure 3-6**). Construct mechanical and biochemical properties were assessed though 56 days of culture, and generally followed these histological observations (**Figure 3-6**).

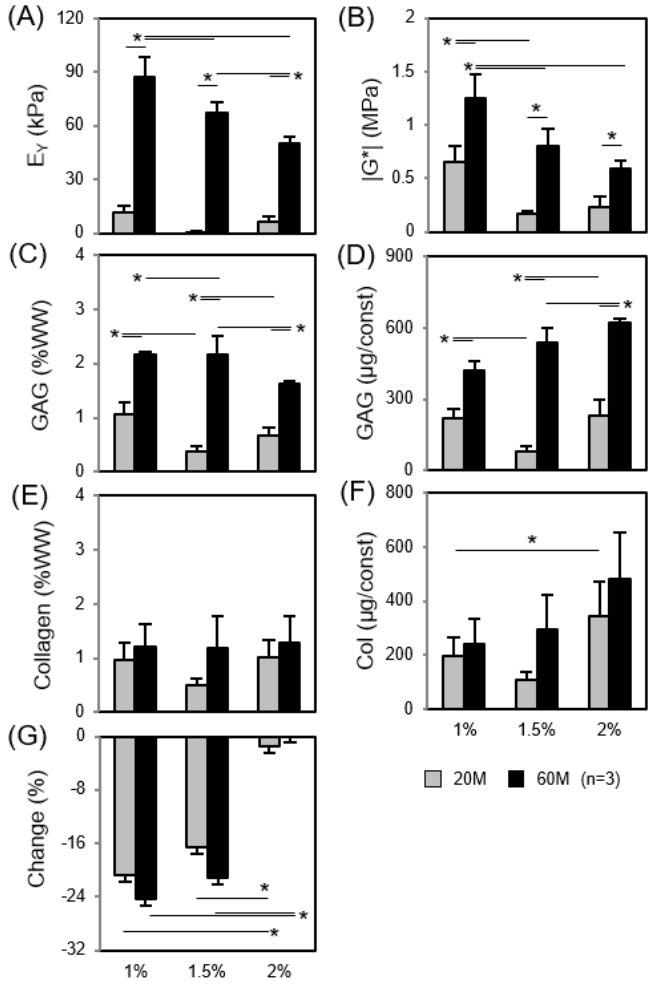

Figure 3-7: Functional properties of hMSC-laden HA constructs formed at varying cell and macromer densities after 8 weeks of culture. (A) Equilibrium modulus (E_Y; kPa), (B) Dynamic modulus (|G*|; MPa), (C and D) GAG content (%WW and µg/construct), (E and F) collagen content (%WW and µg/construct), and (G) Volumetric change (diameter; %change) (Lighter bars = 20M cells/mL; Darker bars = 60M cells/mL; n = 3/group, *p<0.05)

Mechanical properties of hMSC-laden HA hydrogel constructs increased with time in culture, reaching equilibrium (E_Y) and dynamic (|G*|) moduli of 87kPa and 1.25 MPa (1% HA), 67kPa and 0.8MPa (1.5% HA), and 50kPa and 0.59MPa (2% HA), respectively (**Figure 3-7A and B**). The equilibrium modulus (E_Y) of 1% HA constructs was 30% and 74% greater than 1.5% and 2% HA, respectively (*p<0.05). Evaluation of GAG content showed a similar trend, with 1% HA (2.2% WW) and 1.5% HA (2.2% WW) levels markedly higher than 2% HA (1.6% WW, *p<0.05). On a per construct basis, however, the reverse trend was noted, with 422µg (1% HA), 540µg (1.5% HA) and 620µg (2% HA) of GAG produced (**Figure 3-7C and D**). Collagen content followed similar trends, with 1.2% WW and 240µg (1% HA), 1.2% WW and 295µg (1.5% HA) and 1.3% WW and 481µg (2% HA), respectively (**Figure 3-7E and F**). High levels of contraction were noted for 1% HA (-20% and -24%; 20M and 60M cells) and 1.5% HA (-16% and -21%) constructs; contraction was much less in 2% HA constructs (-1.5% and +1.0%) (**Figure 3-7G**).

3.4 Discussion

In this study, we evaluated the chondrogenic potential of MSCs from multiple human donors in pellet and three dimensional HA hydrogel culture. When encapsulated in HA hydrogels and induced to undergo chondrogenesis, hMSCs from different donors showed a differential response to the 3D microenvironment. Some donors interacted

positively with their microenvironment to accumulate extracellular matrix while others self-aggregated and showed little matrix production, while still others appeared to degrade the HA and constructs disintegrated early in culture. Of the eight donors initially assayed, only two young/healthy and one old/aged donor remained viable and produced a matrix rich in PG and collagen with increasing mechanical properties. Conversely, donor hMSCs from the remaining five old/aged donors severely contracted or rapidly dissolved the hydrogel, making further analysis impossible. The above data showed that MSCs from different donors react to the same microenvironment in a different way. It should be noted, however, that despite the fact that some did not respond well to HA, two of the old/aged donors did form small pellets with some PG content when cultured in this alternative 3D format. The remaining three donors, which failed in HA culture, also failed to produce matrix in pellet culture. This differential matrix production in HA compared to pellet suggests a microenvironmental influence on differentiation and maturation processes. Some of these differences might be compounded by age-related changes in MSCs, specifically acting to accelerate compaction and decrease chondrogenic capacity (Erickson, van Veen et al. 2011). Similar findings have been noted in the bovine system, where adult bovine MSCs seeded in HA produced the least matrix and lowest properties while contraction the most compared to fetal and juvenile MSCs (Erickson, van Veen et al. 2011). Our data may also suggest that the disease status (and perhaps endogenous inflammatory state) of the OA donors might impact outcomes by accelerating hydrogel dissolution via the secretion of degradative enzymes (e.g., hyaluronidase or MMPs), compromising initial construct integrity.

For clinical application, an engineered cartilage construct should possess mechanical and biochemical properties comparable to native tissue and achieve a stable 3D configuration. Our data suggest that not every donor will yield such an outcome. We

found that for some donors, HA hydrogels with low macromer density yielded constructs with greater mechanical properties, but these had severely contracted, precluding clinical application. To address this issue of contraction, we first sought to reduce cytoskeletal tension by treating MSC-laden constructs with the Rho/ROCK pathway inhibitor Y27632 during chondrogenic induction. The Rho/ROCK pathway is a major regulator of cytoskeletal tension, and plays important roles in stem cell activities involved in cell-cell interactions and chondrogenesis (Woods, Wang et al. 2005, Amano, Nakayama et al. 2010). For instance, Woods et al showed that Rho/ROCK pathway activation inhibited chondrogenesis of limb bud chondrocytes. Treatment of hMSC-seeded HA constructs with Y27632 clearly blocked intercellular self-aggregation, but resulted in little to no change in the dynamic modulus or GAG content of constructs.

Based on the finding that inhibition of contractility did not improve outcomes, we next explored whether modulation of cell and/or HA macromer concentration could influence initial construct dimensional stability and functional matrix accumulation over time. MSCs-laden hydrogel constructs seeded at 20M cells/mL in 1% HA showed marked volumetric changes and cell and matrix compaction, whereas those at 1.5 and 2% HA maintained an even cell distribution and relatively uniform matrix distribution. This suggests that macromer density can mediate against the contraction we observed at low gel densities. However, we also observed that the dynamic modulus (|G*|) of 1% HA constructs was 3-4 times greater than either the 1.5 and 2% HA constructs, suggesting that concentrating deposited ECM improves functional outcomes.

To realize such an outcome at higher wet percent gels, which better maintain their initial morphology, we next assayed the impact of a higher hMSC seeding density. Gels seeded at 60M cells/mL yielded high mechanical properties (E_Y: 50-87 kPa and |G*|:

0.59-1.25MPa) and GAG content (1.6-2.2%WW) after 8 weeks in culture. 1% HA constructs again had the highest mechanics (87kPa; 2.2%WW GAG), but also showed the highest amount of contraction (-24%). Conversely, 2% HA constructs produced the least matrix (1.6%WW GAG) and lowest mechanical properties (50kPa), but maintained their original dimensions. This demonstrates that by simultaneously increasing cell and macromer density, one can promote matrix production, functional maturation, and dimensional stability. This is consistent with Erickson et al., who showed similar results using bovine MSCs (Erickson, Huang et al. 2009). Based on these results there appears to be a trade-off between the benefit in functional properties and the risk in structural instability. To take advantage of all benefits, one possible approach would be to cast constructs larger than the defect to be filled, pre-culture these constructs with at high cell and low HA density, and allow the constructs to contract during maturation. These matured constructs with improved functional properties could then be trimmed to match the size of the treated defect.

This study demonstrated donor-to-donor variations of human MSCs in their chondrogenic differentiation in 3D culture. Our findings reveal marked differences across donors that will need to be addressed for any autologous therapy to be successful. Indeed, understanding and characterizing this donor-dependent hMSCs response will enable prediction of donor-specific response, via screening assays, and direct the optimization of their chondrogenic potential for autologous clinical applications. Future studies will investigate additional donors, especially from old/aged populations with varying degeneration status, to establish an effective approach to patient-specific articular cartilage repair using autologous MSCs.

CHAPTER 4: Transient Exposure to TGF-β3 Improves the Functional Chondrogenesis of MSC-laden Hyaluronic Acid Hydrogels

4.1 Introduction

Articular cartilage is the dense white connective tissue lining the ends of long bones in diarthrodial joints and functions to transfer and distribute loads generated with locomotion (Carney and Muir 1988, Ateshian and Hung 2005). Load transfer occurs through the dense extracellular matrix (ECM), which is primarily composed of type II collagen and proteoglcycans (PGs). Matrix mechanical properties are quite high, with an equilibrium modulus on the order of 0.5-1 MPa and a dynamic modulus ranging from 16-40 MPa (Park, Hung et al. 2004, Erickson, van Veen et al. 2011). While the tissue can function remarkably well in a demanding environment over a lifetime of use, focal defects and other trauma can initiate progressive degeneration (Martel-Pelletier 1998, Buckwalter, Martin et al. 2000). As cartilage is avascular, repair processes are limited (Huber, Trattnig et al. 2000), and regenerative strategies, short of total joint replacement, have not yet produced durable and functional repair.

To address this issue, cartilage tissue engineering approaches have been developed with the goal of forming biologic replacement materials with functional mechanical properties (Ateshian and Hung 2005). In addition to cell-based therapies (Knutsen, Engebretsen et al. 2004, Hettrich, Crawford et al. 2008), three dimensional constructs consisting of various hydrogels coupled with chondrocytes have been utilized to generate cell-laden constructs (Buschmann, Gluzband et al. 1995, Mauck, Soltz et al. 2000, Roy, Boskey et al. 2008, Kisiday, Lee et al. 2009). Within this 3D context, a number of culture variables have been explored, including modulation of cell density,

growth factor supplementation, oxygen tension and mechanical stimulation (Blunk, Sieminski et al. 2002, Mauck, Wang et al. 2003, Hung, Mauck et al. 2004, Lima, Bian et al. 2007, Meyer, Buckley et al. 2010), to further the biochemical and mechanical maturation of engineered constructs. Indeed, recent reports employing chondrocytes in agarose hydrogels demonstrate functional equivalence between engineered constructs and native tissue, with equilibrium compressive properties approaching 1MPa (Lima, Bian et al. 2007, Byers, Mauck et al. 2008).

While chondrocytes have been instrumental as a cell source for such approaches, their clinical use may be limited due to a scarcity of healthy cells. Mesenchymal stem cells (MSCs) derived from bone marrow have emerged as an attractive alternative cell type (Pittenger and Martin 2004) as they are multipotent and easy to expand, and so are available in a nearly unlimited supply, and in an autologous fashion. Numerous studies have shown that MSCs within hydrogel constructs cultured in a chemically defined media (CM) undergo chondrogenesis when supplemented transforming growth factor (TGF) family members (Huang, Farrell et al. 2010). We are particularly interested in the translational capacity of hyaluronic acid (HA) hydrogels. HA is a natural constituent of the cartilage extracellular matrix and provides a biologically relevant interface for encapsulated MSCs (Chung and Burdick 2009). Moreover, gel properties are easily tunable (Burdick, Chung et al. 2005, Erickson, Huang et al. 2009), and the gel can be modified to degrade in a controlled fashion (Sahoo, Chung et al. 2008) and to deliver TGF-beta through co-encapsulated alginate microspheres (Bian, Zhai et al. 2011). Indeed, using methacrylated (and so photo-crosslinkable) HA as a starting point, we have optimized gel formation and functional matrix production by MSCs with variations in gel density (1%, (Erickson, Huang et al. 2009)) and MSC (~60 million cells/mL,

(Erickson, Kestle et al. 2011)) concentration, consistently producing cartilage like constructs with compressive properties in the range of native tissue levels (200-300kPa).

In addition to the hydrogel environment, the timing and dose of pro-chondrogenic factors can modulate the growth of MSC-based constructs. In early work with human MSCs in alginate, it was reported that a single high dose of TGF (50ng/mL) resulted in comparable molecular level induction of cartilage genes at day 21 compared to continuous exposure to TGF at much lower levels (10 ng/mL) (Caterson, Nesti et al. 2001). More recently, we showed that transient exposure of MSCs in agarose to 10ng/mL TGF-β3 (for three weeks) induced a stable chondrogenic phenotype, with functional properties at six weeks greater than continual exposure at this same level (Huang, Stein et al. 2009). This suggests that timing, dose, and duration of exposure to chondrogenic factors can influence the long-term growth of engineered constructs formed with MSCs.

Transient exposure presents an interesting paradigm with clinical relevance; *in vivo* defect filling will require robust maturation of the engineered tissue driven by TGF-β3 delivered from the material itself in a controlled and sustained fashion. As most delivery systems offer the capacity for only a short term, high dose delivery, the purpose of this study was to determine the minimal TGF-β3 dosage and duration of exposure required to promote the most robust chondrogenesis and functional maturation of MSCs in this HA hydrogel system. To this end, MSCs were seeded in 1% HA hydrogels at a high cell density (60 million cells/mL) and cultured under different levels (10, 50, and 100 ng/mL) of TGF-β3 for varying durations (3, 7, and 21 days) in a chemically defined medium. After removal of the growth factor at these defined time points, construct mechanics,

biochemical content, and histological features were evaluated through 9 weeks of *in vitro* culture.

4.2 Materials and Methods

4.2.1 MSC Isolation and Expansion

MSCs were isolated from femoral and tibial bone marrow from juvenile calves (3 months old, Research 87, Bolyston, MA) and maintained in basal medium consisting of high-glucose Dulbecco's modified Eagle's medium supplemented with 10% fetal bovine serum (Gibco-Invitrogen, Grand Island, NY) and 1% penicillin/streptomycin/fungizone (PSF) (Gibco-Invitrogen, Grand Island, NY). MSCs were expanded in culture through passage three prior to encapsulation.

4.2.2 Construct Fabrication and Long-term 3D Culture

MSCs were suspended in a chemically defined medium (CM) consisting of high glucose DMEM supplemented with 1% PSF, 0.1 µM dexamethasone, 50mg/mL ascorbate 2-phosphate, 40mg/mL L-proline, 100mg/mL sodium pyruvate, 6.25µg/mL insulin, 6.25µg/mL transferrin, 6.25µg/mL selenious acid, 1.25mg/mL bovine serum albumin (BSA), and 5.35µg/mL linoleic acid. The cell solution was centrifuged, and the supernatant was removed. The cells were resuspended in 1% w/v methacrylated hyaluronic acid (HA) solution. Specifics on the synthesis of this photocrosslinkable HA macromer have previously been reported in detail (Burdick, Chung et al. 2005, Erickson, Huang et al. 2009). Briefly, 1 wt% sodium hyaluronate (Lifecore Biomedical, Chaska, MN) was reacted with methacrylic anhydride (Sigma, St. Louis, MO) at pH 8.0, followed by dialysis to remove unreacted byproducts and lyophilization and storage at -20^{o}C. To form cell-seeded constructs, the methacrylated HA was dissolved at 1% w/vol in PBS with 0.05% w/vol photoinitiator (Irgacure I2959, Ciba, Basel, Switzerland). MSCs were

resuspended at a concentration of 60 million cells/mL, cast into a mold, and exposed to UV for 10 min at room temperature. Cylindrical cores (Ø4mm × 2.25mm) were removed from the resulting HA sheet with a sterile biopsy punch.

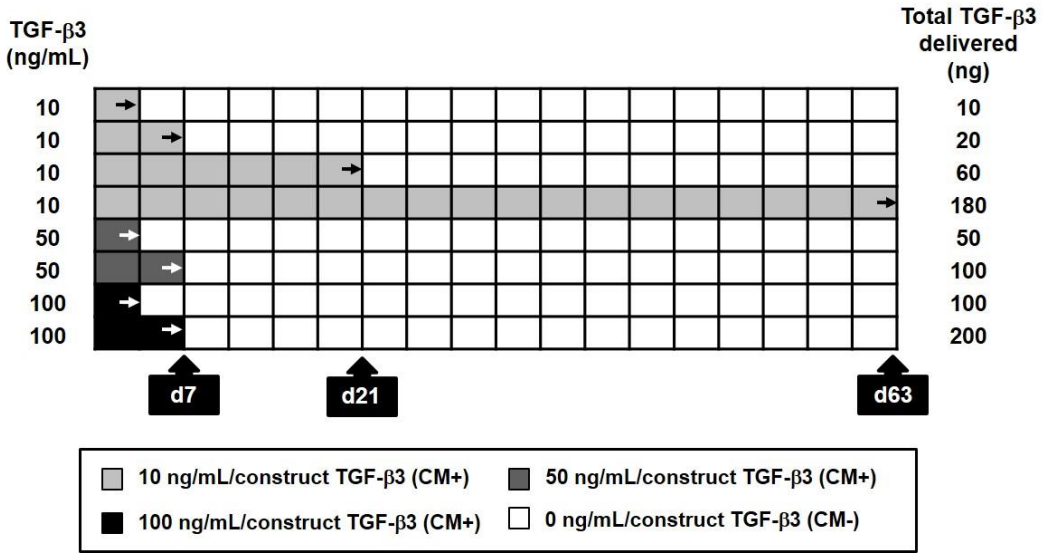

Figure 4-1: Schematic of transient exposure to TGF-β3 at varying doses and durations

Constructs were cultured in chemically defined media (CM) (1mL per construct) for the duration of the study. TGF-β3 (R&D Systems, Minneapolis, MN) was introduced at several different concentrations and durations (**Figure 4-1**). TGF-β3 dose was varied from a standard concentration of 10ng/mL to a high dose of 50ng/mL, or to a very high dose of 100ng/mL. For these higher concentrations, exposure times were limited to 3 or 7 days, with media changed one time over the first week. For the lower dose, exposure was for 3, 7, 21, or 63 days. A total of 8 groups were thus evaluated (10-d3, 10-d7, 10-d21, 10-d63, 50-d3, 50-d7, 100-d3 and 100-7d), where the first number indicates dose, and the second number indicates duration of exposure to TGF-β3. Media was changed twice weekly for the duration of study.

4.2.3 Mechanical Analysis

A custom-built mechanical testing device was utilized to examine compressive properties of engineered constructs (Mauck, Soltz et al. 2000). Unconfined compression was applied via a non-porous indenter with constructs hydrated in PBS during testing. Constructs underwent creep loading to 0.02 N for 5 min to ensure even contact between the construct and platens. After equilibration of this creep load, samples were compressed at 0.05%/sec to 10% strain, calculated from the post creep thickness of the construct. Constructs were then allowed to relax for 1000 sec, and the equilibrium stress noted. Subsequently, a 1% sinusoidal deformation was applied at 1.0 Hz. Equilibrium and dynamic moduli were calculated from stress-strain response and the sample geometry.

4.2.4 Biochemical Analysis

After mechanical testing, wet weight of constructs was measured followed by digestion in papain (1 mL/construct, 0.56U/mL in 0.1M sodium acetate, 10M cysteine hydrochloric acid, 0.05M ethylenediaminetetraacetic acid, pH 6.0) at 60°C for 16 hours. Glycosaminoglycan (GAG) content was determined using the 1,9-dimethylmethlene blue (DMMB) dye-binding assay and collagen content using the orthohydroxyproline (OHP) assay, with a 1:7.14 OHP:collagen ratio, as previously described (Stegemann and Stalder 1967)**.** DNA content was assessed via the PicoGreen double strand DNA assay (Molecular Probes, Eugene, OR).

4.2.5 Histological Analysis and Cell Viability

Constructs were fixed in 4% paraformaldehyde and embedded in paraffin. Sections (8µm thick) were deparaffinized in a graded series of ethanol and stained with Alcian Blue (pH 1.0) and Picrosirius Red (0,1% w/v in saturated picric acid) for proteoglycans

(PG) and collagens, respectively. Viability was assessed on fresh constructs on days 21, 42 and 63 using the LIVE/DEAD staining kit (Molecular Probes, Eugene, OR).

4.2.6 Fourier Transform Infrared Imaging Spectroscopy (FT-IRIS)

FT-IRIS analysis of construct matrix composition and distribution was carried out with a Spectrum Spotlight 300 imaging system (Perkin-Elmer, Waltham, MA) as in (Kim, Bi et al. 2005, Kim, Foo et al. 2010). The system consists of an FTIR spectrometer in conjunction with a light microscope and linear array detector under N_2 purge (Boskey and Pleshko Camacho 2007). Molecular characteristics are determined in a rectangular region of interest. IR absorption for cartilage ranges from 800 – 2000 cm^{-1} (i.e., within the mid infrared (MIR) region; 400 – 4000 cm^{-1}). Histological sections (8μm) from the day 63 groups were mounted onto Low-e Microscope Slides (1 × 3 inch, Kevely Technologies, Chesterland, OH) and dehydrated completely to avoid spectral interference from water molecules prior to data acquisition (6.25μm^2 pixel resolution and 4cm^{-1} spectral resolution). During IR penetration, molecules within the tissue absorb IR and vibrate at a specific frequency (wave number; cm^{-1}) based on the characteristics of the molecular bond (composition) and the number of molecules (intensity) at that location. Collagen (C=O stretching) signal is apparent in the amide I (1655cm^{-1}), amide II (1550cm^{-1}) and amide III (1250cm^{-1}) regions. Proteoglycan (C-O-C, C-OH, C-C ring vibration) signal is apparent in the amide I (1640cm^{-1}), amide II (1545cm^{-1}), sulfate (1245cm^{-1}) and sugar (1125-920 and 850cm^{-1}) regions. In native tissue, the Amide I band primarily represents type II collagen while the sugar groups primarily represent proteoglycans. Although proteoglycans contribute to the amide I and II bands, their contributions are minute compared to that of collagen in native tissue (Camacho, West et al. 2001). However, in this study, because proteoglycan content was significantly higher than collagen content (see results), proteoglycan absorbance contributed markedly to the amide I peak.

Therefore, the proteoglycan contributions to Amide I signal were spatially subtracted to allow for quantification of collagen alone. Data processing was carried out using the ISys software (version 5.0, Malvern Instruments Ltd., Worcestershire, UK).

4.2.7 Statistical analysis

Statistical analysis was performed using the SYSTAT software (v10.2, SYSTAT software Inc., San Jose, CA). Significance was determined by two-way ANOVA with Tukey's post hoc test ($p<0.05$).

4.3 Results

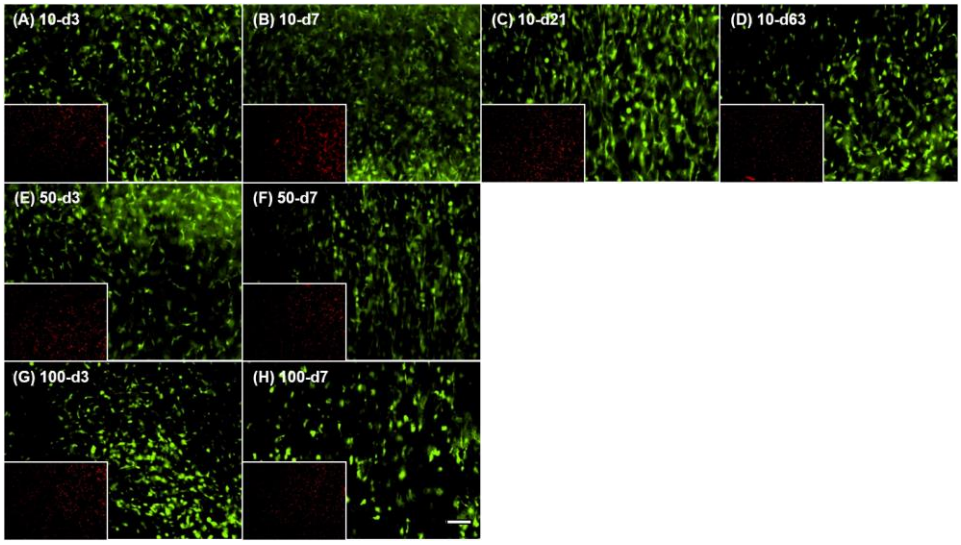

Figure 4-2: Viability within MSCs-seeded HA hydrogels with different exposure conditions. Live (Green; 10X) and dead (Red; Inset: 2X) staining show comparable cell viability in HA hydrogels with each treatment condition. (A-D) 10 ng/mL TGF- β3 for 3, 7, 21 or 63 days, (E and F) 50 ng/mL for 3 or 7 days, and (G and H) 100 ng/mL for 3 or 7 days. Scale bar indicates 100 µm.

4.3.1 Mechanical properties of MSC-seeded HA constructs

The effect of varying dose and duration of TGF-β3 exposure on the chondrogenesis and functional maturation of MSC-laden HA hydrogels was assessed under free swelling conditions. MSCs were viable and biosynthetically active in HA hydrogels under each condition assessed (**Figure 4-2**). Construct diameters were similar between groups and did not change during the culture period **(Figure 4-3A)**.

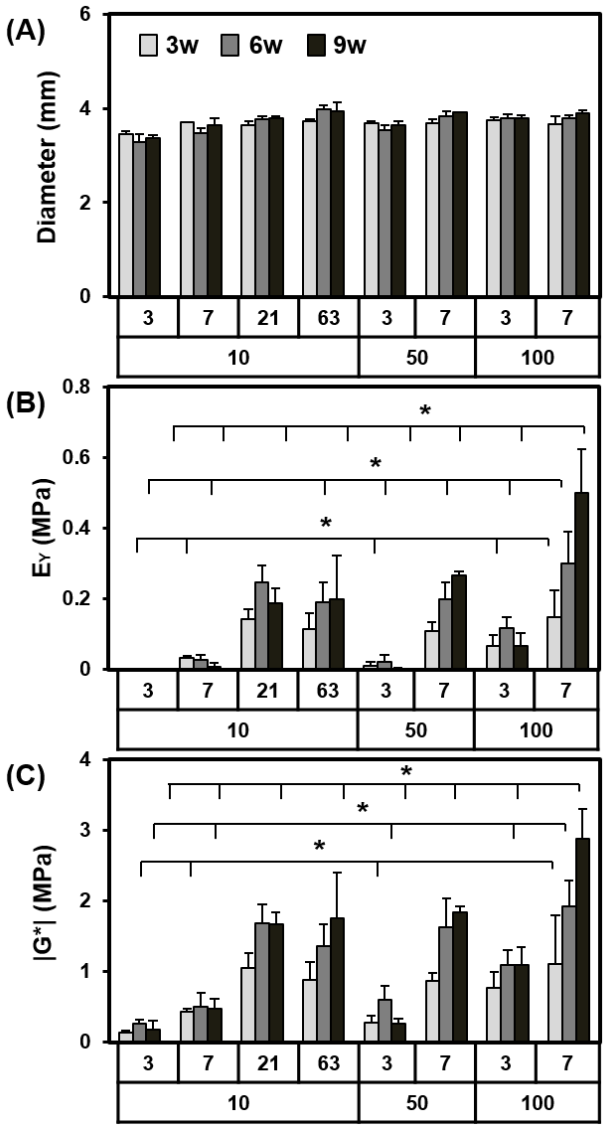

Figure 4-3: Transient exposure to high levels of TGF-β3 enhances the mechanical properties of MSC-seeded HA constructs. Transient exposure time (day) and concentration of TGF- β3 (ng/mL) over the entire culture period (9 weeks, 9w) shown on x-

axis. (A) Construct diameter, (B) Equilibrium modulus (E_Y; MPa), and (C) Dynamic modulus (|G*|; MPa) as a function of treatment (n=5/group; *p<0.05 for groups at 3w, 6w, or 9w compared to the 100-d7 group at same the time point).

While constructs were geometrically stable, transient exposure of TGF-β3 altered construct mechanical properties, depending on the dose and duration of exposure. Compared to conditions where TGF-β3 was provided at each media change at 10 ng/mL, constructs exposed to either 10 ng/mL for only the first three weeks, or constructs exposed to higher concentrations (50 and 100 ng/mL) for even shorter periods of time (one week), reached equivalent or higher mechanical properties. For example, the equilibrium (and dynamic) modulus for constructs exposed to TGF-β3 at a high dose (100-d7; two feedings at 100ng/construct) reached ~500 kPa (and ~2.9 MPa) at nine weeks, the highest level achieved in this study (**Figure 4-3**).

Control constructs with continuous delivery of TGF-β3 at the standard concentration (10ng/mL) for the entire culture duration (10-d63) reached only ~200 kPa (and 1.7 MPa) over this same time course. This differential growth occurred despite similar levels of TGF delivery over the culture duration (200ng/construct for 100-d7, 180ng/construct for 10-d63). Groups intermediate to these two extremes (50-d7 and 100-d3) yielded constructs with lower mechanical properties. Equilibrium (and dynamic) modulus for these groups (50-d7 and 100-d3) was 267 kPa (and 1.8 MPa) and 67 kPa (and 1.1 MPa) by 9 weeks, respectively. Groups exposed to 10ng/mL for only 3 or 7 days (10-d3, 10-d7) did not show marked increase in mechanical properties. However, at this low dose, 21 days of exposure (10-d21) was sufficient to match properties in constructs with continual exposure (10-d63).

4.3.2 Biochemical content of MSC-seeded HA constructs

Consistent with the mechanical properties, biochemical content of constructs depended on dose and duration of exposure to TGF (**Figure 4-4**). In control conditions (10-d63, continuous exposure, 10 ng/mL), GAG and collagen content increased with time. By 9 weeks, GAG content in these constructs reached ~3.7%.

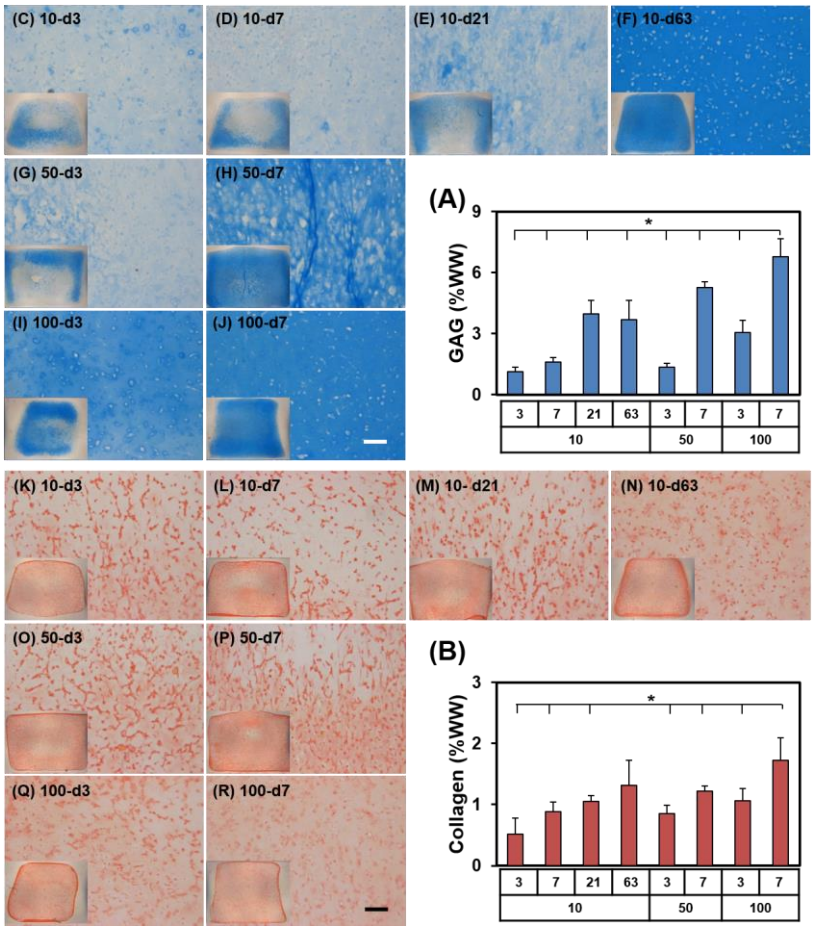

Figure 4-4: Transient exposure to high levels of TGF-β3 enhances biochemical content and matrix distribution of MSC-seeded HA constructs. (A) GAG (%WW), (B) Collagen (%WW), (C-J) Alcian blue, (K-R) Picrosirius red (n=5/group for biochemical analysis; A and B; *p<0.05 for 9w group compared to 100-d7 group at the same time point). Histological images were captured at 9w at a magnification of 10X (Inset: 2X). Scale bar indicates 100μm.

Interestingly, comparable GAG content was achieved in constructs exposed to this concentration of TGF for only three weeks (10-d21, ~4.0%), while shorter durations at this level resulted in less GAG accumulation (10-d3, 1.1%; 10-d7, 1.6%). With higher doses of TGF exposure, even with short durations of exposure, GAG content of constructs was markedly higher. Indeed, the short-term, high dose TGF-β3 group (100-d7) reached GAG contents higher than all other groups. In these constructs, GAG content was ~6.8% (per wet weight) by 9 weeks, matching or exceeding native tissue levels (Erickson, van Veen et al. 2011). Intermediate groups (i.e., 50-d7 and 100-d3) produced GAG contents comparable to the continuous low concentration group (10-d63). DNA content for most groups decreased slightly with culture duration (not shown). Collagen content followed this same general trend, though the difference between groups was less marked. Transient exposure to a high dose of TGF-β3 (i.e., 50-d7, 10-d3 and 100-d7) resulted in comparable levels of collagen content to the control group (10-d63) by week 9 (**Figure 4-4**). The highest collagen content achieved was ~1.7% in the 100-d7 group at 9 weeks.

4.3.3 Histological analysis of MSC-seeded HA constructs

Histological evaluation generally supported bulk biochemical measures (**Figure 4-4**). Low doses of TGF-β3 applied for short periods of time (10-d3, 10-d7) resulted in very little proteoglycan deposition (as evidenced by lack of Alcian Blue staining), while longer periods of exposure (10-d21 and 10-d63) resulted in robust staining (**Figure 4-4J-Q**) throughout the construct. Interestingly, with a short duration of exposure, PG staining was only apparent at the periphery of the construct. When TGF-β3 was added at higher concentrations for one week (50-d7 and 100-d7), staining patterns were similar to that of continuous exposure in the low dose (10-d63) group. At high doses, with only one exposure (50-d3 and 100-d3), staining was intense only at the construct periphery.

Picrosirius red staining of collagen likewise matched bulk biochemical assessment, where collagen staining intensity was not markedly different between groups (**Figure 4-4A-H**).

4.3.4 FT-IRIS analysis of MSC-seeded HA constructs

Because collagen staining may have been compromised by the large amount of proteoglycan in constructs, a more sensitive method of analysis was employed. FT-IRIS allows for the deconvolution of collagen and proteoglycan signal based on specific signatures of these molecules in the IR spectrum. This analysis showed that collagen matrix production was initiated near the outer edge of constructs. With longer durations of exposure, central regions of the construct contained progressively more collagen (**Figure 4-5**). Continuous exposure constructs (10-d63) showed abundant collagen distributed throughout the construct. Groups exposed to TGF-β3 at higher concentrations (50-d7, 100-d3 and 100-d7) showed comparable collagen distributions, while those at lower concentrations and for shorter times of exposure (10-d3 and 10-d7) produced less collagen. Summation of the FT-IRIS signal across the construct expanse matched patterns of bulk collagen content determined through biochemical analysis.

4.4 Discussion

In this study, we evaluated the impact of TGF-β3 dose and duration of exposure on the functional maturation of MSC-laden HA hydrogels. Our results show that, even with a very short exposure time, a sufficiently high TGF-β3 dose can produce functional cartilage-like materials over a 9 week period. Indeed, these constructs achieved mechanical and biochemical properties greater than those achieved with continuous exposure to TGF-β3 at a lower dose. This 'release' response is consistent with that observed previously in both chondrocytes (Lima, Bian et al. 2007, Byers, Mauck et al.

2008) and MSCs (Huang, Stein et al. 2009), though in this study it was apparent after an even shorter exposure period (1 week vs. 3 weeks), though a higher dose was required.

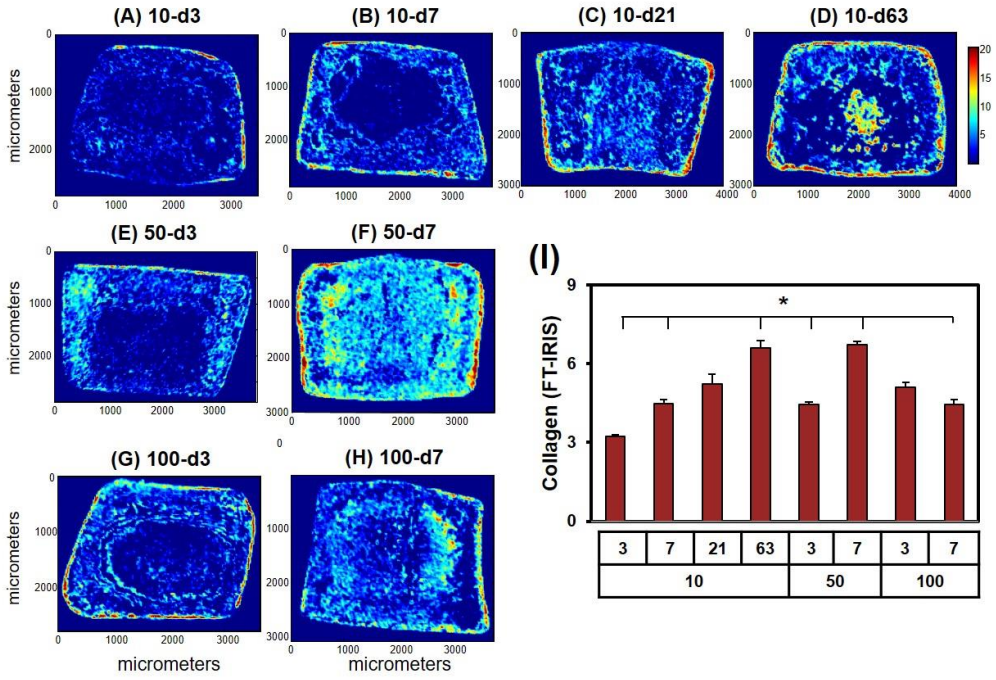

Figure 4-5: FT-IRIS assessment of collagen distribution with transient exposure to TGF-β3. Cross-sectional images showing distribution of collagen within MSC-seeded HA constructs on day 63 (A-H). Collagen intensity was quantified and averaged from 3 serial sections for each group (I). Pixel (25 x 25μm) intensity defined by color bar. *p<0.05 for 9w groups compared to 100-d7 group at the same time point.

Interestingly, chondrogenic differentiation (as evidenced by continued accrual of proteoglycans) progressed over the entire 9 weeks, despite only 1 week of exposure to chondrogenic factors. In the most auspicious conditions identified (100-d7, 100 ng/mL TGF-β3 exposed for 7 days), constructs showed a dramatic increase in mechanical properties and biochemical content, reaching an equilibrium modulus of ~500 kPa and ~6.8% GAG (per wet weight) at 9 weeks. These properties were higher than those in the

continual exposure group (~200 kPa and 3.7% GAG), and nearly match those of native bovine cartilage (Erickson, van Veen et al. 2011). Indeed, these are the highest yet reported in this HA system when seeding with MSCs. This finding confirms that a robust and persistent chondrogenic state can be induced with very short exposure durations to TGF, and has bearing on the clinical translation of this system.

The finding of time and dose varying effects of TGF on progenitor cell behavior should not be surprising, given its developmental relevance. In development, multiple morphogen gradients are established in a temporally and spatially varying manner to direct cellular behavior and tissue differentiation (Wolpert 1969, Gurdon and Bourillot 2001, Ibanes and Izpisua Belmonte 2008, Berezhkovskii, Sample et al. 2011). These soluble factor gradients are established when a local accumulation of differentiated cells initiates production of a given factor. From this origin to cells at a distant location, the morphogen concentration will decrease, depending on simple diffusion and/or consumption/binding of the factor (Gurdon and Bourillot 2001). In some instances, there exist critical concentration thresholds for phenotypic conversion (Raj, Rifkin et al. 2010), allowing for distinct boundaries to form along continuous gradients. The impact of a morphogen gradient can be transient, where either it establishes a pattern of differentiation after which the source cells cease production, or the cells initially regulated by the gradient move away from the point source through other growth mechanisms. An example of such as system is the cartilaginous growth plate in long bones, where multiple gradients of competing factors regulate progenitor cell chondrogenesis and eventual hypertrophy (Farnum, Turgai et al. 1990).

Some of these developmental features are present in our system as well, where the presentation of TGF in the soluble environment rapidly establishes a morphogen

gradient, with the highest (and defined) levels located at the construct periphery. Overall concentration of TGF in the bathing solution most likely falls between feedings as cellular utilization occurs, eventually depleting the source. This has been shown for other media components (such as glucose) in engineered chondrocyte-based cartilage constructs (Heywood, Bader et al. 2006), and may be pronounced in this study where a very high cell concentration was used. While the 'source' concentration may vary with time between feedings, the local concentration is also expected to vary with distance from the boundary. Cells at the periphery are first exposed to the morphogen, and likely bind and sequester it, decreasing its availability to cells in the center. Indeed, under static conditions, MSCs within agarose hydrogels with continuous exposure to TGF at 10 ng/mL deposit matrix inhomogeneously through the depth, with the centers having significantly lower properties and matrix content than the edge regions (Farrell, Comeau et al. 2011). This is apparent in the current study as well, visualized both by variations in staining intensity across the construct expanse (Figure 4) and FT-IRIS imaging (Figure 5). With short exposure (three days), increasing the dosage of TGF resulted in increasing penetration of proteoglycan staining. Of note, distinct boundaries were apparent where the staining intensity decreased rapidly from high to low levels, perhaps indicating a threshold concentration necessary to achieve chondrogenesis. This drop off in staining could be attenuated when a second delivery with TGF was applied at the higher doses (e.g., 50-d7 and 100-d7). In these conditions, a contiguous proteoglycan rich matrix was observed through the depth of constructs. These findings suggest short term application of TGF at high doses can provide a sufficient supply of the morphogen to reach critical thresholds of exposure to initiate chondrogenesis even at the construct center. When a repeat dosing was provided (i.e., at both 3 and 7 days), the chondrocyte phenotype was 'locked in' in cells throughout the depth of the construct, allowing them to

produce cartilage like matrix through the entire 9 week culture period, long after the morphogen was removed from the culture environment.

The above findings provide both a cost-effective approach to long-term *in vitro* culture studies, and also point to the translational potential of this system. In the current study, essentially the same amount of TGF was delivered (200 ng for the 100-d7 group, 180 ng for the 10-d63 group), with the transient delivery groups reaching mechanical and biochemical properties exceeding the continuous delivery groups. Even at intermediate doses (i.e., 50-d7, where only 100 ng was delivered over the first week), properties matching the continuous exposure group were achieved. While the study terminated at this point, these findings suggest that for culture durations in excess of 9 weeks, it will be cost-effective to deliver a high dose of TGF in a bolus fashion during the first week. In terms of translation, our findings suggest that a finite (but large) dose of TGF-β3 need only be delivered for a short period of time to achieve functional chondrogenesis. While material delivery systems are improving, most still only offer the potential for a short term 'burst' followed by a much slower sustained release (Lee and Shin 2007, Ionescu, Lee et al. 2010, Meyerrose, Olson et al. 2010). We have recently shown that short term (7 day) delivery of chondrogenic factors can be achieved from co-encapsulated alginate microspheres, both *in vitro* and *in vivo* (Bian, Zhai et al. 2011). An important advantage of this system is that TGF can be released at a 'high' dose throughout the gel, and so lower overall delivery may be required (i.e., one will not have to create such steep concentration gradients to service cells at the center as the microspheres will establish a near uniform supply throughout the construct expanse). Data from the current study will help define optimal delivery doses for clinical translation of this technology to testing in a large animal cartilage defect model.

While the current findings are exciting, with native tissue properties achieved in our MSC-seeded HA hydrogel system with transient TGF exposure, additional work remains to fully optimize this system. In particular, it will be important to define the molecular basis of this phenotypic transition with transient exposure, and to monitor both chondrogenic and hypertrophic markers that could indicate a shift or loss in MSC phenotype after TGF withdrawal. The effect of transient TGF delivery must also be evaluated in the context of a changing chemical environment, as the construct will be expected mature within the synovial space. Such an environment may provide 'conflict' signals that alter the response to transient TGF exposure. Finally, these studies must be extended to cell types of clinical relevance, namely porcine and human cells from aged patients, so as to enable rapid transition to pre-clinical and clinical testing scenarios. Taken together, this data suggests that, when coupled with even simple delivery systems providing controlled release for as little as one week, HA-based MSC-seeded constructs may provide effective and functional cartilage repair. Such progress would improve the health and mobility of millions of patients worldwide suffering from the ravages of progressive cartilage degeneration and loss of function.

CHAPTER 5: Role of Dexamethasone in the Long-term Functional Maturation of MSC-laden Hyaluronic Acid (HA) Hydrogels for Cartilage Tissue Engineering

5.1 Introduction

Strategies to engineer cartilaginous tissues using mesenchymal stem cells (MSCs) are promising given that these multipotent cells can undergo chondrogenesis in a variety of 3D contexts and produce robust extracellular matrix equivalent to that produced by articular chondrocytes (Huang, Farrell et al. 2010). While numerous materials and methods have been utilized, we are particularly interested in hydrogels based on hyaluronic acid (HA), a natural constituent of the cartilage extracellular matrix that provides a biologically relevant interface for encapsulated cells (Burdick, Chung et al. 2005, Chung and Burdick 2009, Erickson, Huang et al. 2009). Additionally, HA gel properties are readily tunable based on variations in polymer backbone density (Burdick, Chung et al. 2005, Sahoo, Chung et al. 2008, Khetan, Chung et al. 2009), degradation mechanisms (Chung, Beecham et al. 2009), and can be modified with biologically relevant moieties (Bian, Guvendiren et al. 2013, Cosgrove, Mui et al. 2016). Using a simple methacrylated version of HA (termed MeHA), we recently optimized functional matrix production by MSCs via variations in gel macromer density (Erickson, Huang et al. 2009) and MSC seeding density (Erickson, Kestle et al. 2012). As a consequence of this optimization, MSC-laden HA hydrogel constructs consistently achieve near-native compressive mechanical properties and proteoglycan content (e.g., 700 kPa, 6% WW GAG) when cultured in a chemically defined media (CM) supplemented with pro-chondrogenic factors (i.e, TGF-β3) (CM+) (Mackay, Beck et al. 1998, Yoo, Barthel et al. 1998, Pittenger, Mackay et al. 1999).

Building from the initial description of the chemically defined media formulation that supports chondrogenesis (Johnstone, Hering et al. 1998, Pittenger, Mackay et al. 1999), a number of studies have explored which components are absolutely necessary, and over what time course. For instance, using both chondrocytes and MSCs, several studies have shown that transient inclusion of TGF-β3 in the source media results in greater properties than continual exposure to this factor (Lima, Bian et al. 2006, Byers, Mauck et al. 2008, Huang, Stein et al. 2009, Kim, Erickson et al. 2012). Indeed, very high doses of TGF-β3 (100 ng/mL), for short periods of time (7 days), were most effective in producing robust tissue constructs in this chemically defined setting (Kim, Erickson et al. 2012). Translating this finding, others have shown that alginate-coated TGF-β3 microspheres that were co-encapsulated with human MSCs in HA hydrogels resulted in robust chondrogenesis. This study showed that the release of a high dose of TGF-β3 over a relatively short period (less than two weeks) could promote comparable construct properties as those cultured in CM+ with a lower and continual dose of TGF-β3 (Bian, Zhai et al. 2011).

While these previous results are compelling, the transition to the in vivo environment may be more complicated, particularly when the in vivo environment is the synovial joint. Successful strategies for cartilage repair require not only an engineered construct with native-like functional properties, but also stability of these properties within the native load-bearing synovial environment. Synovial fluid is a dialysate of the blood that is comparable to serum and additionally contains hyaluronic acid, lubricin, proteinases, collagenases, and occasionally lymphocytes, monocytes, and neutrophils (Schmidt, Gastelum et al. 2007). In a recent study, we showed that when engineered MSC-based constructs were transferred to serum containing media (e.g., basal media: BM; 10% FBS) at the time of TGF withdrawal, construct properties rapidly decreased with marked

GAG loss (Kim, Erickson et al. 2012). This suggests that while chemically defined pro-chondrogenic media (CM) can foster maturation, conflict signals present in serum and synovial fluid may compromise long term functionality, and so may limit clinical translation.

One additional factor in CM, dexamethasone (DEX), is a synthetic glucocorticoid that is known to have pro-chondrogenic (Johnstone, Hering et al. 1998, Mackay, Beck et al. 1998) and anti-inflammatory effects (Florine, Miller et al. 2013). Dexamethasone suppresses inflammatory signaling (e.g., IL-8 secretion regulated by p38MAPK, AP-1 and NF-kB activity) (Rebeyrol, Saint-Criq et al. 2012). A recent study also showed that this glucocorticoid combined with HA enhances glucocorticoid receptor (GR) activity to inhibit activation of p38 MAPK signaling pathway (Lv 2016). Interestingly, several studies have shown that dexamethasone is an indispensable component in chondrogenic media (Johnstone, Hering et al. 1998, Mackay, Beck et al. 1998). One recent combinatorial screen coupled with RNA profiling showed that dexamethasone acted synergistically with TGF beta to promote MSC chondrogenesis (Jakobsen, Ostrup et al. 2014). In another recent study, however, it was shown that dexamethasone inhibits BMP-2 induced MSC chondrogenesis, and that removal of dexamethasone in defined media improved GAG deposition in synovial explants (Shintani and Hunziker 2011). In chick limb bud cultures, the dose of dexamethasone played a role, where lower doses improved chondrogenesis and higher doses promoted osteogenic conversion (Cheng, Chen et al. 2014). Similarly, others have reported a different impact of dexamethasone in young bovine and adult human MSCs in agarose and self-assembling peptide hydrogels (Florine, Miller et al. 2013). Further, in short term cultures of equine MSCs in agarose hydrogels, withdrawal of dexamethasone had an adverse impact on matrix accumulation when this factor was absent for longer than two days (Tangtrongsup and

Kisiday 2016). Collectively, these data suggest there are species, age, cell source, material context, and time dependent effects of dexamethasone on mesenchymal stem and progenitor cell chondrogenesis.

Given these findings, the goal of this study was to investigate the effect of dexamethasone in long term cultures of MSCs in HA hydrogels, both in chemically defined condition and under 'conflict' condition wherein the constructs were transferred to a more in vivo-like serum containing setting. In a first set of studies, we investigated the maturation of MSC-laden HA constructs with various combinations of media components that make up chemically defined media, with a particular focus on dexamethasone and serum substitutes (e.g., ITS+ Premix) and the presence of serum. In a subsequent study, based on the differential effect of dexamethasone on functional properties during the culture period, we examined the short and long term effect of dexamethasone presence and absence in chemically defined media conditions. Finally, given that previous studies indicated an anti-inflammatory role for dexamethasone, we assayed its role in attenuating matrix disruption when constructs were transferred to serum containing 'conflict' media for extended culture.

5.2 Materials and Methods

5.2.1 Preparation of cell/tissue culture media

Basal media (BM; serum containing), chemically defined media (CM), or media with addition/removal of CM components were prepared as outlined in **Table 5-1**. Basal media (BM) consisted of high glucose DMEM with 10% fetal bovine serum (Gibco-Invitrogen, Grand Island, NY) and 1% penicillin/streptomycin/fungizone (PSF) (Gibco-Invitrogen, Grand Island, NY).

Table 5-1: Combinatorial analysis of media components

Media component	Media combinations			
	CM+	DEX-	ITS/BSA/LA-	Serum+
DMEM (High glucose)	+	+	+	+
Penicillin/ Streptomycin/ Fungizone (PSF)	+	+	+	+
Ascorbate 2-Phosphate (AP) Proline (PRO) Sodium Pyruvate (SP)	+	+	+	+
Dexamethasone (DEX)	+	-	+	-
Insulin/Transferrin/Selenium Supplements (ITS) Bovine Serum Albumin (BSA) Lenoleic Acid (LA)	+	+	-	-
Fetal bovine serum (FBS)	-	-	-	+
TGF-ß3	+	+	+	+

This media was used to isolate and expand mesenchymal stem cells (MSCs). Chemically defined media (CM) consisted of high glucose DMEM with 1x penicillin/streptomycin/fungizone (PSF), 0.1 µM dexamethasone (DEX), 50 µg/mL ascorbate 2-phosphate (AP), 40 µg/mL L-proline (PRO), 100 µg/mL sodium pyruvate (SP), 6.25 µg/mL insulin, 6.25 µg/mL transferrin, 6.25 ng/mL selenious acid, 1.25 mg/mL bovine serum albumin (BSA), and 5.36 µg/mL linoleic acid (LA). This chemically defined media (CM) was further supplemented with 10ng/mL TGF-ß3 (R&D Systems, Minneapolis, MN) to produce a chondrogenic induction media (CM+). To identify the effect of the specific media components in CM+, additional formulations were developed including DEX- (removal of dexamethasone from CM+), ITS/BSA/LA- (removal of serum substitute from CM+) or Serum+ (addition of serum and removal of dexamethasone and ITS/BSA/LA). These various media formulations are detailed in **Table 5-1**.

5.2.2 Preparation of mesenchymal stem cells (MSCs)

MSCs were isolated from juvenile bovine knees (Research 87, Bolyston, MA). To extract bone marrow, cubes of trabecular bone were segmented from the epi- and metaphyseal

region of the femur and tibia and were washed with medium containing 0.2% heparin (Sigma-Aldrich, St. Louis, MO) in BM. The diluted bone marrow was washed in BM, resuspended and plated onto tissue culture plastic. Adherent cells were noted within 5 days, and were expanded to passage 3 to obtain sufficient cell numbers for hydrogel encapsulation.

5.2.3 MeHA synthesis

Synthesis of methacrylated hyaluronic acid (MeHA) was as previously described by Burdick and co-workers (Burdick, Chung et al. 2005). Briefly, 1% w/v sodium hyaluronate (65 kDa MW; Lifecore, Chaska, MN) dissolved in deionized water was reacted with methacrylic anhydride (Sigma-Aldrich, St. Louis, MO) on ice at a pH of 8.0 with 5N NaOH (Sigma-Aldrich, St. Louis, MO) for 6 hours. This was followed by dialysis (No.132670, 6kDa MWCO, Spectrum Laboratories, Inc, Rancho Dominguez, CA) to remove unreacted byproducts for one week with repeated changes of distilled water. The methacrylated HA (MeHA) solution was lyophilized and stored at -20°C.

5.2.4 MSC encapsulation and construct culture

To form gels, lyophilized MeHA was dissolved at 1% w/v in PBS with 0.05% w/v photoinitiator (Irgacure I2959, Ciba-Geigy, Tarrytown, NY). MSCs were resuspended at a concentration of 60 million cells/mL and poured into a gel casting apparatus (Hoefer, Inc., Hollison, MA) (Mauck, Soltz et al. 2000) and exposed to UV using a 365nm Blak Ray UV lamp (UVL-56, San Gabriel, CA) for 10 minutes. The range of the UV was 320-400 nm with a transmission maximum of 70% at 365 nm. To explore the effect of media components in chondrogenic maturation of MSCs laden in HA hydrogels, cylindrical constructs (Ø4 mm × 2.25 mm) were cored using a biopsy punch from the resulting hydrogel slabs and cultured in CM+, DEX- (removal of dexamethasone in CM+),

ITS/BSA/LA- (removal of serum substitute in CM+) or Serum+ (addition/removal of serum, dexamethasone or ITS/BSA/LA) for 8 weeks **(Table 5-1)**. Each construct received 1 mL of media, which was changed thrice weekly for the duration of the study.

5.2.5 Effect of dexamethasone on construct maturation

In preliminary studies, we found that after 4 weeks, in the absence of dexamethasone (DEX-), functional properties of MSC-laden constructs were greater than those cultured in the presence of DEX (i.e, CM+). However, the constructs cultured in the continued absence of DEX showed a markedly decrease in properties after 8 weeks while those in CM+ increased to a greater extent. To explore the short and long-term effects of DEX inclusion or exclusion, MSC-laden HA constructs were cultured in CM+ (group C) for 4 weeks (0 – 4w), and then were maintained in CM+ (group C-C) or were transferred to DEX- (group C-D; removal of DEX from CM+) for the next 4 weeks (4 – 8w). Likewise, constructs cultured in DEX- (group D) for the first 4 weeks were converted to CM+ (group D-C) or were continuously cultured in DEX- conditions (group D-D) through 8 weeks **(Table 5-2)**. The level and timing of GAG, collagen, and nitrite released from constructs during the culture period were assessed using supernatants collected from each media change.

Table 5-2: Study design to test for the effect of dexamethasone (DEX) on MSC chondrogenesis

Group	Culture Period	
	0-4w	4-8w
C-C	**C**M+	CM+
C-D		DEX-
D-C	DEX-	CM+
D-D		DEX-

5.2.6 Inhibitory effect of dexamethasone in the conflicting signal environment

Early results showed that transfer of constructs from CM+ to serum containing media resulted in rapid loss of mechanical properties. To assess whether DEX could inhibit GAG loss in the context of serum containing media, constructs were first cultured for 4 weeks in CM+ or Serum with or without DEX and/or TGF (TGF-/DEX+, TGF+/DEX- or TGF+/DEX+) (see **Table 5-3**). Constructs cultured in Serum were harvested at 4 weeks, while constructs maintained in CM+ for the first 4 weeks were either continuously cultured in CM+ (CM+_CM+) or were converted to BM with or without DEX (TGF+/DEX- or TGF+/DEX+) for the next 4 weeks (**Table 5-3**).

Table 5-3: Study design to test for the effect of serum containing media and the effect of DEX.

0-4w	4-8w
CM+	CM+
	Serum(TGF+/DEX+)
	Serum(TGF+/DEX-)
Serum(TGF+/DEX+)	
Serum(TGF+/DEX-)	
Serum(TGF-/DEX+)	

5.2.7 Cell viability

Cell viability was assessed using the LIVE/DEAD staining kit (Molecular Probes, Invitrogen). Live (green) and dead (red) cells were determined by calcein AM and ethidium homodimer (EthD-1), respectively.

5.2.8 Analysis of mechanical properties

Unconfined compression testing was carried out to determine bulk compressive equilibrium (E_Y) and dynamic (|G*|) moduli of constructs as in Mauck et al (Mauck, Soltz et al. 2000, Mauck, Wang et al. 2003). Compressive modulus was determined via a stress-relaxation test including a step compression at 0.05%/sec to 10% strain after creep loading to 0.02 N for 5 min. The relaxation phase was for 1000 seconds. Subsequently, a 1% sinusoidal deformation was applied at 1.0 Hz to obtain the dynamic modulus. Prior to mechanical testing, the top and bottom surfaces of constructs were carefully planed using a freezing stage microtome to ensure an even contact surface.

5.2.9 Biochemical analysis

After mechanical testing, construct wet weight was measured followed by papain digestion (1mL/construct, 0.56U/mL in 0.1M sodium acetate, 10M cysteine hydrochloric acid, 0.05M ethylenediaminetetraacetic acid, pH 6.0) at 60°C for 16 hours. Sulfated glycosaminoglycan (s-GAG) content was assessed using 1,9-dimethylmethylene blue (DMMB) assays (Farndale, Buttle et al. 1986) . Orthohydroxyproline (OHP) content was measured via reaction with chloramine T and diaminobenzaldehyde. Collagen content was extrapolated from OHP using a 1:7.14 ratio of OHP (Neuman and Logan 1950). DNA content was determined using Picogreen dsDNA assay kit (Molecular Probes, Eugene, OR). In some studies, GAG, collagen, nitrite (Promega, Madison, WI), and

MMP (AnaSpec, Fremont, CA) released from constructs was assessed using supernatants collected each media change over the entire culture period.

5.2.10 Histological analysis

Constructs were fixed in 4% paraformaldehyde (PFA) for 24 hours and embedded in paraffin. Sections (8 μm thick) were deparaffinized in a graded series of ethanol and stained with Alcian Blue (pH 1.0) for proteoglycans (PG). Immunohistochemistry was carried out to visualize type I, II collagen and chondroitin sulfate (CS). Samples underwent antigen retrieval using hyaluranidase (HASE) from type IV bovine tests (Sigma-Aldrich, St. Louis, MO) for 1 hour and followed by Protease-K (DAKO, Glostrup, Denmark) for 4 minutes at room temperature. Endogenous peroxidase activity was quenched by pretreating sections with 3% hydrogen peroxide. To block nonspecific background staining, sections were incubated with 10% normal goat serum (Sigma-Aldrich, St. Louis, MO). Primary antibodies to type I collagen (MAB3391; Millipore, Billerica, MA), type II collagen (II-II6B3; Developmental Studies Hybridoma Bank, Iowa City, IA), and chondroitin sulfate (C8035, Sigma-Aldrich, St. Louis, MO) were used for immunolabeling. Antibody diluent solution (DAKO, Glostrup, Denmark) was used to dilute primary antibodies. After incubation with primary antibodies (overnight at 4ºC), sections were washed and treated with bioinylated goat anti-rabbit IgG secondary antibodies followed by streptavidin horseradish peroxidase (HRP). Sections were reacted with DAB chromogen reagent for 10-20 min (DAB150 IHC Select, Millipore, Billerica, MA). Native tissues (osteochondral plug and tendon) were used as negative or positive controls. Color images were captured at magnification of 2.5 or 25X using a light microscope (Leica DMLP, Leica Microsystems) or Eclipse 90i upright microscope (Nikon Corp).

5.2.11 Statistical Analysis

Statistical analysis was performed using the SYSTAT software (v10.2, SYSTAT software Inc., San Jose, CA). Significance was determined by two-way ANOVA with Tukey's post hoc test ($p<0.05$).

5.3 Results

5.3.1 Influence of media components on the functional maturation of MSC-laden HA hydrogel constructs

Four media formulations were initially screened (**Table 5-1**). Live/Dead staining showed that MSCs were viable only in CM+ and DEX- conditions, and that constructs in these conditions maintained their initial shape and produced robust matrix **(Fig 5-1A, Table 5-4)**. Conversely, cells in ITS/BSA/LA- and Serum+ conditions did not remain viable, and these constructs contracted significantly over the culture period. Equilibrium modulus (E_Y) and GAG content of constructs in CM+ and DEX- reached to 181 kPa (3.1 %WW) and 296 kPa (4.2 %WW) at 4 weeks, respectively, while the ITS/BSA/LA- and Serum+ constructs had no mechanical properties and lower GAG content (1.1 and 1.5%WW, respectively) **(Fig 5-1A and B)**. At 4 weeks, the mechanical properties and GAG content of constructs in the absence of dexamethasone (DEX-) were 63% ($p=0.838$) and 37% ($p=0.461$) greater than those cultured in the presence of dexamethasone (CM+), respectively. Interestingly, however, properties in CM+ and DEX- conditions reversed at 8 weeks, reaching 480 kPa/4.7 %WW and 211 kPa/3.3 %WW, respectively. Mechanical properties and GAG content of constructs in CM+ were 2.2 ($p=0.002$) and 1.42 ($p=0.032$) times greater than those cultured in DEX- at this 8 week time point. Collagen content increased with time for all media conditions, except for Serum+, regardless of the presence or absence of DEX **(Fig 5-1C)**. Similarly, Alcian blue staining showed marked PG production in constructs cultured in CM+ and DEX- at 4 weeks compared to

ITS/BSA/LA- and Serum+ conditions. However, PG accumulation of constructs in the absence of dexamethasone (DEX-) decreased in extracellular matrix (ECM) after 8 weeks. **(Fig 5-1D and 5-2)**

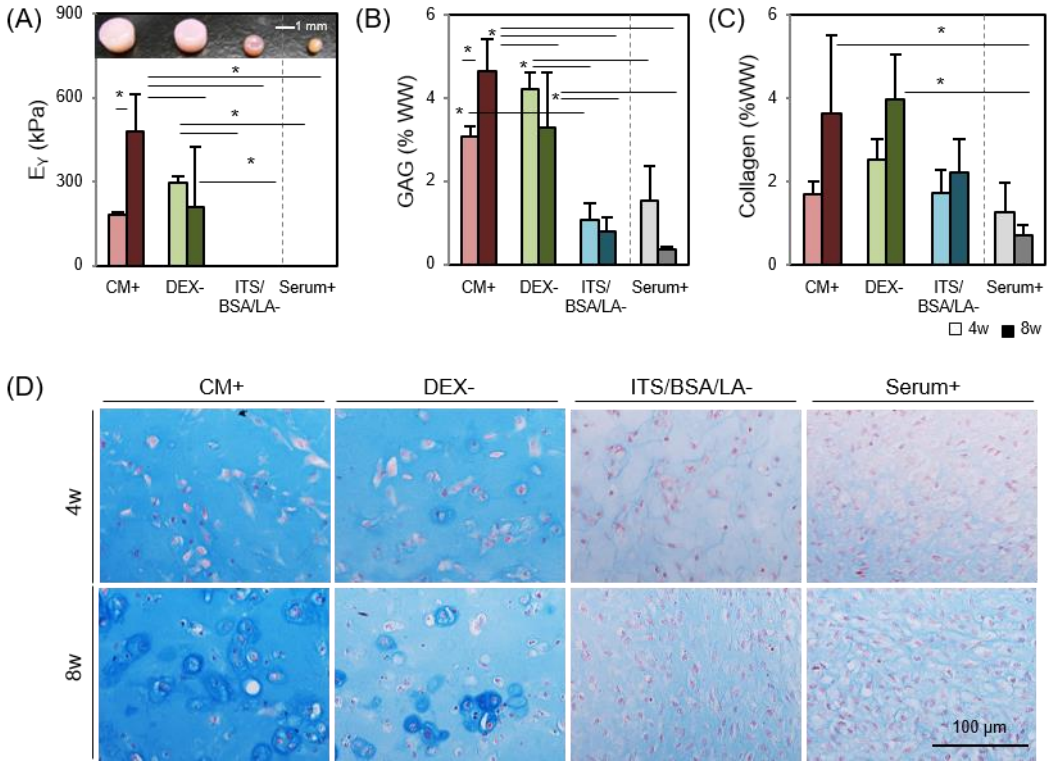

Figure 5-1: Influence of media components on functional properties of MSC-laden HA constructs. (A) Equilibrium modulus (E_Y; kPa) (Inset: gross images of constructs cultured in different media combinations at 8 weeks), (B) GAG (%WW), (C) Collagen (%WW) (D) Alcian blue staining at 4 weeks (top) and 8 weeks (bottom). (N = 4/group; Lighter bars = 4w, Darker bars = 8w; Scale bar = 100 µm; *p<0.05)

5.3.2 Short and long term effects of dexamethasone on construct maturation

Given that dexamethasone seemed dispensable in the first period of culture, we next carried out a study exploring the timing of exposure. Consistent with the previous study, the mechanical properties and GAG content of constructs in the DEX- condition (267

kPa and 3.5% WW) were greater than these in CM+ (198 kPa and 3.1% WW) at 4 weeks **(Fig 5-3A and B, Table 5-5)**.

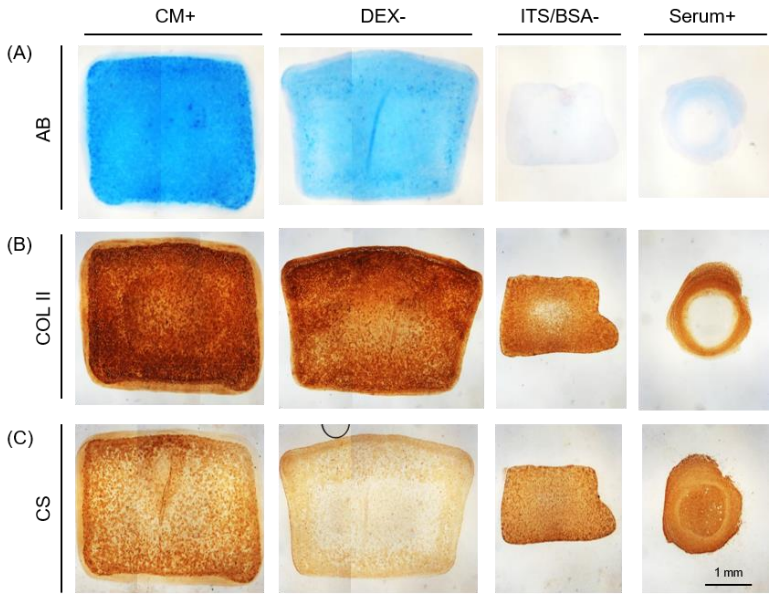

Figure 5-2: Histological analysis of MSC-laden constructs cultured in different media. (A) Alcian blue (B) Type II collagen, (C) Chondroitin sulfate at 8 weeks. (Scale bar = 1 mm)

Table 5-4: Mechanical and biochemical properties of MSC-laden constructs with various media formulations at 4 and 8 weeks (mean ± SD; N=4 /group)

	CM+		DEX-		ITS/BSA/LA-		Serum+	
	4w	8w	4w	8w	4w	8w	4w	8w
E_Y(kPa)	182 ± 12	480 ± 132	297 ± 23	211 ± 215	0	0	0	0
|G*| (kPa)	2181 ± 181	3835 ± 597	3009 ± 193	2527 ± 1330	151 ± 80	674 ± 241	0	0
Diameter (mm)	3.8 ± 0.1	4.1 ± 0.2	3.8 ± 0.2	3.9 ± 0.2	2.7 ± 0.2	2.4 ± 0.2	1	1
GAG (%WW)	3.1 ± 0.3	4.7 ± 0.8	4.2 ± 0.4	3.3 ± 1.4	1.1 ± 0.4	0.8 ± 0.3	1.5 ± 0.8	0.4 ± 0.1
GAG (µg/const)	756 ± 67	1543 ± 275	951 ± 156	804 ± 490	62 ± 11	47 ± 9	14 ± 2	15 ± 8
GAG/DNA (µg/µg)	538 ± 123	1251 ± 883	430 ± 125	417 ± 327	97 ± 44	47 ± 39	68 ± 13	43 ± 31
Collagen (%WW)	1.7 ± 0.3	3.6 ± 1.9	2.5 ± 0.5	4.0 ± 1.1	1.7 ± 0.5	2.2 ± 0.8	1.3 ± 0.7	0.7 ± 0.2
Collagen (µg/const)	414 ± 89	1243 ± 795	559 ± 69	926 ± 292	102 ± 11	135 ± 22	11 ± 4	27 ± 5
Col/DNA (µg/µg)	298 ± 94	763 ± 386	260 ± 102	439 ± 283	154 ± 57	217 ± 191	56 ± 21	72 ± 10

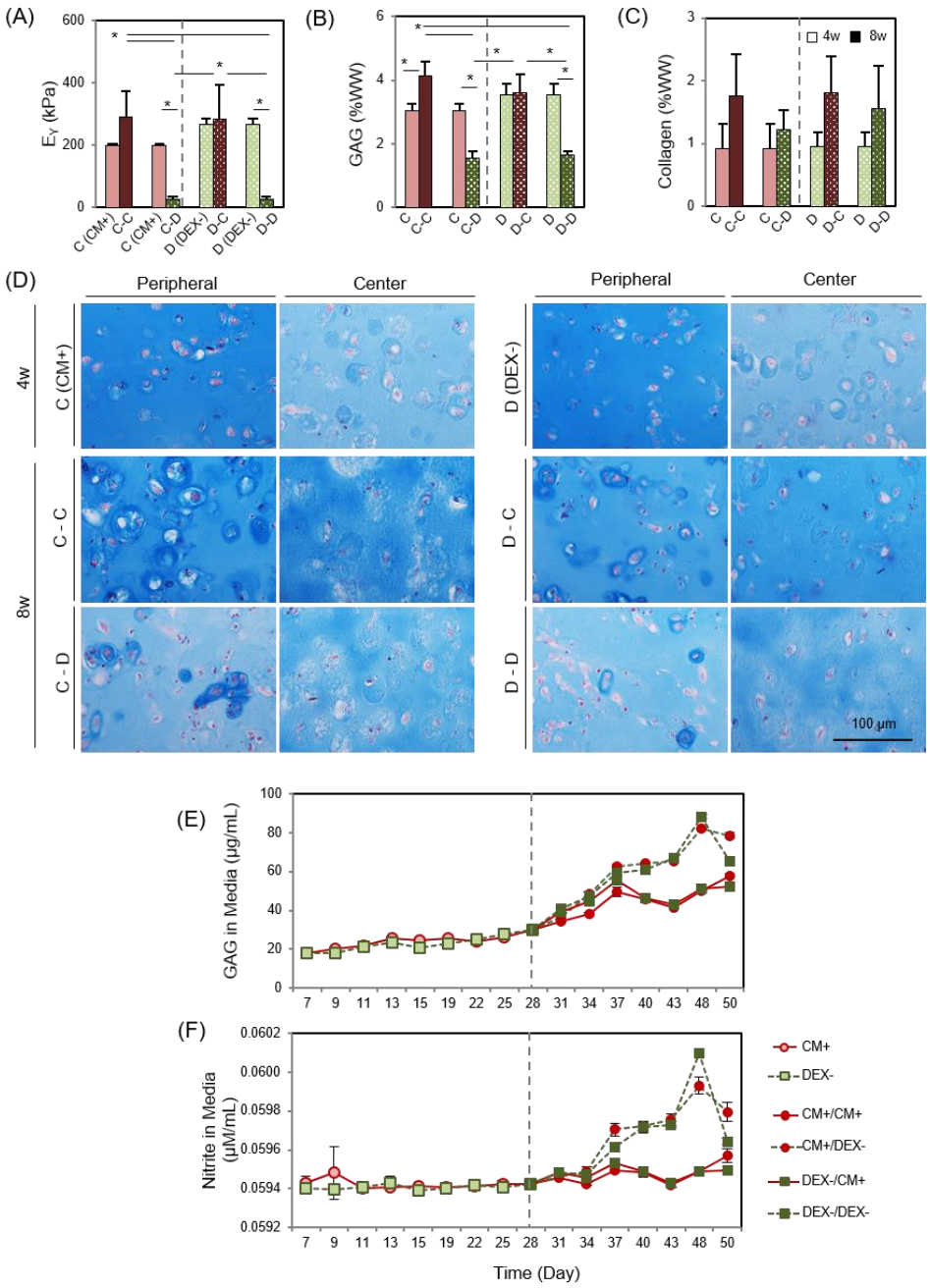

Figure 5-3: Short- and long-term effect of dexamethasone on MSC-laden HA constructs. (A) Equilibrium modulus (E_Y; kPa), (B) GAG (%WW), (C) Collagen (%WW), (D) Alcian blue staining at 4 weeks (CM+ or DEX-; Top) and 8 weeks (C-C, C-D, D-C or D-D; Middle and Bottom), (E) GAG in media (μg/mL), (F) Nitrite in media (μM/mL) (N = 4/group; Lighter bars = 4w, Darker bars = 8w; Solid fill = CM+; Pattern fill = DEX-; Scale bar = 100 μm; 20X magnification; *p<0.05). (C-C group: constructs cultured in CM+ for the first 4 weeks

followed by 4 weeks in CM+; C-D groups: constructs cultured in CM+ for the first 4 weeks followed by 4 weeks in DEX-; D-C group: DEX- for the first 4 weeks followed by CM+ for 4 weeks; D-D group: DEX- for the first 4 weeks followed by DEX- for 4).

However, when continuously cultured in DEX- conditions, construct properties decreased by 8 weeks (25 kPa; $p<0.0001$ and 1.6% WW; $p<0.0001$, respectively). Likewise, when constructs cultured in CM+ were switched to DEX- conditions, construct properties markedly decreased (25 kPa; $p=0.008$ and 1.5% WW; $p<0.0001$, respectively) by 8 weeks. However, constructs that were continuously cultured in CM+ or were switched to CM+ after the first 4 week of culture in DEX- slightly increased or maintained their properties (290 kPa and 4.1 %WW ($p=0.009$) for the C-C group and 285 kPa and 3.6 %WW for the D-C group). Consistent with the previous study, collagen content was independent of the addition or removal of dexamethasone, generally increasing with culture duration **(Fig 5-3C)**.

Table 5-5: Effect of DEX on the functional maturation of MSC-laden HA constructs at 4 and 8 weeks (mean ± SD; N=4 /group).

	CM+ (4w)	C-C (8w)	CM+ (4w)	C-D (8w)	DEX- (4w)	D-C (8w)	DEX- (4w)	D-D (8w)
E_Y(kPa)	198 ± 8	291 ± 83	198 ± 8	26 ± 83	267 ± 19	286 ± 109	267 ± 19	26 ± 9
|G*| (MPa)	1518 ± 96	2279 ± 382	1518 ± 96	921 ± 229	2125 ± 100	2507 ± 671	2125 ± 100	812 ± 66
Diameter (mm)	4.1 ± 0.1	4.2 ± 0.1	4.1 ± 0.1	4.1 ± 0.1	4.1 ± 0.06	4.1 ± 0.1	4.1 ± 0.1	4.1 ± 0.1
GAG (%WW)	3.1 ± 0.2	4.1 ± 0.5	3.1 ± 0.2	1.5 ± 0.2	3.5 ± 0.4	3.6 ± 0.6	3.5 ± 0.4	1.6 ± 0.1
GAG (µg/const)	1087 ± 49	1501 ± 310	1087 ± 49	484 ± 82	1120 ± 153	1027 ± 272	1120 ± 153	436 ± 43
GAG/DNA (µg/µg)	582 ± 38	1994 ± 415	582 ± 38	445 ± 185	487 ± 103	2281 ± 752	487 ± 103	294 ± 106
Collagen (%WW)	0.9 ± 0.4	1.8 ± 0. 7	0.9 ± 0.4	1.2 ± 0.3	1.0 ± 0.2	1.8 ± 0.6	1.0 ± 0.2	1.6 ± 0.7
Collagen (µg/const)	325 ± 119	645 ± 269	325 ± 119	381 ± 96	309 ± 104	524 ± 239	309 ± 104	494 ± 180
Col/DNA (µg/µg)	175 ± 72	846 ± 356	175 ± 72	361 ± 219	138 ± 65	1205 ± 426	138 ± 65	343 ± 169

Alcian blue staining showed robust PG deposition in CM+ and DEX- after 4 weeks, with greater intensity in the peripheral region compared to the core. Constructs continuously cultured or switched to CM+ accumulated intense ECM and PCM in the periphery and core regions, whereas those cultured or switched to DEX- decreased in PG content, particularly in the peripheral region **(Fig 5-3D and 5-4)**. GAG and nitrite release from constructs increased with the switch to DEX- conditions (at week 4) and continued to increase over the next 3 weeks whereas constructs maintained in CM+ conditions showed a lower release of both **(Fig 5-3E and F)**. Collagen release was low and unchanged, regardless of media condition (data not shown).

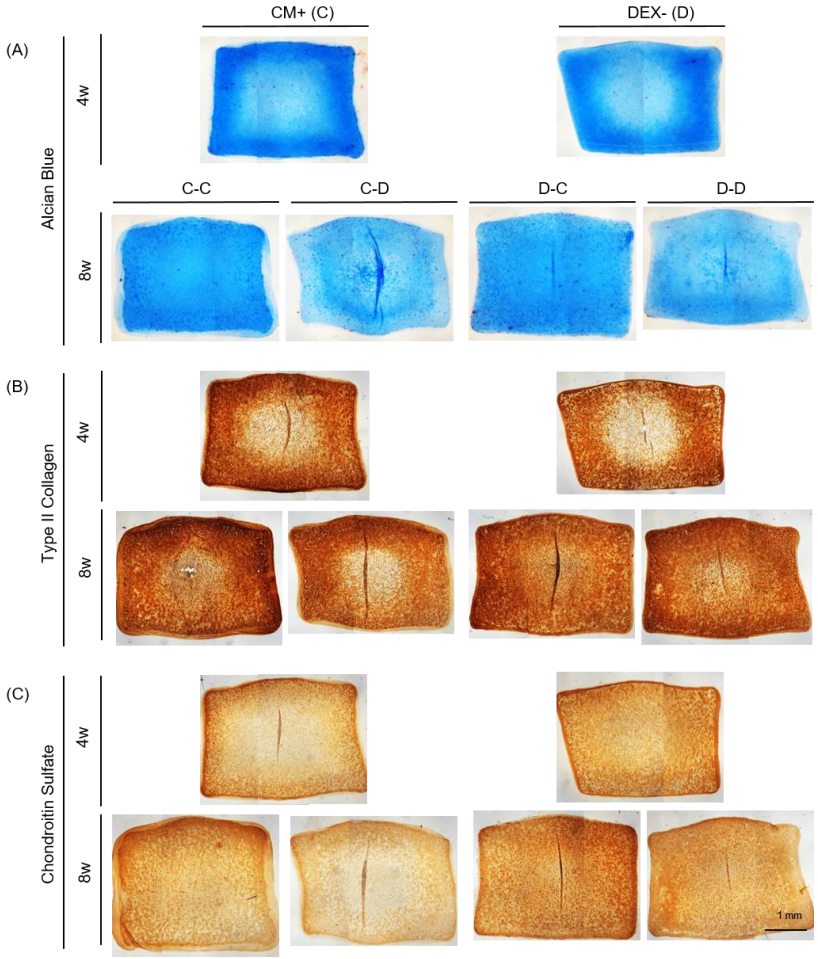

Figure 5-4: Histological analysis of MSC-laden constructs to determine the effect of DEX in defined media. (A) Alcian blue, (B) Type II collagen, (C) Chondroitin sulfate at 4 (top) and 8 weeks (bottom). (2.5X; scale bar = 1 mm). (Construct cultured in CM+ [C) or DEX- [D] for the first 4 weeks (top) with continuous (C-C or D-D) or addition/removal (C-D or D-C) of dexamethasone in defined media for the following 4 weeks (bottom) (2.5X; scale bar=1 mm)

5.3.3 Dexamethasone attenuates GAG loss with transfer to serum-containing media

Constructs cultured in Serum in the absence or presence of TGF and/or DEX (Serum [TGF-/DEX+], Serum [TGF+/DEX-] and Serum [TGF+/DEX+]) failed to mature from the outset, contracted and/or produce little matrix after 4 weeks (0 kPa and 0.2-0.8 %WW). Conversely, those in CM+ produced robust matrix (230 kPa; p=0.001 vs. all Serum conditions and 2.9 %WW; p=0.001, 0.009 and 0.005 vs. Serum conditions, respectively) **(Fig 5-5A-C, Table 5-6)**. Likewise, GAG release from Serum media conditions was low, similar to day 0 levels **(Fig 5-5D)**. When constructs were switched to Serum (Serum[TGF+/DEX-] or Serum[TGF+/DEX+]) after pre-culture in CM+ for 4 weeks, constructs lost mechanical properties entirely (0 kPa for Serum[TGF+/DEX-]; $p<0.0001$) or significantly (21 kPa for Serum[TGF+/DEX+]; $p<0.0001$) compared to those that were in CM+ for the entire 8 weeks. Interestingly, their gross appearance did not change **(Fig 5-5A)**. However, GAG loss in the group cultured in the presence of DEX (Serum[TGF+/DEX+]) was only 34% compared to the level at 4 weeks while that in the absence of DEX (Serum[TGF+/DEX-]), GAG loss reached 80% over the ensuing 4 weeks **(Fig 5-5B)**. Consistent with previous findings, collagen content did not change **(Fig 5-5C)**. GAG release from constructs occurred almost immediately when converted to Serum, and lasted through the culture duration. GAG loss in Serum supplemented with dexamethasone was slightly lower **(Fig 5-5E)**. MMPs release to the media was

similar to GAG, with no pronounced effect of dexamethasone **(Fig 5-5F)**. Nitrite and collagen release (data not shown) had no changes. Alcian blue staining showed that constructs cultured in Serum produced little to no matrix and showed with marked contraction (left column). Constructs in CM+ grew well and produced robust matrix with time in culture (middle). However, when the constructs were switched to Serum, GAG loss was partially inhibited for constructs in the presence of dexamethasone, whereas constructs switched to Serum in the absence of dexamethasone showed marked GAG depletion **(Fig 5-5G** and **6**; right).

Table 5-6: Impact of serum containing media and the effect of DEX on the functional properties of MSC-laden constructs (mean ± SD; N=4 /group).

	4w				8w		
	Serum			CM+	Serum		CM+
	TGF-/DEX+	TGF+/DEX-	TGF+/DEX+		TGF+/DEX-	TGF+/DEX+	
E_Y (kPa)	0	0	0	231 ± 26	0	21±10	426±128
|G*| (kPa)	95 ± 21	0	123 ± 33	2208 ± 162	284 ± 63	916 ± 247	3330 ± 603
Diameter (mm)	3 ± 0.01	1 ± 0.01	2.4 ± 0.1	4 ± 0.03	3.81 ± 0.04	3.89 ± 0.14	4.04 ± 0.01
GAG (%WW)	0.2 ± 0.03	0.8 ± 0.04	0.6 ± 0.4	2.9 ± 0.1	0.7 ± 0.1	1.9 ± 0.4	4.6 ± 0.7
GAG (µg/const)	15.4±3.7	11.6±2.5	26.1±1.6	795±16.3	193±35	524±92	1247±209
GAG/DNA (µg/µg)	124 ± 21	92 ±20	225 ± 20	2743 ± 1000	461 ± 10	1421 ± 600	4524 ± 1200
COL (%WW)	0.83±0.9	3.18±1.7	1.97±1.5	2.12±0.6	2.37±0.6	2.35±0.4	2.75±0.6
COL (µg/const)	48±37	45±20	86±38	581±193	654±184	647±95	757±154
COL/DNA (µg/µg)	421 ± 370	366 ± 190	723 ± 240	2011 ± 680	1595 ± 640	1744 ± 650	2659 ± 310

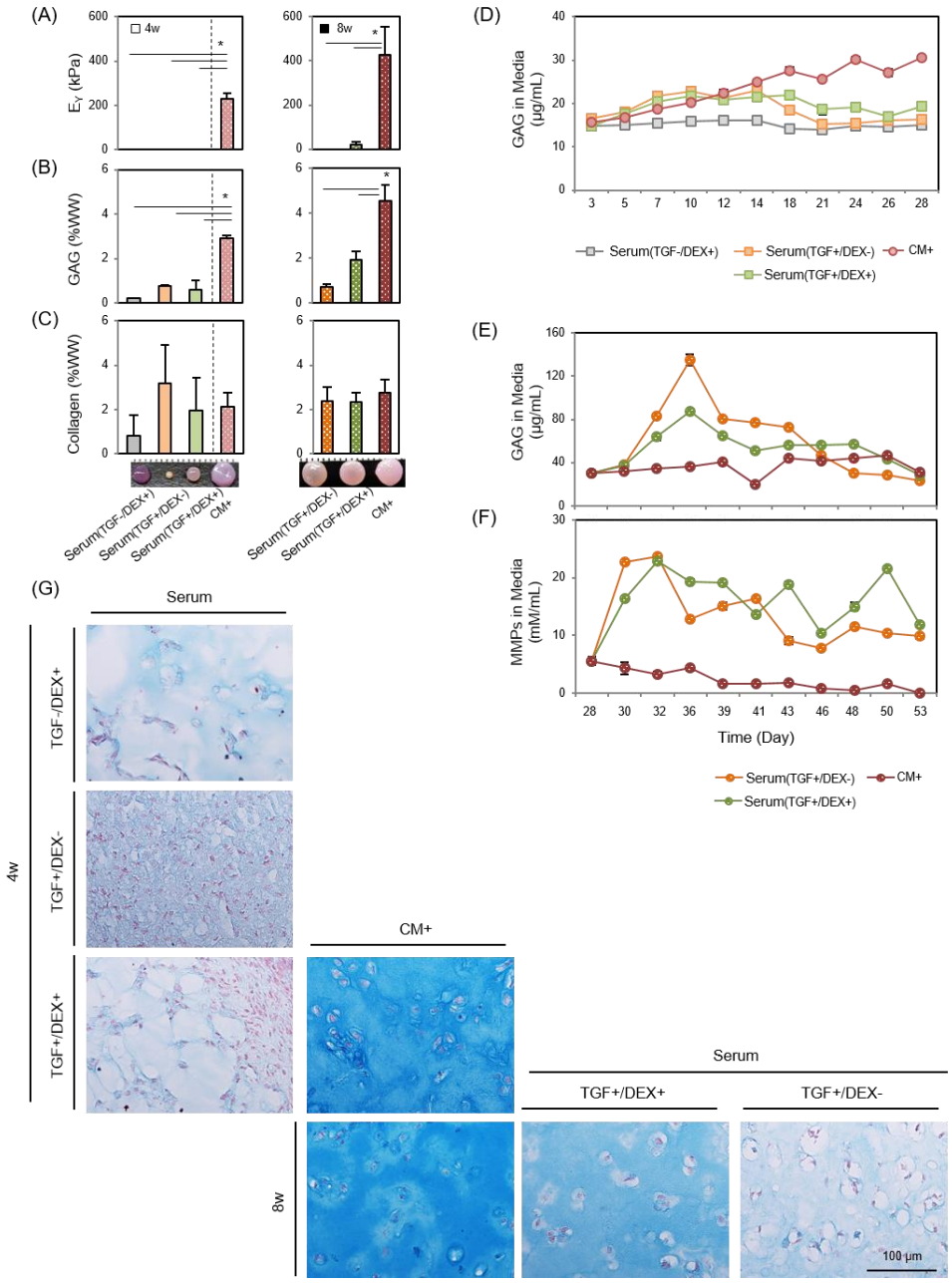

Figure 5-5: Functional properties of MSC-laden HA constructs in defined media or with transfer to serum containing media. (A) Equilibrium modulus (E_Y; kPa), (B) GAG (%WW), (C) Collagen (%WW). (D and E) GAG in media (μg/mL) over first 4 weeks (D) and following 4 weeks (E). (F) MMPs in media (mM/mL) (N = 3/group; *p<0.05), (G) Alcian blue staining: constructs were cultured in serum containing media for 4 weeks with the addition/removal of DEX or TGF (Left). Constructs were cultured in CM+ for the first 4 weeks and continued in CM+ or switched to Serum with the removal/addition of DEX/TGF.

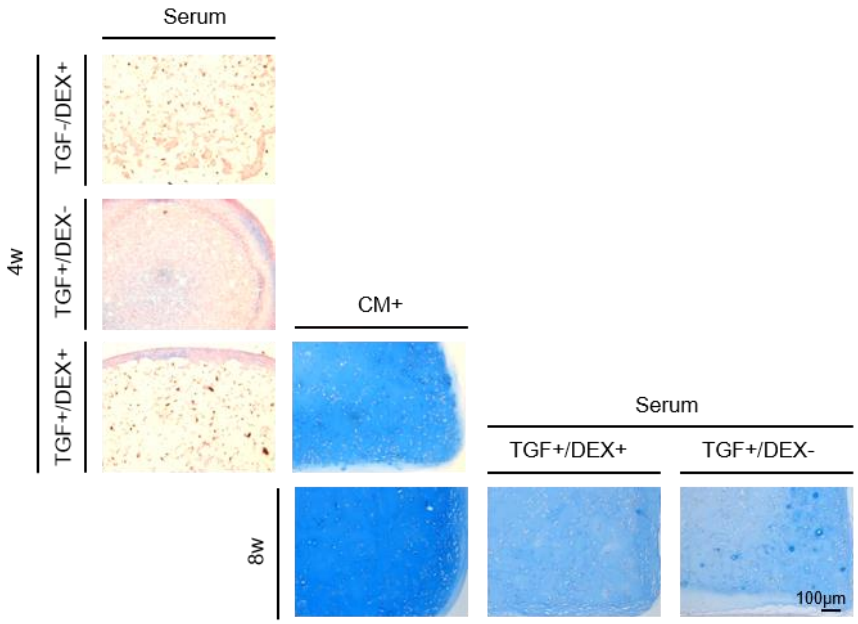

Figure 5-6: Histological analysis of MSC-laden constructs cultured with transfer to serum containing media at 4 and 8 weeks with or without dexamethasone and TGF-β3. (10X; scale bar = 100 μm)

5.4 Discussion

In this study, we determined the roles of various chemically defined media components on the chondrogenesis and functional maturation of MSCs-laden constructs. Further, we defined the role of dexamethasone during culture in these chemically defined conditions and after transition of constructs to a conflicting (in vivo-like) environment. Our findings show that MSC-laden constructs produce robust matrix in CM+ conditions, and that mechanical properties and GAG content were greater in the absence of dexamethasone (DEX- condition) after 4 weeks. However, we also noted that with the prolonged absence of dexamethasone, the mechanical properties and GAG content of these constructs markedly decreased by 8 weeks, whereas those constructs cultured in CM+ conditions for entire period shoed persistent increases throughout this time period. This indicates that dexamethasone plays a key role in regulating pro-chondrogenic and anti-

inflammatory activities, consistent with previous studies (Mackay, Beck et al. 1998, Florine, Miller et al. 2013), and supports long term tissue formation and maturation.

Our data also showed that no matrix was produced when constructs were cultured in absence of a serum substitute (ITS/BSA/LA- condition) or in serum containing media (Serum+ condition). ITS/BSA/LA include essential components in chemically defined media, namely insulin, transferrin, selenium, bovine serum albumin (BSA) and linoleic acid (Yamane, Murakami et al. 1975, Morris, Cripe et al. 1984, Gstraunthaler 2003), and is commonly used as a serum replacement (i.e., ITS Premix+) to improve consistency of in vitro studies. Insulin is crucial for glucose transport into cultured cells, and transferrin is an ion carrier reducing toxic levels. Selenium, as sodium selenite, is a cofactor for selenium-dependent enzyme activities (e.g., glutathione reductase, glutathione peroxidase), and inhibits oxidation. Linoleic acid is a precursor of prostaglandins, glycolipids, and vitamins, while albumin serves as a plasma substitute for the growth of cultured cells. The absence of growth of constructs in media formulations lacking ITS/BSA/LA indicate that these molecules are indispensable in chemically defined media formulations. We also noted that constructs cultured in Serum+ conditions contracted immediately, showing aggregation of MSCs that culminated in the formation of a central pellet-like structure that separated from the HA hydrogel. These data indicate that serum elements are essential for construct growth, but that other elements in serum can limit matrix formation by MSCs.

Based on our observation of a differential effect of dexamethasone on functional maturation during the culture period, we further investigated how dexamethasone regulated functional properties with time in culture. Consistent with previous results, constructs produced greater mechanical properties and GAG content in the absence of

dexamethasone (DEX- condition) through 4 weeks, compared to constructs cultured in the presence of dexamethasone (CM+ condition). However, constructs cultured with the continuous absence of dexamethasone (the D-D condition) showed a marked decrease in properties by 8 weeks compared to those with the continuous addition of dexamethasone (the C-C condition. Interestingly, when dexamethasone was added later in culture (the D-C group), construct properties were maintained through the 8 weeks. Conversely, when dexamethasone was withdrawn at 4 weeks (the C-D condition), construct properties decreased to the level of the D-D condition. This suggests that the presence of dexamethasone is essential during the latter phases of construct maintenance, but may not be necessary during the rapid growth phase of construct maturation.

These mechanical and biochemical analyses were largely confirmed by histological assessment, which also showed that constructs with continuous addition of dexamethasone (the C-C condition) or with dexamethasone added later (the D-C condition) retained a dense matrix in both peripheral and central regions. Conversely, the removal or absence of dexamethasone resulted in marked depletion of GAG, with greater loss in the peripheral region. Analysis of loss of GAG and nitrite content (indicative of inflammation) in media showed that all groups had low levels, regardless of the presence of dexamethasone, at 4 weeks. Later, however, levels of both indicators of a catabolic state gradually increased for constructs cultured without dexamethasone (the C-D and D-D conditions), while release of GAG and nitrite production by constructs with dexamethasone remained lower. These data are consistent with reports suggesting that constructs produce greater properties in the absence of dexamethasone over the short term (through week 4), but are also consistent with the requirement of dexamethasone to retain these properties over longer durations (through week 8). Given the finding of

increased nitrite in media over this period, the role of dexamethasone during this period may arise from the state of cells after maturation is complete. It has been reported that IGF-1 (insulin-like growth factor-1) signaling, which maintains cartilage homeostasis in healthy cartilage, is sensitive to nitric oxide (NO). The presence of NO decreases IGF receptor expression and makes cartilage insensitive to the anabolic effects of IGF-1 (Studer, Levicoff et al. 2000, Studer 2004). This effect of NO was enhanced when glutathione (an anti-oxidant) was depleted from the media (Studer 2004). This implies that reactive oxygen species (ROS) that arise during long term culture (due to cell stress) may be mitigated by the action of dexamethasone, making this factor essential for the stability of MSC-based engineered cartilage cultured in vitro for long periods.

Based on the finding that dexamethasone is essential for the long term stability of chondrogenic MSC-based constructs, we next queried the potential protective role of this factor when constructs were transferred to in vivo like conditions including serum, a 'conflict' signal. Constructs cultured from the outset in serum containing media (Serum+), with or without dexamethasone, failed to mature and produced no matrix. However, when constructs were pre-cultured in CM+ for 4 weeks, and then converted to Serum+, dexamethasone had a positive effect on long term outcomes. That is, while all constructs lost mechanical properties compared to their week 4 values in serum containing media, GAG loss was attenuated with dexamethasone (34% loss compared to 80% loss without dexamethasone at 8 weeks). Interestingly, GAG release after transfer to serum containing media (Serum+) occurred very rapidly, reaching a maximum in one week. This suggests that dexamethasone delivery may be optimized to sustain construct properties in the long term by systemic or local delivery post-implantation.

Since local delivery of dexamethasone may be required, it is auspicious that numerous methods to deliver dexamethasone and other growth factors have been introduced for cartilage repair. For example, early work by Nuttelman et al. generated dexamethasone-releasing poly(ethylene glycol) (PEG)-based hydrogels, where dexamethasone was covalently linked to a photo-reactive PEG molecule via a degradable lactide bond. This allowed for sustained release of dexamethasone with in vivo hydrolysis of the ester bond (Nuttelman, Tripodi et al. 2006). Other work, by Na et al., fabricated a thermo-reversible hydrogel using poly(NiPAAm-*co*-AAc) as an injectable drug delivery vehicle with co-encapsulated dexamethasone and TGFβ3 (Na, Park et al. 2006, Na, Kim et al. 2007). Similarly, local dual delivery of dexamethasone/TGF-β3 via with heparin in or on PLGA microspheres has been demonstrated to promote rabbit MSC chondrogenesis (Park, Na et al. 2009). Most recently, Roach et al. demonstrated delivery of dexamethasone via PLGA microspheres in a chondrocyte-laden agarose hydrogel (Roach, Kelmendi-Doko et al. 2016). Kopesky et al., utilized a self-assembled peptide hydrogel (i.e., AcN-$(KLDL)_3$-CNH_2) encapsulated with TGF-β1 for sustained delivery of TGF-β1 (Kopesky, Byun et al. 2014). Jung et al., introduced monoCB[6]/DAH-HA (monofunctionalized cucurbit[6]uril-HA (CB[6]-HA), diamino-hexane conjugated HA (DAH-HA), and drug conjugated CB[6] (drug-CB[6])) for controlled chondrogenesis of human MSCs (Jung, Park et al. 2014). Finally, Bajpayee et al. introduced avidin for charge based intraarticular delivery of a single dose of dexamethasone, and demonstrated that this single dose was both quickly and slowly released (Bajpayee, Wong et al. 2014, Bajpayee, Quadir et al. 2016).

Collectively, our findings support the importance of dexamethasone in improving and maintaining functional MSC chondrogenesis in HA hydrogels. Targeted delivery and controlled release of dexamethasone (and TGF-β3) and recent advances in drug

delivery systems to enable their release, may enable successful cartilage repair with MSC-based engineered tissue constructs by controlling tissue homoeostasis and promoting long term function.

CHAPTER 6: Extracellular Vesicles Mediate Improved Functional Outcomes in Engineered Cartilage Produced from MSC/Chondrocyte Co-cultures

6.1 Introduction

Mesenchymal stem cells (MSCs) are an attractive cell source for regenerative medicine and especially for cartilage therapeutics as these cells can undergo chondrogenesis in a variety of 3D contexts (Huang, Yeger-McKeever et al. 2008). Focused efforts in MSC-based cartilage tissue engineering have culminated in the reliable formation of cell-based materials possessing biochemical and functional properties that are equivalent to that of the native tissue (Erickson, Kestle et al. 2012). Despite the promise of this approach, MSCs are and remain a multipotent cell type (Pittenger, Mackay et al. 1999), and show an unfortunate predilection towards hypertrophic conversion when removed from carefully controlled chemically defined *in vitro* media conditions (Mueller and Tuan 2008). Furthermore, it has been well established that both the number and chondrogenic capacity of MSCs decreases with organismal aging (Erickson, van Veen et al. 2011). This decline in MSC number and capacity with aging makes cartilage repair procedures that rely on an endogenous progenitor cell source contraindicated in aged persons (Kretlow, Jin et al. 2008). Although chondrocytes (CH) are the current clinical cell source for cartilage repair procedures (Huang, Hu et al. 2016), and are generally superior to MSCs in matrix production and phenotypic stability (Erickson, Huang et al. 2009), the scarcity of this cell type limits their more widespread application, as does their loss of phenotype with monolayer expansion, their decrease in potential with aging, and the requirement for two independent surgical events for this procedure (Darling and Athanasiou 2005, Kretlow, Jin et al. 2008, Ruta, Villarreal et al. 2016).

To address these issues, a number of studies have explored the co-culture of chondrocytes and chondrocyte-like cells with MSCs in monolayer, pellet, and 3D hydrogel culture environments (Richardson, Walker et al. 2006, Fischer, Dickhut et al. 2010, Aung, Gupta et al. 2011, Bian, Zhai et al. 2011, Meretoja, Dahlin et al. 2012, Strassburg, Hodson et al. 2012, Wu, Prins et al. 2012). While most such studies report some positive effect of co-culture, the directionality of intercellular communication remains controversial. That is, some groups have suggested that CHs enhance the initial efficiency of MSC chondrogenesis, as well as limit hypertrophic changes, and that CHs accomplish this through secretion of morphogens that are taken up by neighboring MSCs (Fischer, Dickhut et al. 2010, Aung, Gupta et al. 2011, Bian, Zhai et al. 2011). Conversely, others have suggested that MSCs improve CH proliferation and function while attenuating inflammation, resulting in improved matrix deposition (Meretoja, Dahlin et al. 2012, Wu, Prins et al. 2012). Still other studies suggest a bi-directional exchange between the two cell types during co-culture (Strassburg, Hodson et al. 2012).

Despite the distinct findings, it is generally agreed that the molecular factors mediate the intercellular communication of co-culture. However, it also remains unclear as to the distinct mechanism by which these intercellular signals are conveyed. For instance, cells may signal over a long distance or influence only neighboring or connected cells, and they might do so through direct cytoplasmic transfer (i.e., through gap junctions), via local secretion of the factor, or via facilitated transport through the extracellular space. Some studies have reported different outcomes of co-culture based on either the intercellular distance or the density of the intervening materials (Lai, Kajiyama et al. 2013, de Windt, Saris et al. 2015). These findings may in part be explained by the recent description of cell-derived extracellular vesicles (EVs; exosomes and micro-vesicles) that can carry proteins, enzymes, mRNAs, miRNAs and DNA between cells (Muralidharan-

Chari, Clancy et al. 2010, Gyorgy, Szabo et al. 2011, Raposo and Stoorvogel 2013, Malda, Boere et al. 2016). Given that the diffusivity of these larger particles through a porous medium may be hindered, it is possible that EVs play an important role in intercellular communication during co-culture (Chen, Liang et al. 2012, Malda, Boere et al. 2016).

To explore these questions in detail, we developed a 3D hyaluronic acid (HA) hydrogel culture system in which to better define the mechanism of MSC/CH co-culture. Because CHs from different regions of articular cartilage retain different matrix forming capacity and phenotype (Cheng, Conte et al. 2007), we first assayed whether zonal origin impacted co-culture outcomes, and whether this depended on the age of the recipient MSCs. Next, we identified the distance over which the molecular factors could effectively induce the co-culture effect. Finally, we queried the molecular factors and pathways that mediated the co-culture effect, and determined how these factors were transferred between releasing and recipient cells. Our results demonstrate that passaged CHs from all zones retain their zonal characteristics and the ability to rejuvenate the chondrogenic capacity of adult MSCs in co-culture. Our data further support the idea that co-culture can only function when the two cell types are close to one another, and that the recipient MSC population undergoes marked shifts in expression profiles. Finally, we demonstrate that extracellular micro-vesicular transport is a primary mediator and requisite feature of intercellular communication in this co-culture system. These findings will forward the development of new therapeutic agents and more effective delivery systems to promote functional cartilage tissue formation by adult autologous MSCs.

6.2 Materials and Methods

6.2.1 Isolation of zonal chondrocytes (CHs) and mesenchymal stem cells (MSCs)

Chondrocytes and MSCs were isolated from bovine stifle joints (Juvenile: Research 87, Bolyston, MA; Adult: Animal Technologies, Tyler, TX) **(Figure 6-1A)**. Full-thickness juvenile cartilage segments were excised from the femoral condyle and divided into three layers (Ng, Ateshian et al. 2009). The top-most 100μm thick layer at the articular surface was carefully removed and taken as the superficial zone (S). The segment from the bony surface to just above the tide mark was removed and discarded. The remaining "top" half of the tissue segment was considered as middle zone (M) and the "bottom" half as deep zone (D) cartilage. These separated zonal cartilage tissues were minced and digested with collagenase to obtain respective zonal CH populations. MSCs were isolated from juvenile (JMSC) or adult (AMSC) bone marrow as described previously (Huang, Yeger-McKeever et al. 2008, Erickson, van Veen et al. 2011). These zonal CHs and MSCs were separately maintained in basal medium consisting of high glucose Dulbecco's modified Eagle's medium (DMEM; ThermoFisher, Grand Island, NY) supplemented with 10% fetal bovine serum (FBS; ThermoFisher, Grand Island, NY) and 1% penicillin/streptomycin/fungizone (PSF; ThermoFisher, Grand Island, NY). Cells of both type were expanded in culture through passage 3~4. To monitor the distribution of each cell population in 3D culture, cells were trypsinized, washed with PBS, and labeled with CellTracker (Molecular Probes, Eugene, OR; CHs = Red and MSCs = Green) prior to encapsulation.

6.2.2 MeHA synthesis and cell encapsulation

Methacrylated hyaluronic acid (MeHA) was synthesized as described previously. Briefly, 1% w/v sodium hyaluronate (65 kDa HA; Lifecore Biomedical, Chaska, MN) was reacted with methacrylic anhydride (Sigma, St. Louis, MO) on ice at pH 8.0 for 6 hours followed by dialysis (6kDa MW cutoff, Spectrum Labs, Rancho Dominguez, CA) to remove unreacted byproducts for 7 days. Then, the MeHA solution was lyophilized and stored at

−20°C. To form gels, lyophilized MeHA was dissolved at 1% w/v in PBS with 0.05% w/v photoinitiator (Irgacure I2959, CibaGeigy, Tarrytown, NY).

6.2.3 Establishment of zonal CH and MSC co-cultures

To determine whether zonal chondrocyte (CH) identity differentially contributed to MSC fate and/or how aging impacted MSC response to co-culture, CellTracker-labeled juvenile zonal CHs were mixed with juvenile or adult MSCs (zonal JCH:JMSC or zonal JCH:AMSC) at a 1:4 ratio (20% CH:80% MSC). This cell mixture was formed in 1% MeHA solution, with a final cell concentration of 60 million cells/mL. Gel-cell mixtures were poured into a gel casting device (Hoefer, Inc., Hollison, MA) and exposed to UV using a 365 nm BlakRay UV lamp (#UVL56, San Gabriel, CA) for 10 minutes. The range of the UV was 320–400 nm, with a transmission maximum of 70% at 365 nm. Cylindrical cores (Ø4 mm × 2.25 mm) were removed from the resulting HA gel sheets using a sterile biopsy punch. These constructs were then cultured in chemically defined media (CM) (2 mL/construct) with TGF-β3 (10ng/mL; R&D Systems, Minneapolis, MN) (CM+). CM consisted of high glucose DMEM supplemented with 1% PSF, 0.1 μM dexamethasone, 50 μg/mL ascorbate 2-phosphate, 40 μg/mL L-proline, 100 μg/mL sodium pyruvate, 6.25 μg/mL insulin, 6.25 μg/mL transferrin, 6.25 ng/mL selenious acid, 1.25 mg/mL bovine serum albumin (BSA), and 5.36 μg/mL linoleic acid. Media were changed thrice weekly for up to 8 weeks. Tracker-labeled cells were observed using a Nikon Eclipse TE2000-U inverted microscope (Nikon Instruments Inc., Melville, NY, USA) or a Nikon A1R confocal microscope (Nikon Instruments Inc., Melville, NY, USA).

6.2.4 Assessment of co-culture efficacy

To determine whether co-culture of zonal CHs and MSCs in HA hydrogels resulted in an improvement in outcomes, we determined the efficacy of co-culture by computing a ratio

of the actual (Y-axis) to the expected (X-axis) outcomes (mechanical properties and biochemical content, described below) based on the relative contribution of each cell type and their individual performance **(Fig 6-1C and D; Fig 6-2A and B; 6-4A and B)**. Expected values were calculated based on the rule of mixtures, where the expected outcome was the sum of 20% of the performance of zonal CHs on their own and 80% of the performance of MSCs on their own (Expected = 0.2* Actual CH + 0.8* Actual MSC). In cases where there was a 'synergistic' effect, the actual value was greater than expected (actual>expected), and these samples were located on the upper-left quadrant of the plot. In cases where there was a 'negative' effect (actual<expected), samples were located the lower-right quadrant of the plot. Finally, in cases where the two cell types were 'independent' or had no synergistic/co-culture effect (actual=expected), the samples fell along the diagonal (dashed) line.

6.2.5 Influence of intercellular distance on co-culture outcomes

To investigate how far molecular factors might travel from releasing to recipient cells within HA culture, JCHs and AMSCs were seeded in constructs at varying distances to provide increasing separation between two cell populations: these included 'mixed', 'fused', or 'distanced' configurations **(Figure 6-5A)**. JCHs and AMSCs were isolated, expanded (P2-3), and seeded at 60 million cells/mL in 1% w/v HA hydrogels (JCH:AMSC = 1:4) at varying distances. First, "mixed" populations were seeded as a single mixture in one layer to provide the shortest possible distance over which molecular factors might travel. Second, CH-seeded and MSC-seeded layers were "fused" by creating a bi-layered construct. Finally, CH-seeded and MSC-seeded layers were constructed as a tri-layered 'barrier' construct, with an acellular HA gel segment interposed between the cell-seeded layers in the middle of the construct (MSC-barrier-

CH) **(Figure 6-5B)**. These constructs were cultured in CM+, with media changed thrice weekly for 56 days.

6.2.6 Molecular profiling of MSCs during co-culture

To investigate molecular pathways that might mediate the co-culture effect, we evaluated genome-wide changes in mRNA expression in AMSCs that had been co-cultured with JCHs for a short period of time, in the absence or presence of TGF, compared to AMSCs that were cultured alone. To enable sorting of distinct cell populations, AMSCs (green) and JCHs (red) were labeled with CellTracker (Molecular Probes) prior to encapsulation **(Figure 6-7A)**. AMSCs alone *(AMSC)* or mixed *(co-culture, CO)* cell populations (MSC:CH ratio = 4:1) were encapsulated at 20×10^6 cells/mL in 1% MeHA. Constructs (Ø4 × 0.75 mm) were cultured in CM in the absence *(TGF-)* or presence *(TGF+)* of TGF-β3 (10ng/mL). On day 10, constructs were minced and digested with hyaluronidase (100U/mL) (Burdick, Chung et al. 2005) to re-isolate cells from constructs. Isolated cells were suspended in PBS with 1% BSA and maintained on ice prior to sorting. Cell mixtures underwent fluorescence activated cell sorting (FACS) using a BD Aria II cell sorter (BD Biosciences, San Jose, CA). Cell populations were sorted into Trizol (in 1.5 mL Eppendorf tubes), vortexed for 10 min, and stored at -80C until RNA isolation.

Sorting resulted in AMSC populations remained green in co-culture (AMSC: CO G) or had become double positive (AMSC: CO DP) as well as those that were cultured alone (green; AMSC: G) in the absence or presence of TGF. RNA was isolated from these populations (microRNeasy mini kit, Qiagen) and subjected to microarray analysis (Bovine Genome 1.0st, Affymetrix) by the Penn Microarray Facility. This included quality control tests of total RNA by Nanodrop spectrophotometry and analysis of RNA quality

via Bioanalyzer. All protocols used to carry out RNA isolation, quality control, and microarray analysis were as previously described (Huang, Stein et al. 2010). The study was repeated three times with mixed donor sets used in each replicate. The Ingenuity software was used to identify pathways associated with co-culture, grouping genes that were differentially regulated with a false discovery rate (q-value) of 0.25 and fold change of >1.5. Fold change was compared across four groups (CO+ vs. MSC+, MSC+ vs. MSC-, CO- vs. MSC- and CO+ vs. CO-) to assess how the molecular factors secreted from CH in the absence (JCH-TGF) or presence of (JCH+TGF) TGF altered the expression profiles of AMSCs compared to AMSCs that were exposed to only TGF.

6.2.7 Probing mechanisms of intercellular communication

To identify whether intercellular communication occurred through the release of extracellular vesicles (EVs), we first inhibited endocytic pathways. Co-culture constructs were maintained in CM+ (control) supplemented with a high dose of Dyngo 4a (50μM; Abcam, to inhibit dynamin and t-SNARE mediated vesicle fusion) or Pitstop2 (50μM; Abcam, to inhibit clathrin mediated vesicle formation) for 42 days. To determine the dose-dependent impact and reversibility of Pitstop2 in exocytic release of extracellular proteins, JCH-laden constructs were cultured in CM+ in the presence of Pitstop2 at a varying concentration (0, 10, 25, and 50μM) for the first 21 days (D0-21) followed by culture for an additional 21 days (D22-42) in the absence of Pitstop2 **(Figure 6-9A)**. Cell viability was evaluated using the Live/Dead assay (Molecular Probes) at day 42. After determining an optimal dose of Pitstop 2 (25μM), cell-laden constructs (JCH, AMSC alone, or co-cultured) were cultured in CM+ supplemented with Pitstop2 (0 or 25μM) for 42 days **(Figure 6-10A)**.

6.2.8 Analysis of mechanical properties

To determine mechanical properties of constructs, unconfined compression testing was carried out as in (Mauck, Soltz et al. 2000). The equilibrium modulus was determined via a stress-relaxation test. Constructs underwent creep loading to 0.02 N applied over 5 minutes. After creep loading, samples were compressed at 10% strain from the post creep construct thickness with a step compression at 0.05%/sec, followed by a relaxation phase lasting for 1000 seconds. After stress relaxation, a 1% sinusoidal deformation was applied at 1.0 Hz to obtain the dynamic modulus.

6.2.9 Biochemical Analysis

After mechanical testing, construct wet weight was measured followed by papain digestion at 60°C for 16 hours. Glycosaminoglycan (GAG) content was determined using the 1,9 dimethylmethylene blue (DMMB) assay (Farndale, Buttle et al. 1986). Collagen content was extrapolated from orthohydroxyproline (OHP) content assessed by reaction with chloramine T, using a 1:7.14 (OHP: collagen) ratio (Neuman and Logan 1950).

6.2.10 Histological Analysis

Constructs were fixed in 4% paraformaldehyde (PFA) and embedded in paraffin. Sections (8μm thick) were deparaffinized in a graded series of ethanol and stained with Alcian Blue (pH 1.0) for proteoglycans (PG). Immunohistochemistry was carried out to visualize type I and type II collagen and chondroitin sulfate (CS). Samples underwent antigen retrieval using hyaluronidase (HASE) from type IV bovine testes (Sigma-Aldrich, St. Louis, MO) followed by Protease-K treatment (DAKO, Glostrup, Denmark). Endogenous peroxidase activity was quenched by pretreating sections with 3% hydrogen peroxide. To block nonspecific staining, sections were incubated with 10% normal goat serum (Sigma-Aldrich, St. Louis, MO). Primary antibodies for type I (MAB3391, Millipore, Billerica, MA) and type II collagen (II-II6B3; Developmental Studies Hybridoma Bank, Iowa City, IA) and chondroitin sulfate (C8035, Sigma-Aldrich, St.

Louis, MO) were used. After incubation with primary antibodies (overnight at 4ºC), sections were treated with biotinylated goat anti-rabbit IgG secondary antibodies followed by streptavidin horseradish peroxidase (HRP) and reacted with DAB chromogen reagent for 10-20 min (DAB150 IHC Select, Millipore, Billerica, MA). Stained images were captured using a light microscope (Leica DMLP, Leica Microsystems).

6.2.11 Statistical Analysis

Statistical analysis was performed using the SYSTAT software (v10.2, SYSTAT Software Inc., San Jose, CA). Significance was determined by two-way ANOVA with Tukey's post hoc test ($p < 0.05$). Data represent the mean ± the standard deviation.

6.3 Results

6.3.1 Co-culture of juvenile CHs with adult MSCs improves functional outcomes.

Constructs seeded with zonal JCHs, JMSCs alone, or mixed co-cultured (JMSC/JCH) cell populations in HA hydrogels were geometrically stable with time and slightly increased in volume for all groups **(Figure 6-1)**. AMSCs cultured alone aggregated together and separated from the HA, resulting in the formation of a small single mass **(Figure 6-1C and D)**. However, co-culture constructs seeded with both cell populations (AMSC/JCH) in HA slightly contracted early in culture but were geometrically stable over 56 days **(Figure 6-1D-F)**. CHs and MSCs seeded in HA hydrogels retained CellTracker signal through the culture period, and their ratio (MSC/CH) on day 56 was only slightly lower than that at the day 0 **(Figure 6-2B)**. Construct mechanical property and GAG content for JCH-laden construct groups (S, M and D) increased with time and depended on the zonal origin of the JCHs; lower properties were achieved with superficial JCHs (202-387 kPa and 2.9-3.4 %WW GAG) and higher properties with deep zone JCHs (515-702 kPa and 5.5-5.8 %WW GAG).

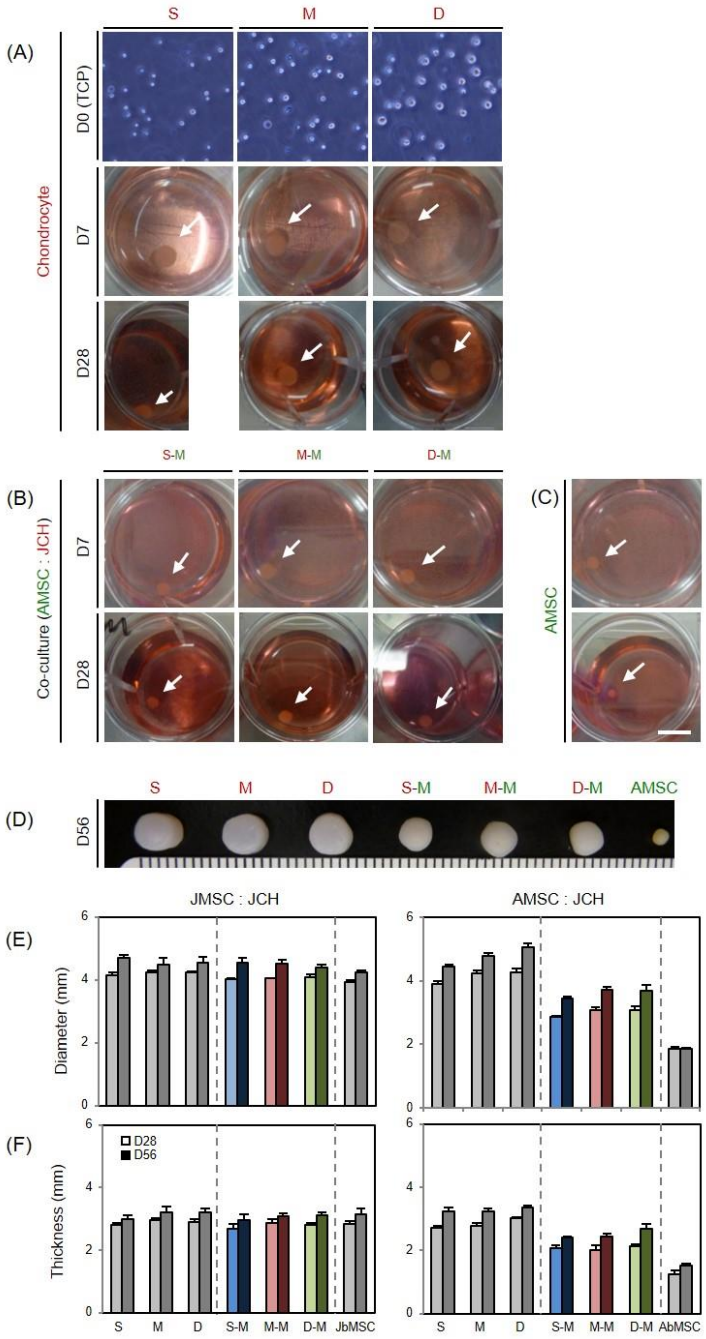

Figure 6-1: Growth of zonal JCH-, AMSC- and Co-cultured HA constructs.

(A) Zonal JCHs, (B) JCH/AMSC co-cultures, and (C) AMSCs alone at day 0 (zonal CHs on TCP, prior to encapsulation), day 7, and day 28. (D) Gross images of cell-laden constructs at day 56. (E and F) Construct dimensions (diameter and thickness) on day 28 and day 56 (Left column = JMSC:JCH, Right column = AMSC:JCH, Lighter bars = day 28 and Darker bars = day 56).

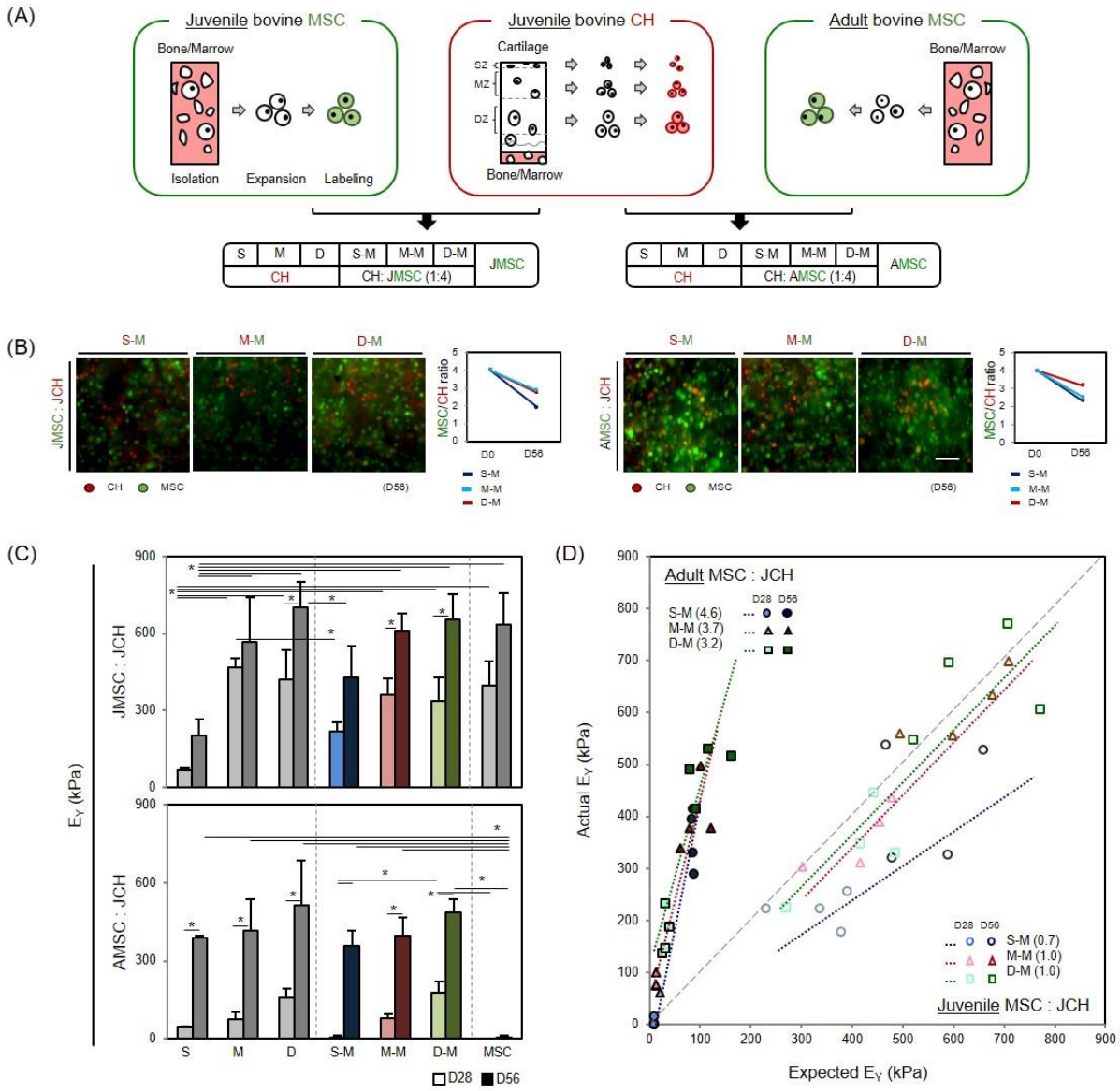

Figure 6-2: Impact of zonal-CH co-culture with MSCs of juvenile and adult origin.

(A) MSCs and CHs were isolated from bone marrow and articular cartilage. Zonal CHs were isolated from the superficial (S), middle (M), and deep zone (D) of juvenile cartilage. Isolated cells were expanded and labeled with CellTracker (MSC: green and CH: red). Juvenile (J) MSCs and Adult (A) MSCs were mixed with zonal CH subpopulations (mixture ratio = CH:MSC = 1:4) at 60 million cells per mL of 1% HA. Constructs (Ø4 x 2.25mm) were cultured in CM+. (B) Mixed cell populations in all groups (S-M, M-M and D-M) were well distributed within the constructs after 56 days of culture (JMSC:JCH (Left) and AMSC:JCH

(Right)). Quantification of CH and MSC sub-populations over time showed that by 8 weeks, 25~30% of cells were CH and 70~75% were MSCs. (C) Equilibrium modulus (E_Y; kPa) of juvenile MSC/juvenile CH co-cultures (JMSC:JCH, Top) and adult MSC/juvenile CH co-cultures (AMSC:JCH, Bottom) where zonal origin is indicated by S, M, or D. Additional groups included zonal CH alone (S, M, and D, Left-most groups) and MSC alone (MSC, Right-most group). Constructs formed from JMSCs grew well on their own, while those formed from AMSCs failed to mature. No synergistic effect of co-culture was observed for JCH/JMSC groups, whereas AMSCs co-cultured with JCHs exceeded expectations based on individual cultures (Lighter bars = Day 28, Darker bars = Day 56; N=4/group; $p<0.05$). (D) To assess the efficacy of co-culture, actual ($E_{Y\ Actual}$; Y-axis) and expected E_Y ($E_{Y\ Expected}$; X-axis) values for S-M, M-M and D-M co-cultures were plotted. Expected E_Y was calculated based on the rule of mixtures, equating to the sum of 20% of $E_{Y\ zonal\ CH}$ and 80% of $E_{Y\ MSC}$ ($E_{Y\ Expected\ Mixed} = 0.2 * E_{Y\ Actual\ CH} + 0.8 * E_{Y\ Actual\ MSC}$). Slopes (◢; dotted line) in each group indicate the growth rate between 4 and 8 weeks. JMSC:JCH co-cultures showed mainly negative or independent effects of co-culture while AMSC:JCH co-cultures showed a positive effect of co-culture, outperforming expectations (Solid shapes = AMSC:JCH and Hollow shapes = JMSC:JCH; Circle = S-M, Triangle = M-M and Square = D-M).

These passaged JCHs produced robust ECM in CM+, and construct properties reached near native levels after 56 days **(Figure 6-2C and 3A)**. JMSCs alone also grew well (reaching 633 kPa and 6.1 %WW GAG), matching the properties of deep zone CHs. Construct properties for JMSC/JCH co- culture groups also reflected zonal origins of JCHs, but their combination (428-655 kPa and 4.3-5.9 %WW GAG) did not enhance functional properties. Conversely, AMSCs alone failed to mature (5 kPa and 1.2 %WW GAG) in HA hydrogels. When co-cultured with JCHs, however, these constructs achieved markedly higher properties and ECM content (357-488 kPa and 3.7-4.1 %WW

GAG). Unlike mechanical properties and GAG content, collagen content was independent of co-culture **(Figure 6-4A)**.

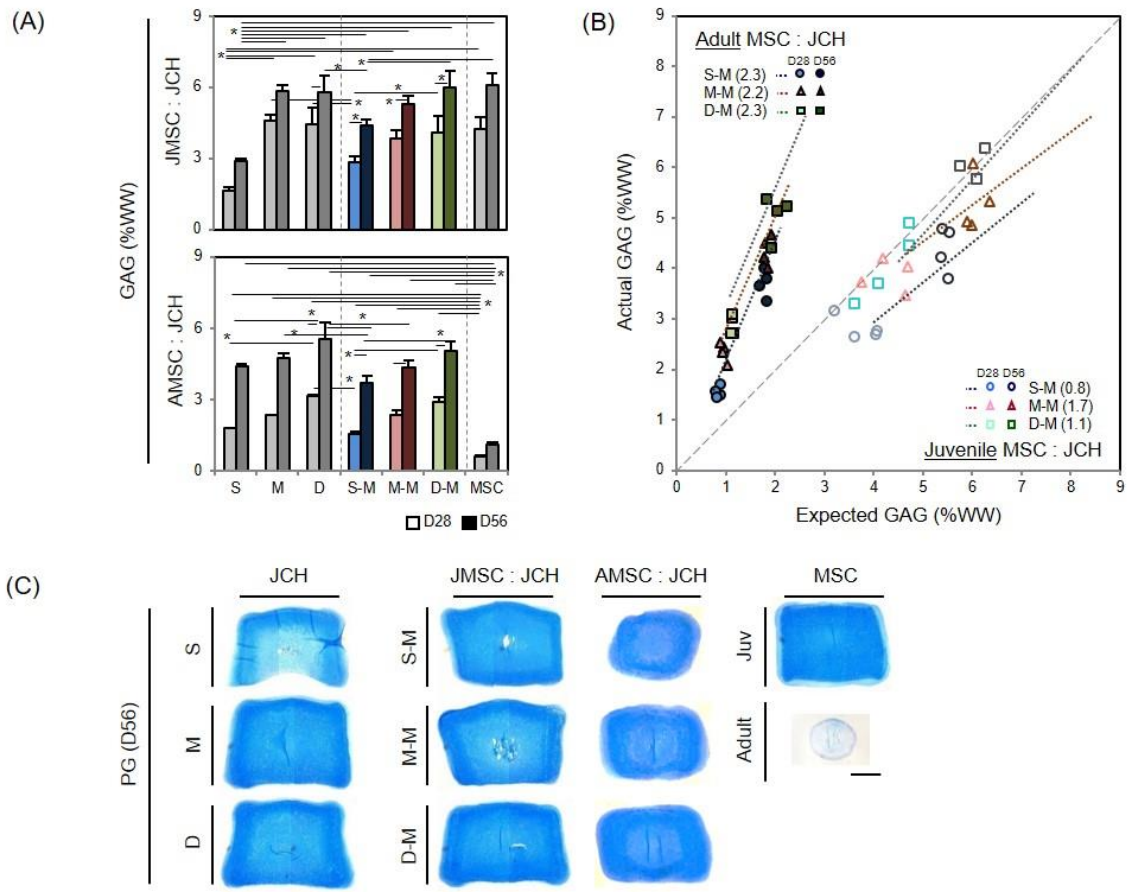

Figure 6-3: Proteoglycan content of zonal CH/MSC co-cultures.

(A) GAG content (% wet weight) for juvenile and adult MSC co-cultures with zonal juvenile CH. Consistent with the mechanical properties, AMSCs showed greater than expected GAG deposition when co-cultured with JCHs. (B) GAG content in AMSC:JCH co-cultures showed a greater than expected result based on GAG deposition in CH and MSC alone cultures, while little synergism was observed in JMSC:JCH co-cultures. (C) Alcian blue staining for proteoglycans (PG) on day 56: zonal JCHs alone (Left), co-cultures (Middle; JMSC:JCH and AMSC:JCH) and juvenile and adult MSCs cultured alone (Right). (Scale bar = 1 mm).

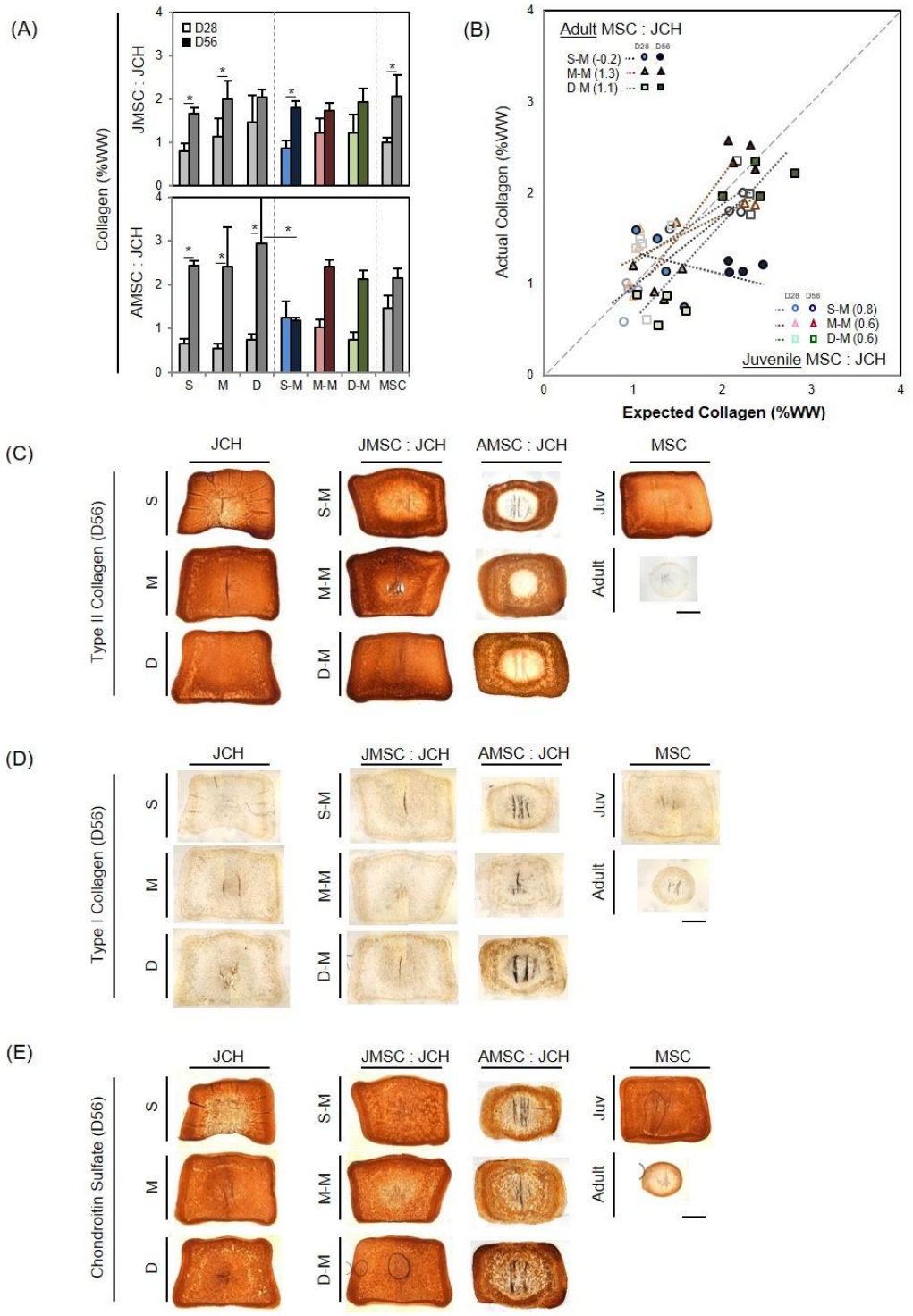

Figure 6-4: Collagen content and immunohistochemistry. (A) Collagen content (% WW). (B) Plot of co-culture efficacy for collagen content. (C-E) Immunohistochemistry for type II collagen (C), Type I collagen (D), and chondroitin sulfate (E) at day 56 (JCH = Left, Co-cultures = Middle, MSC = Right; Scale bar = 1 mm; $p<0.05$).

To evaluate efficacy of co-culture, mechanical properties and biochemical content was plotted on an X-Y plane based on expected versus actual findings **(Figure 6-2D, 3B and 4B)**. JMSC/JCH co-cultures groups (hollow shapes) showed largely independent contributions from each cell type (with no synergistic effect) in mechanical properties and biochemical content. That is, data largely fell on the line representing unity, where expected outcomes were the sum of the individual cell types. Conversely, there was a marked synergistic effect in AMSC/JCH co-cultures (solid shapes). Middle and deep zone CHs co-cultured with MSCs produced greater construct properties in both co-culture groups. However, collagen content showed independent effects **(**no synergism, **Figure 6-4B)**. Histological assessment confirmed these findings, showing that Alcian Blue staining for proteoglycan (PG) and immunohistochemistry for chondroitin sulfate (CS) was evident for all groups except for AMSC-laden constructs **(Figure 6-3C and 4E)**. Type II collagen staining was distributed throughout the constructs for all groups, except for AMSCs cultured alone **(Figure 6-4C)**.

6.3.2 Close proximity is required for the co-culture effect.

AMSCs and JCHs were either well distributed or well separated (by design) throughout the constructs based on their respective culture configurations **(Figure 6-5B)**. AMSCs in both the 'fused' and 'barrier' group aggregated together, resulting in the formation of several small masses or a single mass with a 70% decrease in diameter **(Figure 6-5B and 6-6)**. Conversely, those formed into the 'mixed' configuration maintained initial construct geometry with only mild contraction (-25%) **(Figure 6-5C)**. Mechanical properties and GAG content for the 'mixed' group increased with time, reaching 240 kPa and 3%WW by day 56, while properties in the 'fused' and 'distanced' groups (combined from both MSCs and CHs sublayers) were significantly lower (36 kPa and 1.5% WW for the 'fused' group and 2 kPa and 1.4 %WW for the 'distanced' group) **(Figure 6-5D and**

E). The equilibrium modulus of the 'mixed' group was 6.7 ($p<0.001$) and 120 times ($p<0.001$) higher than the fused and barrier groups, respectively.

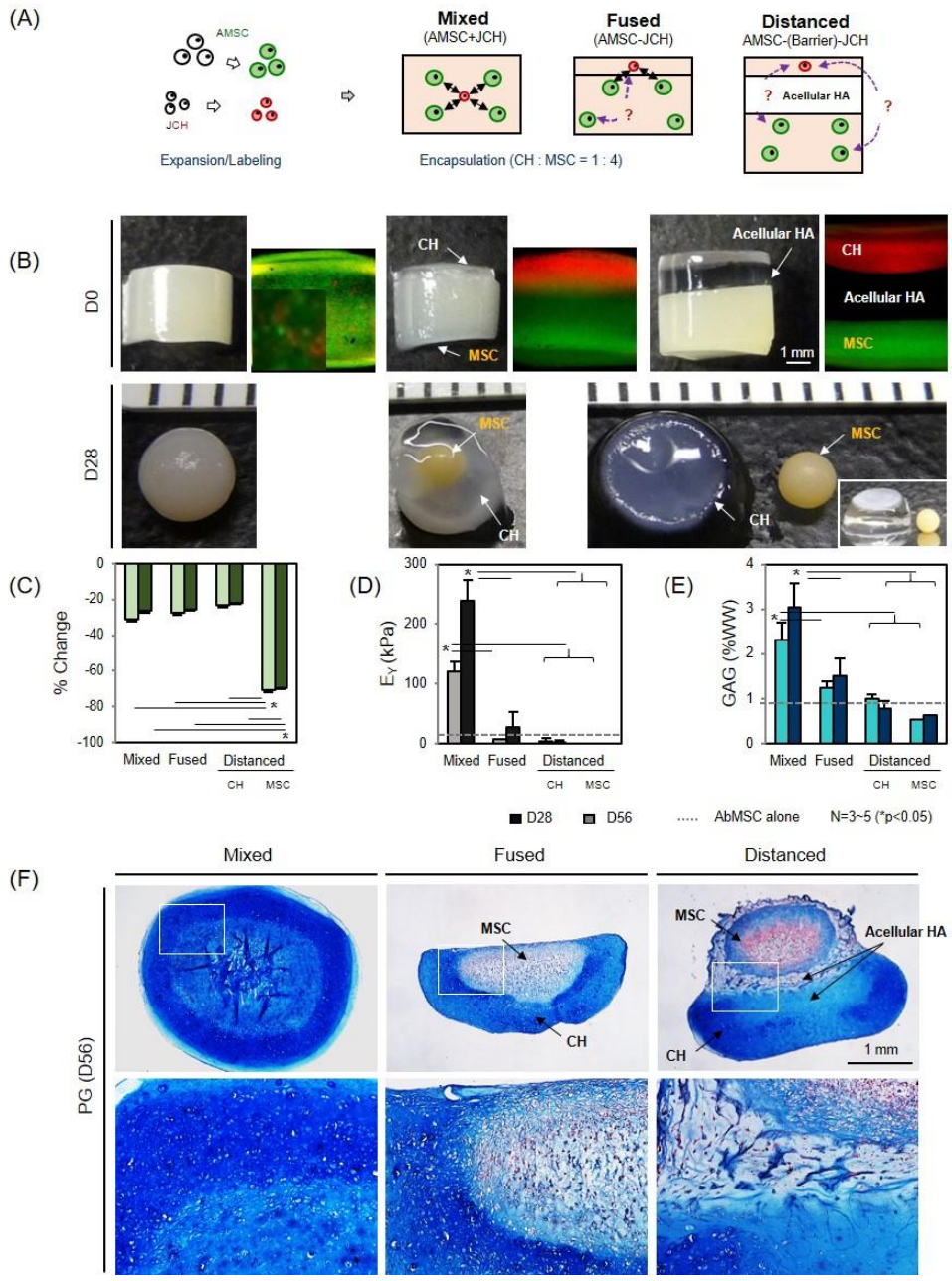

Figure 6-5: CH/MSC co-cultures require close cell proximity.

(A) AMSCs (green) and JCHs (red) were labeled using CellTracker and seeded in HA hydrogels (60 million cells/mL; JCH:AMSC = 1:4) at varying distances by forming

constructs that were 'mixed' (close cell-cell relationship), 'fused' (further cell-cell relationship), or 'distanced' (distanced cell-cell relationship). (B) Gross images of the three different configurations at day 0 and 28. Mixed (Left), Fused (Middle) and Distanced (Right) configurations and the distribution of individual subpopulations (AMSC=green and JCH=red). (C) Percent (%) change in construct volume (D), Equilibrium modulus (E_Y), (E) GAG content (%WW) (Darker bars = day 28, Lighter bars = day 56; dashed line = AMSC alone at day 56; N=3-5/group). (F) Alcian blue staining on day 56 of constructs formed in the mixed (left), fused (middle), and distanced (right) configurations (scale bar = 1 mm).

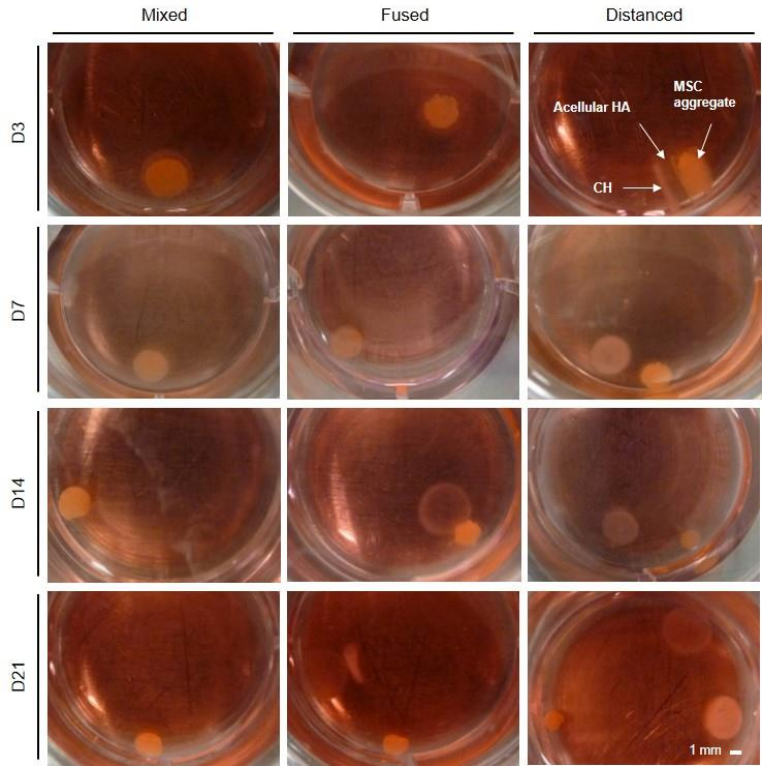

Figure 6-6: Gross appearance of 'mixed', 'fused' and 'distanced' co-cultures of juvenile CH and Adult MSC. Images of mixed (Left), fused (Middle) and distanced (Right) constructs on day 3, 7, 14 and 21 (Scale bar = 1 mm).

Similarly, GAG content for the mixed group was 2 times higher than the other groups ($p<0.001$). The 'mixed' group showed robust PG deposition through the construct at day

56, whereas the ‘fused’ and ‘barrier’ groups showed dense matrix deposition only on the area where JCHs were located **(Figure 6-5F)**. Interestingly, AMSCs, with no close contact to JCHs in the ‘fused’ and ‘distanced’ groups, produced little or no matrix, whereas some AMSCs near the border of JCHs produced some matrix in the ‘fused’ group. These findings support the notion that CH and MSC must be in close proximity for the co-culture effect to operate.

6.3.3 AMSCs in co-culture internalize intracellular factors released from JCHs, altering their transcriptional profile

To investigate molecular pathways involved in the co-culture effect, we evaluated the molecular profiles of AMSCs that were co-cultured (CO) with JCHs, and compared them to AMSCs that were cultured alone (AMSC). AMSCs that were cultured alone (AMSC_green) mostly retained their initial (green) CellTracker label, regardless of TGF supplementation (90% retention) **(Figure 6-7B)**. JCHs cultured alone (red) showed varying signal intensities, with 55% being bright red, 12.6% being dim red, and 15% that were negative (data not shown). For the AMSC/JCH co-culture group, some AMSCs were retained their original green (CO_green) label in the absence or presence of TGF (50% retention), while other AMSCs became double positive (CO_DP, a 40~50% shift in the population). To further investigate this phenomenon, we closely examined these cells in constructs at early time points in culture to determine when and how they began to manifest this double positive characteristics. Mixed cell-laden constructs (AMSC/JCH) were first observed after 15 hours in co-culture, and no exchange of intracellular contents was observed **(Figure 6-7B and 8)**.

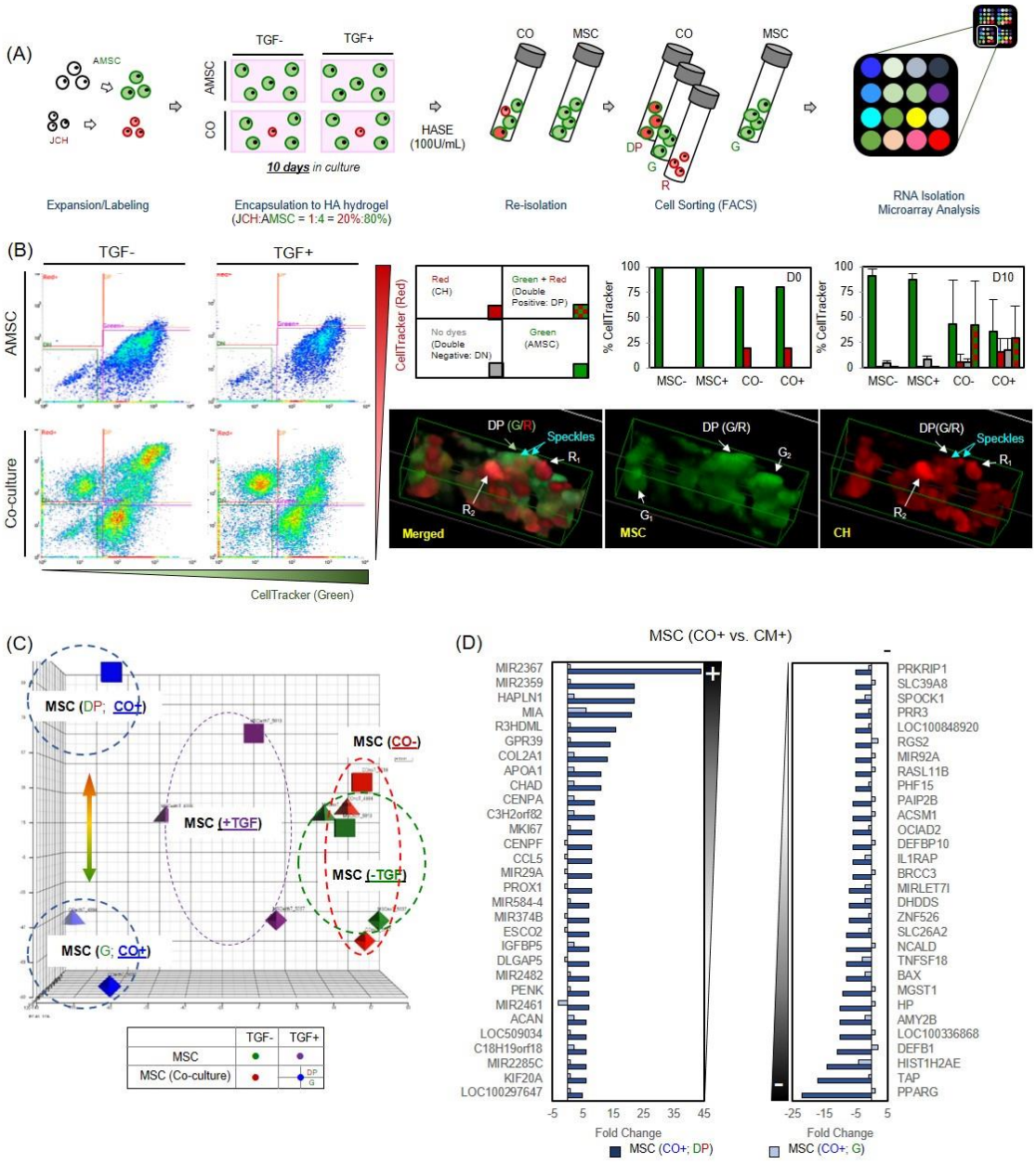

Figure 6-7: Molecular profiling of co-culture pathways in adult MSCs.

(A) AMSC (green) alone or AMSC/JCH (green/red) co-cultured populations were seeded in HA hydrogels at 20 million cells (JCH:AMSC = 1:4) and cultured in the presence (CM+) or absence (CM-) of TGF. After 10 days, cells were re-isolated by hyaluronidase digestion and sorted based on their CellTracker dyes using FACS. Sorted MSCs (green or double positive (DP)) were used for RNA isolation, followed by microarray and pathway analyses. (B) FACS results (left) showed double-positive expression in co-culture groups, regardless

of TGF inclusion. Some MSCs in co-culture groups became double positive (DP; ~50% MSCs) after 10 days (Top right). 3D reconstructions from confocal microscopy showed the appearance of red speckles in otherwise green cells (Bottom right). (C) Principle component analysis (PCA) showed no differences between MSCs alone and MSCs that were in co-culture in the absence of TGF. In the presence of TGF, the MSC alone group shifted away from undifferentiated MSCs. MSCs that were co-cultured with CHs for 10 days showed an even further shifted from MSCs alone with TGF. Moreover, MSCs that from co-cultures that were double positive (DP) were distinct from those that were only green. (D) List detailing the 30 genes showing the greatest fold change with co-culture (positive on left and negative on right). AMSCs (DP and G only) co-cultured with JCHs were compared to AMSC cultured alone (Darker bars = CO+: DP vs. MSC+: G; Lighter bars = CO+: G vs. MSC+ G)

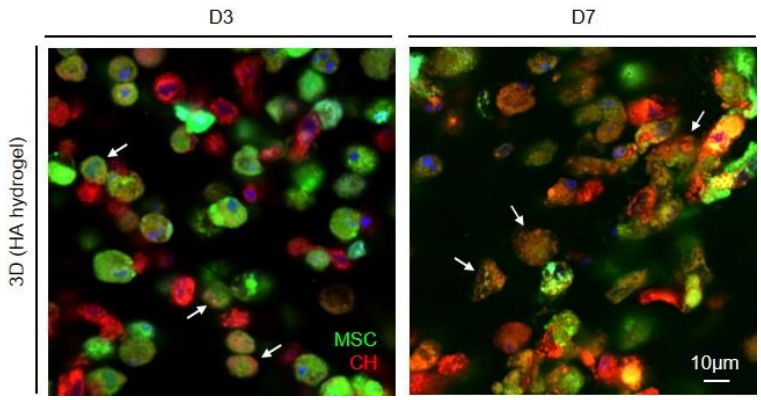

Figure 6-8: Transfer of intracellular contents in JCH /AMSC co-cultures.

Confocal images of CH (red) and MSCs (green) in HA hydrogels on days 3 and 7, showing increasing number of double positive cells (DP, arrow heads) (Scale bar = 10 μm)

By day 3 in co-culture, however, we noted cells that showed both green and red (double positive), in addition to the majority green only and red only cells. When these cells were reconstructed in 3D, there was the clear area of overlap, where red speckles appeared within in green cells, suggesting transfer from the CH population to the MSC population.

By day 7, more red speckles were observed in otherwise green cells, and some red cells had dimmed, losing the majority of their red dye.

Molecular profiling and principal component analysis (PCA) showed that there was no effect of co-culture in the absence of TGF (CO- vs. AMSC-) **(Figure 6-7C)**. Conversely, in the presence of TGF, the expression cluster for AMSCs markedly shifted (AMSC+ vs. AMSC-). AMSCs taken from the co-culture group that had retained their green signal (CO+ G) had further shifted in expression compared to AMSCs alone (AMSC+), and AMSCs that were double positive (CO+ DP) also differed from those remained green (CO+ G). To further define these differences, we evaluated the fold change in CO+ vs. CM+ (e.g., [CO+ DP vs. MSC+ G] or [CO+ G vs. MSC+G]) and outline the 30 genes with the greatest fold changes **(Table 6-1)**. Interestingly, this list was quite distinct based on whether the AMSC was green or double positive. Further, when comparing DP and G directly, the list of genes from AMSCs was highly related to cartilage development and matrix formation (e.g., HAPLN1, MIA, COL2A1, CHAD, IGFBP5 and ACAN), proliferation/mitosis, anti-apoptosis, anti-inflammation, and suppression of osteogenesis and adipogenesis **(Table 6-2~6-4)**. In comparison to green only AMSCs, those that were double positive group had expression changes of 5 to 44 fold **(Figure 6-7D)**.

Table 6-1: Positive and negative fold changes in AMSCs that became double positive (DP) or remained green (G) over 10 days of culture, with and without TGF-beta, compared to AMSCs that were cultured on their own (MSC+ G)

AMSC (CO+ DP)

Gene Symbol	CO+ vs. CM+	CM+ vs. CM-	CO- vs. CM-	CO+ vs. CO-
MIR2367	44	1	1	41
MIR2359	22	-2	5	3
HAPLN1	22	2	35	1
MIA	21	3	35	2
R3HDML	16	1	-1	18
GPR39	14	-1	-1	20
COL2A1	13	-1	1	8
APOA1	11	2	2	10
CHAD	11	5	-2	85
CENPA	9	1	-1	15
C3H2orf82	9	1	2	4
MKI67	8	-1	-1	9
CENPF	8	2	1	13
CCL5	8	1	2	6
MIR29A	8	-1	-1	8
PROX1	8	-1	-1	8
MIR584-4	7	-1	2	4
MIR374B	7	-2	-1	5
ESCO2	7	-2	-1	4
IGFBP5	7	-3	-1	3
DLGAP5	7	1	1	8
MIR2482	7	-1	-1	6
PENK	7	5	-1	39
MIR2461	7	2	1	10
ACAN	6	9	12	5
LOC509034	6	-1	1	4
C18H19orf18	6	-1	-1	6
MIR2285C	6	2	2	6
KIF20A	6	1	-1	7
LOC100297647	5	-1	-1	7

Gene Symbol	CO+ vs. CM+	CM+ vs. CM-	CO- vs. CM-	CO+ vs. CO-
PRKRIP1	-5	-1	-2	-3
SLC39A8	-5	-6	-1	-18
SPOCK1	-5	-3	-1	-10
PRR3	-5	2	-1	-3
LOC100848920	-5	-2	-1	-9
RGS2	-5	-1	-2	-4
MIR92A	-5	1	1	-5
RASL11B	-5	5	1	-1
PHF15	-5	-2	-1	-8
PAIP2B	-6	2	2	-6
ACSM1	-6	-13	-1	-77
OCIAD2	-6	-3	2	-31
DEFB10	-6	-2	-2	-6
IL1RAP	-6	-2	1	-14
BRCC3	-6	-1	1	-8
MIRLET7I	-7	-1	1	-9
DHDDS	-7	-1	-2	-4
ZNF526	-7	1	-1	-5
SLC26A2	-8	-3	1	-26
NCALD	-8	4	-2	-1
TNFSF18	-8	8	-1	1
BAX	-8	-1	-1	-8
MGST1	-9	-6	1	-64
HP	-10	-3	-1	-26
AMY2B	-10	-3	-1	-30
LOC100336868	-10	2	2	-12
DEFB1	-11	-2	-1	-15
HIST1H2AE	-14	-1	1	-16
TAP	-17	2	-1	-9
PPARG	-22	-3	-1	-53

AMSC (CO+ G)

Gene Symbol	CO+ vs. CM+	CM+ vs. CM-	CO- vs. CM-	CO+ vs. CO-
MIR2335	6	-1	-1	6
LOC100337095	6	-1	-1	5
LOC100847384	6	1	-1	7
MIA	6	4	10	2
LOC100847384	5	1	-1	6
LOC100140002	5	1	1	6
TSPY	5	-1	1	5
ANGPTL5	5	-1	-1	5
LOC100337132	4	1	-1	6
LOC100337080	4	1	-1	5
MIR15A	4	-2	-1	3
OR8U1	4	-1	-1	4
LOC100295153	4	1	1	4
LOC788067	4	1	1	4
LOC617033	4	-1	-1	4
LOC789022	4	-1	1	3
MALL	4	1	2	2
LOC100337227	4	-5	-2	2
SAA3	4	-4	4	-5
LOC517139	4	2	2	4
LOC614886	4	1	1	4
LOC786014	3	1	1	3
LOC100337377	3	1	-1	4
OR8G5	3	1	-1	4
LOC100137758	3	1	1	4
LOC100301420	3	-2	-1	2
TCEANC	3	-1	1	3
TSPY	3	1	1	4
LOC783287	3	1	-1	3
LOC782475	3	-1	-1	3

Gene Symbol	CO+ vs. CM+	CM+ vs. CM-	CO- vs. CM-	CO+ vs. CO-
TNFSF18	-3	2	-1	-1
KPNA6	-3	1	1	-3
IGIP	-3	1	1	-3
SEPX1	-3	-2	-1	-5
COMMD10	-3	-1	-1	-3
CHEK1	-3	3	1	-1
ARHGAP24	-3	2	-1	-1
AKR1B1	-3	2	1	-2
MFAP5	-3	2	1	-2
PIR	-3	-2	-1	-4
EIF2S3Y	-3	1	1	-3
SERPINB10	-3	6	-1	3
CDC6	-3	9	1	2
RSAD2	-3	3	-1	1
RAPGEF4	-3	1	1	-3
CALCRL	-3	-4	-1	-11
IFIT3	-3	1	-1	-2
MIR2414	-3	3	1	-1
CHPT1	-3	2	1	-2
AMTN	-3	20	-1	8
DRD3	-3	3	1	-1
EFEMP1	-3	-8	-1	-19
MIR2463	-3	2	1	-3
CCK	-4	5	-1	2
P2RY1	-4	8	1	2
C8H9orf85	-4	1	-1	-2
HIST1H2AE	-4	2	2	-3
CCRL1	-4	4	1	-2
MIR2384-1	-4	2	-1	-3
GGCT	-5	3	1	-2

Table 6-2: Impact of JCH-derived molecular factors to alter genomic profiles of AMSCs within the same constructs and their gene-matched fold changes

AMSC (CO+ DP)

Gene Symbol	CO+ vs. CM+	CM+ vs. CM-	CO- vs. CM-	CO+ vs. CO-
MIR2367	44	1	1	41
MIR2359	22	-2	5	3
HAPLN1	22	2	35	1
MIA	21	3	35	2
R3HDML	16	1	-1	18
GPR39	14	-1	-1	20
COL2A1	13	-1	1	8
APOA1	11	2	2	10
CHAD	11	5	-2	85
CENPA	9	1	-1	15
C3H2orf82	9	1	2	4
MKI67	8	-1	-1	9
CENPF	8	2	1	13
CCL5	8	1	2	6
MIR29A	8	-1	-1	8
PROX1	8	-1	-1	8
MIR584-4	7	-1	2	4
MIR374B	7	-2	-1	5
ESCO2	7	-2	-1	4
IGFBP5	7	-3	-1	3
DLGAP5	7	1	1	8
MIR2482	7	-1	-1	6
PENK	7	5	-1	39
MIR2461	7	2	1	10
ACAN	6	9	12	5
LOC509034	6	-1	1	4
C18H19orf18	6	-1	-1	6
MIR2285C	6	2	2	6
KIF20A	6	1	-1	7
LOC100297647	5	-1	-1	7

Gene Symbol	CO+ vs. CM+	CM+ vs. CM-	CO- vs. CM-	CO+ vs. CO-
PRKRIP1	-5	-1	-2	-3
SLC39A8	-5	-6	-1	-18
SPOCK1	-5	-3	-1	-10
PRR3	-5	2	-1	-3
LOC100848920	-5	-2	-1	-9
RGS2	-5	-1	-2	-4
MIR92A	-5	1	1	-5
RASL11B	-5	5	1	-1
PHF15	-5	-2	-1	-8
PAIP2B	-6	2	2	-6
ACSM1	-6	-13	-1	-77
OCIAD2	-6	-3	2	-31
DEFB10	-6	-2	-2	-6
IL1RAP	-6	-2	1	-14
BRCC3	-6	-1	1	-8
MIRLET7I	-7	-1	1	-9
DHDDS	-7	-1	-2	-4
ZNF526	-7	1	-1	-5
SLC26A2	-8	-3	1	-26
NCALD	-8	4	-2	-1
TNFSF18	-8	8	-1	1
BAX	-8	-1	-1	-8
MGST1	-9	-6	1	-64
HP	-10	-3	-1	-26
AMY2B	-10	-3	-1	-30
LOC100336868	-10	2	2	-12
DEFB1	-11	-2	-1	-15
HIST1H2AE	-14	-1	1	-16
TAP	-17	2	-1	-9
PPARG	-22	-3	-1	-53

AMSC (CO+ G)

CO+ vs. CM+	CM+ vs. CM-	CO- vs. CM-	CO+ vs. CO-
1	2	1	2
1	-1	4	-5
2	4	7	1
6	4	10	2
1	1	-1	2
1	-1	1	1
2	1	-1	3
2	4	-1	8
2	17	1	27
2	5	1	8
2	1	-1	2
1	5	1	5
-1	3	-1	3
-1	1	1	-1
-1	1	-1	1
-1	1	1	1
1	-1	-1	-1
-1	2	1	1
-1	2	1	1
2	-3	-1	-1
-1	5	1	4
1	-1	1	1
1	4	1	4
-3	1	-1	-2
2	11	7	3
1	-1	1	1
2	-1	1	1
1	-1	2	-2
1	3	1	3
1	-1	-1	-1

CO+ vs. CM+	CM+ vs. CM-	CO- vs. CM-	CO+ vs. CO-
-1	-1	-1	-1
1	-1	-1	-1
-2	-4	-1	-7
-1	-1	1	-2
-1	-9	-2	-4
2	-6	-1	-2
1	-2	2	-3
1	2	1	3
-1	-2	-1	-2
1	-1	1	-1
1	-17	-1	-15
-1	-2	-1	-3
1	-1	1	-2
-2	-3	-1	-6
1	-2	-1	-1
-2	-2	-1	-3
-2	1	1	-3
-1	1	1	-1
-1	-2	1	-2
1	2	1	1
-3	2	-1	-1
-2	-1	-1	-2
1	-6	-1	-5
1	-1	1	-1
-2	-7	-1	-16
1	-1	1	-1
2	-17	-1	-9
-4	2	2	-3
-1	-1	1	-1
1	-10	-1	-8

Table 6-3: Details of genes that showed positive fold changes in AMSCs with co-culture

Gene Symbol	Gene Title	Description/ Function	Reference
MIR2367	microRNA 2367	Bos taurus	NCBI Gene
MIR2359	microRNA 2359	Bos taurus	NCBI Gene
HAPLN1	Hyaluronan/PG link protein 1 (CRTL1: cartilage link protein 1)	Contribute to ECM stability and flexibility; Regulated by SOX9	Binette et al., 1994 JBC Spicer et al., 2003 JBC Ikuyo et al., 2004 JBC Fang et al., 2014 Arteriosc Thromb Vasc Biol
MIA	Melanoma inhibitory activity (CD-RAP: cartilage-derived retinoic acid sensitive protein)	Found in articular cartilage; Regulated by SOX9	Sakano et al., 1999 JBMR Bosserhoff et al., 2003 Biomaterials
R3HDML	R3H domain containing like	Peptidase inhibitor (a putative serine protease inhibitor); Cysteine-rich secretory protein; May act as an anti-fungal agent	Gibbs et al., 2008 Endocr Rev
GPR39	G protein-coupled receptor 39	Block Hedgehog signaling that causes heterotopic ossification	Regard et al., 2013 Nat Med Bassilana et al., 2014 Nat Chem Biol
COL2A1	Collagen, type II, alpha 1	Major component of articular cartilage	
APOA1	Apolipoprotein A-1	Main functional protein of HDL (high-density lipoprotein); Transports endogenous microRNAs to recipient cells; Decrease accumulation of atherosclerosis by removing LDL	Vickers et al., 2011 Nat Cell Biol Chen et al., 2012 Trends Cell Biol Wu et al., 2014 Arterioscler Thromb Vasc Biol Michell et al., 2016 BBA
CHAD	Chondroadherin	A leucine rich repeat ECM protein in cell-matrix interaction; Binds cells via integrin and cell surface PGs; Acts as an anchor to ECM by binding to collagens	Hessle et al., 2013 PLOSOne Batista et al, 2014 Mat Biol Tillgren et al, 2015 JBC
CENPA	Centromere protein A (Histone H3 variant)	Recruited to chromatin in DNA damage; Essential for growth and development;	Van Hooser et al., 2001 JCS Zeitlin et al., 2009 PNAS
C3H2orf82	Chromosome 3 open reading frame, human C2orf82	Chromosome 3 C2orf82 homolog	NCBI Gene
MKI67	Marker of proliferation Ki-67 (Ki-67)	Reflect cellular proliferation rate; Exclusively expressed in proliferating cells (maintaining proliferation); Interact with KIF15	Gerdes et al., 1984 J Immunol Bullwinkel et al, 2006 JCP
CENPF	Centromere protein F (Mitosin)	Involved in proliferation, differentiation and stress response associated with ATF4	Yang et al, 2003 Cell Res Zhou et al., 2005 JBC Yan et al., 2012 Proteomics
CCL5	Chemokine (C-C motif) ligand 5; (RANTES; regulated on activation, normal T cell expressed and secreted)	CCR3 was expressed at the mRNA level and increased during MSC-derived chondrogenesis; Chemokine receptors were expredded in chondrocytes; Expressed in normal and OA cartilage; Exert anti-apoptotic effect mediated by Erk/Akt pathway;	Borzi et al., 2000 Arthritis Rheum Alaaeddine et al., 2001 Arthritis Rheum Mazzetti et al., 2004 Arthritis Rheum Djouad et al., 2007 Arthritis Res Ther Hofer et al., 2016 Stem Cell Res Ther
MIR29A	microRNA 29A	Up-regulated in normal cartilage; Inhibit osteonectin expression	Goldring et al., 2012 Trends Mol Med Shang et al., 2013 J Cell Mol Med Li et al., 2016 Mol. Cells
PROX1	Prospero homeobox 1	Regulate FGFRs expressed in proliferating or hypertrophic chondrocytes	Liu et al., 2002 Genes Dev Audette et al., 2015 Development
MIR584-4	microRNA 584-4	Bos taurus	NCBI Gene
MIR374B	microRNA 374B	Inhibit angiogenesis by targeting VEGF regulated by CCL3 through CCR1 and CCR5	Sohn et al., 2015 J Cancer Liao et al., 2015 Oncotarget
ESCO2	Establishment of sister chromatid cohesion N-acetyltransferase 2	An acetyltransferase that converts chromatin-bound cohesins to a tether-competent state; Induce mitosis and proliferation	Kim et al., 2008 BBRC Banerji et al., 2016 Dev Dyn
IGFBP5	Insulin-like growth factor binding protein 5	Regulate the availability of IGF-1, an anabolic factor involved in matrix synthesis and chondrocyte survival	Buechli et al., 2013 Stem Cells Dev
DLGAP5	Disc, large (Drosophila) homolog-associated protein 5	Promote cell proliferation, migration and invasion	Liao et al., 2013 PLOSOne
MIR2482	microRNA 2482	Bos taurus	NCBI Gene
PENK	Proenkephalin	Attenuate inflammation by stimulating secretion of IL-10	Milwid et al, 2014 Mol Ther
MIR2461	microRNA 2461	Bos taurus	NCBI Gene
ACAN	Aggrecan	Major component of articular cartilage	
LOC509034	Feline leukemia virus subgroup C cellular receptor family, member 2-like (FLVCR2)	Import heme and transport calcium-chelator complex; Regulate growth and calcium metabolism	Braiser et al., 2004 Exp Cell Res Duffy et al., 2010 Mol Cell Biol
C18H19orf18	Chromosome 18 open reading frame, human C19orf18	Chromosome 18 C19orf18 homolog	NCBI Gene
MIR2285C	microRNA 2285C	Bos taurus	NCBI Gene
KIF20A	Kinesin family member 20A	Expressed in healthy DNA; Mitotic cell cycle	Kim et al., 2014 PLOSOne
LOC100297647	Tumor protein, translationally-controlled 1-like (TCTP)	Anti-apoptosis	Liu et al., 2005 Mol Cell Biol Susini et al., 2008 Cell Death Diff Thebault et al., 2016 Sci Rep

Table 6-4: Details of genes that showed negative fold changes in AMSCs with co-culture

Gene Symbol	Gene Title	Description/Function	Reference
PRKRIP1	PRKR interacting protein 1 (IL11 inducible)		
SLC39A8	Solute carrier family 39 (zinc transporter), member 8	Majority of cancer tissues displayed cytoplasmic and/or membranous positivity at a various degree	
SPOCK1	Sparc/osteonectin, cwcv and kazal-like domains proteoglycan (testican) 1	Promote tumor growth and metastasis in cancer cells by activating the PI3K-AKT pathway	Shu et at., 2015, Mol Caner; Yang et al., 2015, Tum Biol; Chen et al., 2016, Drug Design Dev and Ther
PRR3	Proline rich 3	Induced by DNA damage response; Increase DNA-damage-induced apoptosis via mitochondrial death pathway; Localized in mitochondrial and interacted with Bcl-2 (pro-apoptotic activator)	Tibaldi et al., 2011, Biochem J Lou et al., 2013, Mol Oncol;
LOC100848920	Regulator of G-protein signaling 2-like	Accelerate hypertrophic differentiation; Regulate endochondral bone development	James et al., Mol Biol Cell. 2005
RGS2	Regulator of G-protein signaling 2, 24kDa		
MIR92A	microRNA 92A	Directly target Noggin3 mRNA (BMP antagonist), Promote craniofacial development and chondrogenic proliferation; Promote tumor proliferation and inhibit tumor apoptosis;	Ning et al., 2013 Dev Cell; Li et al., 2014, Exp Cell Res
RASL11B	RAS-like, family 11, member B	Play a role in TGFb1-mediated developmental processes such as inflammation, cancer and arteriosclerosis	Stolle et al., BBA 2007
PHF15	PHD finger protein 15	Zinc ion binding	
PAIP2B	Poly(A) binding protein (PABP) interacting protein 2B		
ACSM1 (also known as MACS1, BUCS1)	Acyl-CoA synthetase medium-chain family member 1 (Middle-Chain Acyl-CoA Synthetase 1; Butyryl Coenzyme A Synthetase 1)		
OCIAD2	OCIA domain containing 2	Cancer-related protein; Increase malignant progression	Nagata et al., 2012, Pathol Int; Zhang et al., 2014, Biomed Res Int
DEFB10	Beta-defensin 10	Antibacterial activity; Exist in neutrophils (WBC)	Selsted et al., 1993, JBC Sung et al., 2016, Cell Microbiol
IL1RAP	Interleukin 1 receptor accessory protein	Induce synthesis of pro-inflammatory proteins during infection, tissue damage or stress at the cell membrane	
BRCC3	BRCA1/BRCA2-containing complex, subunit 3	Promote activating inflammation	Py et al., 2012, Mol Cell
MIRLET7I	microRNA let-7i	Repress cell proliferation (i.e., tumor suppression)	Johnson, 2007, Cancer
DHDDS	Dehydrodolichyl diphosphate synthase	Promote trafficking of LDL-derived cholesterol; LDL correlates with ectopic bone formation in OA.	De Munter et al., 2013, Arthritis Res Ther
ZNF526	Zinc finger protein 526		
SLC26A2	Solute carrier family 26 (sulfate transporter), member 2; Diastrophic dysplasia sulfate transporter (DTDST)	Transmembrane glycoprotein. Cause diastophic dysplasia; Play a role in endochondral bone formation	Satoh et al., 1998, JBC; Lamb et al., 2007, Arthritis Rheum
NCALD	Neurocalcin delta	Neuronal calcium sensor family of calcium-binding protein	Terasawa et al., 1992 JBC
TNFSF18	Tumor necrosis factor (ligand) superfamily, member 18	Pro-apoptotic; Mediate NF-kB activation	Liang et al., 2014, Cell Trans
BAX	BCL2-associated X protein	Pro-apoptotic activator; Inhibit caspase activity by preventing the release of cytochrome C from the mitochondria	Oltval et al., 1993, Cell
MGST1	Microsomal glutathione S-transferase 1	Activated by oxidative stress	Aniya et al., 1993, Biochem Pharm
HP	Haptoglobin	Inflammation marker; Bind to hemoglobin in RBC (carrying O2) produced in bone marrow; (Low HP indicates low Hemoglobin (hypoxic condition))	Stevens et al., 2008, Arthritis Rheum; Drueke et al., 2012, Nephrol Dial Trans; Balakrishnan et al., 2014, Clin Proteomics
AMY2B	Amylase, alpha 2B (pancreatic)	Hydrolyze proteoglycan	
LOC100336868	Complement factor H-like	Produced (secreted) by MSCs; increased by TNF-a and interferon-r (IFN-r);	Ruddy et al., 1975 Ann NY Acad Sci; Tu et al., 2010, Stem Cells Dev
; LOC100335230	Beta-defensin 1-like	Microbicidal and cytotoxic peptides made by neutrophils; *Defensin in neutrophils (WBC)	Sung et al., 2016, Cell Microbiol; Selsted et al., 1993, JBC
HIST1H2AE	Histone cluster 1, H2ae/ Histone H2A type 1-B/E		
TAP	Tracheal antimicrobial peptide (Beta defensin)	Antibacterial effect. Beta defensin is secreted from MSCs via TLR4; A family of cysteine-rich antimicrobial peptides from neutrophils (WBC);	Sung et al., 2016, Cell Microbiol; Selsted et al., 1993, JBC
PPARG	Peroxisome proliferator-activated receptor gamma	Adipogenic marker; Promote the progression of PTOA	Ratneswaran et al., 2015 Arth Reum

6.3.4 Intercellular communication in AMSC/JCH co-cultures is mediated by extracellular vesicles.

From the earlier study, we noted that AMSCs became double positive with culture duration, while JCHs tended to remain red and show attenuated signal intensity **(Figure 6-7B and 8)**.

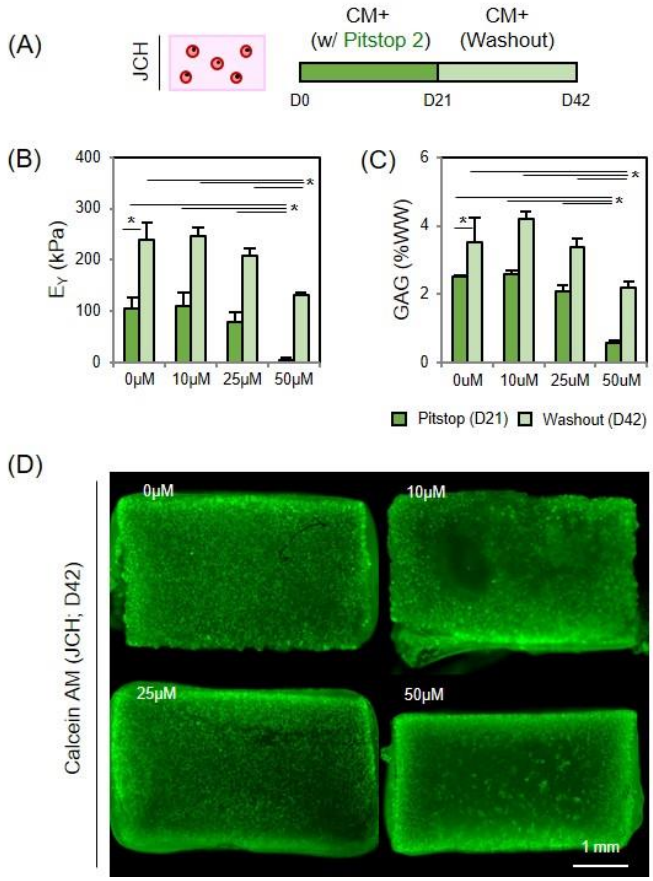

Figure 6-9: Calibration of inhibitors of clathrin mediated vesicle formation in JCH-seeded constructs. (A) To assess effect of Pitstop2 in exocytotic release of extracellular proteins, JCH-laden constructs were cultured in CM+ in the presence of Pitstop2 (0, 10, 25 and 50μM) for the first 21 days (D0-21) followed by 21 days of culture (D22-42) in the absence of Pitstop2. Analysis of mechanical properties (B, E_Y (kPa)), matrix content (C, GAG %WW) and viability (D, Calcein-AM labeling on day 42) indicated that a dose of 25μM would not inhibit normal chondrocyte matrix accumulation or viability (Scale bar = 1 mm, n=3-4/group; $p<0.05$).

Recent studies suggest that one of mechanism for intercellular communication is through the formation and transfer of extracellular vesicles (EVs). To determine whether the improvement in AMSC chondrogenesis resulted from trafficking of molecular factors through EVs, we blocked endocytic pathways through which EVs are internalized using Pitstop2, a blocker of clathrin-mediated endocytosis. To define an effective dose, juvenile CH only constructs were treated with varying doses of this inhibitor. Cells from all groups were viable and produced comparable ECM, though some attenuation in cellularity and construct properties was noted with the highest dose (50μM) employed **(Figure 6-9B-D)**.

Based on this, a moderate dose (25μM) was used. With this dose, the equilibrium modulus of JCH only and AMSC only constructs did not change markedly (JCHs: 389 kPa and 4.3% WW GAG without vs. 309 kPa and 3.5% WW GAG with; AMSCs: 34 kPa and 0.4 %WW GAG without vs. 0 kPa and 0.35 %WW GAG with, **Figure 6-10B and 11)**. Introduction of Pitstop2 at this dose into the co-culture group had an interesting effect, however. That is, construct properties (43 kPa and 1.9 %WW GAG) markedly decreased while those in co-culture without Pitstop2 inhibition reached 195 kPa (4.5 times greater) and 2.4 %WW GAG. Additionally, when imaged early in culture, the number of green AMSCs that had taken on red speckles was notably reduced with Pitstop2 **(Figure 6-10C and D),** with the number of DP AMSCs decreasing by 2.3 fold. Taken together, these data indicate that clathrin mediated endocytosis is essential for the positive co-culture effect to occur.

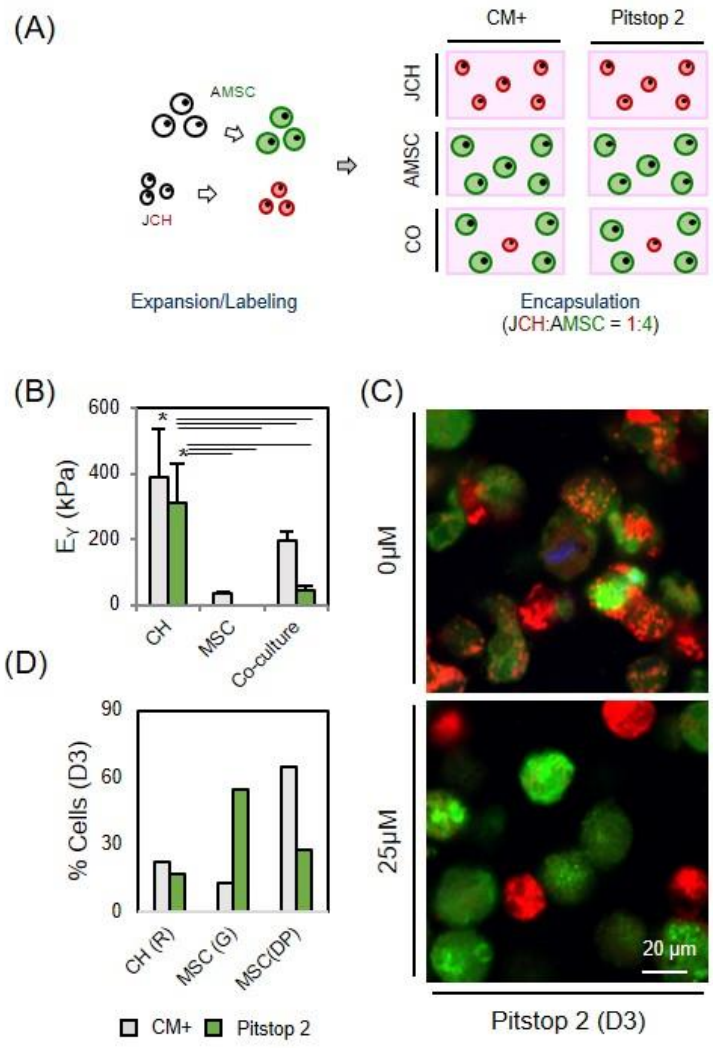

Figure 6-10: Extracellular vesicles (EVs) mediate intercellular communication in CH/MSC co-cultures. (A) AMSC alone (green), JCH alone (red) alone, or mixed co-cultured populations (CH:MSC = 1:4) were seeded in HA hydrogels at 60 million cells/mL and cultured in CM+ with/without Pitstop2 (25μM). Inhibition of vesicular transport with Pitstop2 decreased the mechanical properties of co-cultured constructs (B, E_Y (kPa)) and reduced transfer of cell contents as shown visually (C) and with quantification (D) of green, red, and double positive cells (Scale bar = 20μm; N=3-4; $p<0.05$).

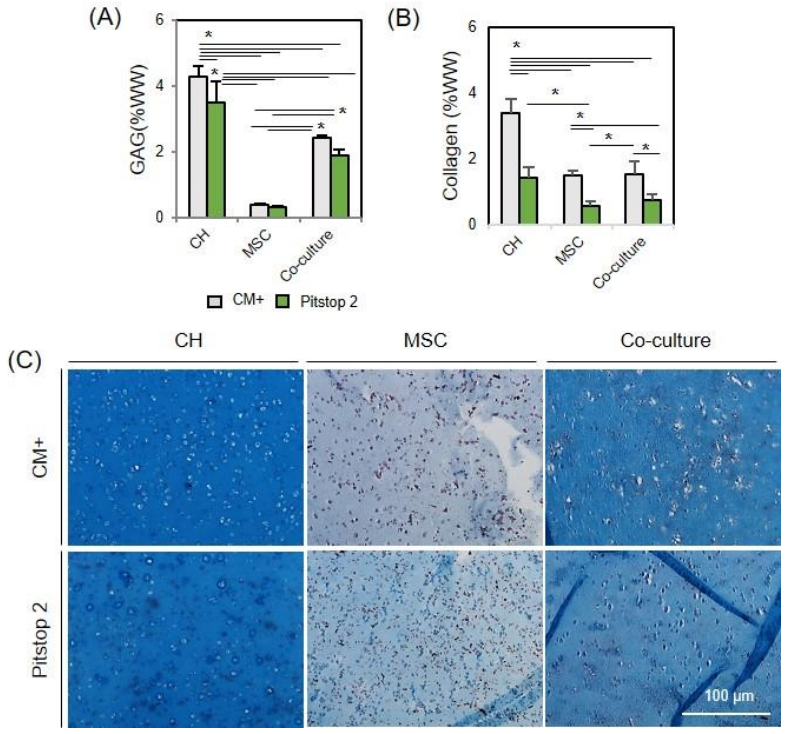

Figure 6-11: Biochemical content of constructs cultured with Pitstop 2

(A) GAG (% WW), (B) Collagen (% WW), (C) Alcian blue staining at day 42. (Scale bar = 100 µm, N=3-4/group; p<0.05)

6.4 Discussion

In this study, we determined the extent to which different zonal articular CHs co-cultured with MSCs in 3D HA hydrogels promoted MSC chondrogenesis. We also explored the impact of MSC age on this co-culture phenomenon. Cells remained viable throughout the culture period, with JCHs more prevalent on day 56 than on day 0. Zonal CH populations retained their native production levels, where superficial zone CH-laden constructs produced the lowest properties while middle and deep zone CH-laden constructs had the highest properties. This suggests that CHs retain their zonal characteristics, even after extensive culture expansion and seeding in this HA hydrogel system in the presence of TGF. We also found that JMSCs in HA culture grew well on

their own, with mechanical properties and GAG content equivalent to those of MZ or DZ CH-laden constructs. Given this already robust growth, no significant increases were observed in JMSC/JCH co-cultures, with measured (actual) properties mostly matching expected properties based on a simple mixture analysis. This result showed that co-culturing with JCHs did not improve JMSC chondrogenesis, indicating that young/healthy MSCs do not require additional chondrogenic induction via co-culture.

Unlike JMSCs, AMSCs failed to mature, even in the presence of TGF, and aggregated together in the HA hydrogel. When placed in co-culture, however, a synergistic enhancement of construct properties was observed for these AMSC/JCH co-cultures. These results are consistent with those using human MSCs from older patients (Fischer, Dickhut et al. 2010, Aung, Gupta et al. 2011, Bian, Zhai et al. 2011), where chondrogenic capacity of old/infirm MSCs was lower than young/healthy MSCs. These adult MSCs thus appear to be more sensitive to molecular factors secreted from juvenile CHs in the co-culture system. Histological analysis confirmed this co-culture effect, with all groups showing dense PG staining through the construct expanse, except for AMSCs cultured alone. Likewise, type II collagen staining for JCHs only, JMSC only and JCH:JMSC co-culture groups was dense through the constructs, except for JCH:AMSC groups, where dense matrix was produced in the peripheral region while little matrix was produced in the core. Type I collagen staining for all groups were generally weak, but the JCH:AMSC groups showed some type I collagen staining, mostly in the core. This might be due to the limited nutrient transport resulting from a contraction at early times in culture. Taken together, these findings show that a small population of juvenile chondrocytes cultured with adult MSCs can rescue the chondrogenic capacity of that adult stem cell population.

To better understand the operative conditions of co-culture, we next queried how the distance between the two cell populations, which may be critical for this intercellular communication, mediated the co-culture effect. We established three different culture designs: cells seeded in the HA hydrogel that were evenly distributed and close to one another (the 'mixed' group), cells separated into different regions of the construct that were adjacent to one another (the 'fused' group), or cells in different regions that were separated by and acellular 'spacer' (the 'distanced' group). Constructs with mixed cell populations maintained their initial geometry with only minor contraction, whereas MSC layers in the fused and distanced group aggregated immediately, with layers that gradually separated from one another. This suggests that the molecular factors operative in co-culture cannot traverse a great distance. When comparing outcomes, we found that the equilibrium modulus of the mixed group was 6.7 or 120 times greater than the fused or distanced groups, respectively. Histological assessment supported this data, showing that AMSCs mixed with JCHs produced dense matrix with homogeneous distribution, whereas in the fused or distanced groups produced little matrix. These results support the prevailing idea that proximity is essential for intercellular communication in co-culture systems (Lai, Kajiyama et al. 2013, de Windt, Saris et al. 2015), but did not address the mechanism or identity of the trafficked factors.

To determine the molecular factors and pathways potentially mediating the co-culture effect, we further carried out genome-wide analyses of fluorescently labeled AMSC populations. While AMSC alone retained their fluorescent staining (color) regardless of TGF, 50% of AMSCs in the co-culture group shifted to a double positive phenotype (CO_DP; expressing green and red in one single cell), while the remainder were green only (CO_G). Confocal microscopy confirmed that red speckles appeared in green cells, but not vice versa, suggesting directional transport of intracellular content from red

chondrocytes to green AMSCs. Microarray analysis showed a strong shift in expression patterns of AMSCs in the presence of TGF (chondrogenically induced AMSCs) compared to those without TGF. Furthermore, in the presence of TGF, AMSCs mixed with JCHs (CO+) were further shifted in their expression from chondrogenically induced AMSCs alone (TGF+). Interestingly, those AMSCs that remained green only (CO+ G) were different from those that had become double positive (CO+ DP).

Analysis of expression profiles from AMSCs that became double positive (AMSCs: CO_DP) or remained green only (AMSCs: CO_G) compared to AMSCs (AMSC: G only) that were never co-cultured with JCHs identified a number of genes highly related to cartilage development and matrix formation. For instance, this data showed that expression of MIA in DP AMSCs or green only AMSCs was 22 or 6 fold higher than in AMSCs alone cultured in the presence of TGF. MIA (melanoma inhibitory activity), also referred to cartilage derived retinoic acid-sensitive protein (CD-RAP), is a small, secreted protein found in cartilage and in malignant melanomas (Bosserhoff, Kondo et al. 1997, Bosserhoff and Buettner 2003). MIA/CD-RAP is an important regulator of chondrogenesis, and activates p54nrb transcription mediated by transcription factor YBX1 (Schmid, Meyer et al. 2013). Of note, although MIA/CD-RAP cannot promote chondrogenic differentiation of human MSCs on its own, when it is combined with it can drive chondrogenic differentiation and block osteogenic differentiation (Schubert, Schlegel et al. 2010). We also noted that expression of PPARG (peroxisome proliferator-activated receptor gamma), an adipogenic marker that promotes the progression posttraumatic osteoarthritis (PTOA), was expressed at a level 22 fold lower in double positive AMSCs compared to AMSCs alone. Moreover, increased expression of GPR39 (G protein-coupled receptor 39) and RGS2 (regulator of G-protein signaling 2) in the double positive group may have also contributed to AMSC chondrogenesis by blocking

hedgehog signaling that causes heterotopic ossification (Regard, Malhotra et al. 2013, Bassilana, Carlson et al. 2014) or suppressing hypertrophic differentiation (James, Appleton et al. 2005). Other important molecular factors include microRNAs (miRNAs) (Chen, Liang et al. 2012), which have been implicated in intercellular communication. These small non-coding RNAs are secreted via extracellular vesicles (EVs). Recent studies have shown that EVs specifically target recipient cells to deliver protein, mRNAs and lipids and also initiate downstream signaling pathways (Valadi, Ekstrom et al. 2007, Kosaka, Iguchi et al. 2010). Several studies have demonstrated that MIR29A is up-regulated in normal cartilage and inhibits osteonectin expression (Goldring and Marcu 2012). We found that expression of MIR29A in double positive AMSCs and green only AMSCs in co-culture was 8 fold higher than AMSC cultured alone in TGF. While the mechanism was not tested in this study, the pathways identified may suggest that, in the context of TGF, JCHs deliver important molecular factors to AMSCs through extracellular vesicles (EVs) to transform their molecular profiles and promote chondrogenesis, proliferation/mitosis, anti-apoptosis, anti-inflammation, and phenotypic stability. Additional pathway analysis and validation of the gene sets that were differentially regulated with co-culture is now underway.

The above findings strongly suggest that EVs are secreted from JCHs and are internalized by the AMSCs to change their phenotype. To validate this hypothesis, we blocked key intercellular communication mechanisms and determined whether such blockade would influence the CH-MSC co-culture phenomenon. Results from these studies showed that the modulus of co-cultured constructs decreased substantially with inhibition of clathrin coated vesicles by Pitstop 2. Further, confocal microscopy showed a reduction in the number of AMSCs that had become double positive. Although GAG content reached similar levels with inhibition of clathrin, expression of link protein

(HAPLN1) was changed by 22 fold, suggesting that this might explain the observed differences in mechanical properties. Recent studies have shown that cell surface receptors (e.g., TGF-β receptors, G-protein-coupled receptors) are internalized via clathrin-coated vesicles that promote TGF-β-mediated Smad activation and transcriptional responses although receptor-mediated endocytosis is not imperative for TGF- β (Di Guglielmo, Le Roy et al. 2003, Chen 2009). This may explain underlying mechanisms of co-culture, at least in part.

Taken together, this work demonstrated that passaged JCHs retain their chondrogenic capacity with zonal characteristics in the presence of TGF, and that rejuvenation of MSCs co-culture with chondrocytes is age-dependent. Additionally, we show that the co-culture phenomenon is only operable when cells are close to one another. Studies blocking mechanisms of intercellular communication suggest that EV-coated molecular factors from JCHs are shuttled to AMSCs using clathrin-mediated endocytosis, and that the contents of these EVs activate anabolic signaling pathways while suppressing catabolic activity in recipient cells **(Figure 6-12)**. This in turn enabled the aged/infirm MSCs to operate as though they were young/healthy functional chondrocyte-like cells. Identifying the molecular factors and vesicular pathways that underlie co-culture might lead to new biologics or other therapeutics to improve functional tissue engineering using adult autologous MSCs, and may ultimately obviate the need for such complicated co-culture systems, increasing the likelihood for clinical translation.

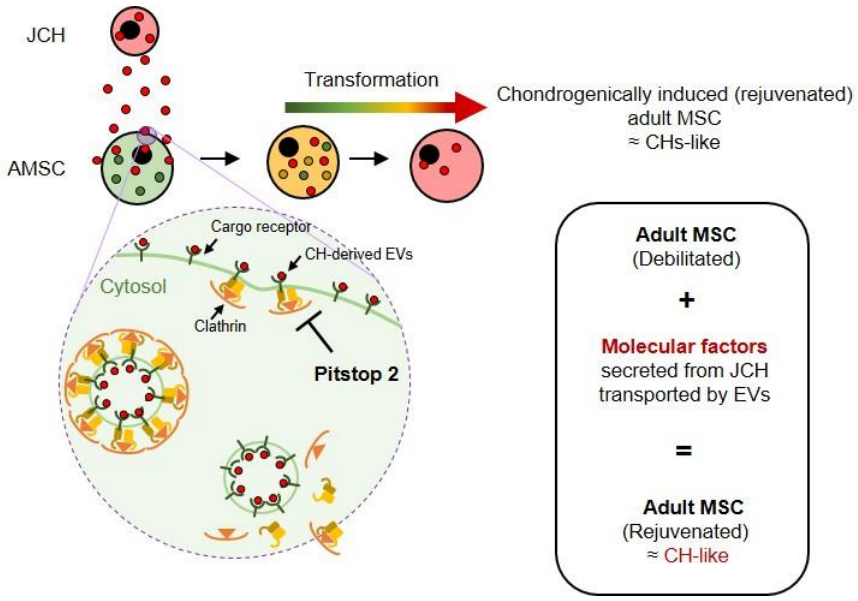

Figure 6-12: Schematic showing how transfer of molecular factors via EVs mediates the CH/MSC co-culture phenomenon. Extracellular vesicles (EVs) secreted from releasing cells (Juvenile CH) travel through the extracellular space to receiving cells (Adult MSC) and enter via clathrin-mediated endocytosis. The contents of these internalized vesicles enable AMSCs to take on an improved chondrogenic capacity, enhancing the function of engineered tissues compared to those formed from MSCs alone.

CHAPTER 7: Enhanced Nutrient Transport Improves the Depth-dependent Properties of Tri-layered Engineered Cartilage Constructs with Zonal Co-culture of Chondrocytes and MSCs

7.1 Introduction

Articular cartilage provides a nearly frictionless load-bearing surface in diarthrodial joints. This functionality is attributed to extracellular matrix (ECM) molecules (e.g., collagens, proteoglycans (PG), lubricin (Rhee, Marcelino et al. 2005) and elastin (Mansfield, Yu et al. 2009, He, Wu et al. 2013)) that are secreted by chondrocytes (CH) residing within the tissue. These cells have a distinct size, morphology, orientation, and matrix forming capacity, based on their zone of origin (e.g., superficial (SZ), middle (MZ), and deep zone (DZ)) (Mow, Wang et al. 1999, Poole, Kojima et al. 2001). The tissue itself also shows marked differences in composition and mechanics as a function of depth, where it is proteoglycan-rich and proteoglycan-rich and stiffest in compression in the deep zone, and collagen-rich and weakest in compression (and strongest in tension) in the superficial zone. Given the complexity of native tissue, recapitulating the morphological and functional properties of articular cartilage has a challenge in cartilage tissue engineering (Buckwalter and Mankin 1998, Poole, Kojima et al. 2001). Indeed, most early studies in the field focused on optimizing bulk properties of cell-laden constructs using a mixed pool of cells, ignoring zonal features. While these constructs achieved overall construct properties approaching native levels, they did not match native tissue depth-dependence. More recently, several groups have taken advantage of persistence of zonal characteristics of CHs isolated from different regions of the tissue. These studies have shown that CHs from different depths retain their zonal characteristics through expansion and in 3D culture systems. For example, CHs isolated from deep zone cartilage produced more PG than those from the superficial zone (Kim, Sharma et

al. 2003, Klein, Schumacher et al. 2003, Cheng, Conte et al. 2007, Klein, Malda et al. 2009, Ng, Ateshian et al. 2009). Interestingly, when these zonal CHs were separately seeded into layered hydrogel constructs, zonal CHs established engineered constructs with some degree of depth dependence (Kim, Sharma et al. 2003, Cheng, Conte et al. 2007, Sharma, Williams et al. 2007, Ng, Ateshian et al. 2009).

While CHs have been broadly used as a primary cell source in cartilage tissue engineering, their scarcity is a major clinical limitation. For that reason, mesenchymal stem cells (MSCs) have been introduced as an alternative cell source for cartilage therapeutics. Unlike CHs, MSCs can be isolated from autologous sources and readily expanded while maintaining differentiation potential. When cultured in the presence of defined factors (i.e., transforming growth factor beta 3; TGF-β3) (Yoo, Barthel et al. 1998, Pittenger, Mackay et al. 1999), these cells can undergo chondrogenesis and produce cartilage-like ECM (Kim, Burdick et al. 2012). It has also been shown that, when MSCs are cultured in 3D with CHs in a 'co-culture' scenario, the two cell types interact and improve matrix formation (Nazempour and Van Wie 2016). This suggests that by adapting a layer-by-layer fabrication scheme, and utilizing MSCs co-cultured with zonal CHs, one might recapitulate the zonal organization and depth-dependent properties of native tissue while decreasing the number of CHs required for tissue formation.

While the choice of cell type and 3D fabrication methods has expanded, a persistent challenge across cartilage tissue engineering is the effective transport of nutrients into (and metabolic waste out of) constructs. This is particularly true for larger constructs, where the core regions show limitations in matrix formation (O'Connell, Lima et al. 2012, Cigan, Durney et al. 2016, Cigan, Nims et al. 2016). Several studies have reported that more and stiffer matrix is produced in the peripheral regions of constructs while less and softer matrix is produced in the innermost core regions (Bian, Angione et al. 2009, Nims,

Cigan et al. 2015, Cigan, Durney et al. 2016). In engineered cartilage established by MSCs, whose metabolic state is more tenuous than CHs, this nutrient deprivation often results in cell death in the central core with extended culture durations. This suggests that insufficient soluble transport compromises cell function in engineered constructs, ultimately resulting in inhomogeneous matrix accumulation (Bian, Angione et al. 2009, O'Connell, Lima et al. 2012). This issue is critical when considering scale up to repair thicker cartilage regions (e.g., the femoral condyle) (Cigan, Nims et al. 2014, Nims, Cigan et al. 2015) or larger defect areas (e.g., partial or total joint resurfacing) (Rowland, Colucci et al. 2016, Saxena, Kim et al. 2016).

To improve nutrient transport and functional properties, a number of possible strategies have been explored. For example, some have used dynamic loading-induced convective transport to encourage fluid movement (Kelly, Ng et al. 2006, Vaughan, Galie et al. 2013). Others have employed encapsulated microbubbles to create additional paths for diffusion (Lima, Durney et al. 2012) or have simply reduced construct thickness to shorten the nutrient path length (Bian, Angione et al. 2009). Perhaps most prominently, several studies have introduced macro-scaled (0.5mm or more) channels into tissue engineered constructs in order to introduce new paths for nutrient transport (Buckley, Thorpe et al. 2009, Cigan, Nims et al. 2014, Nims, Cigan et al. 2015). Interestingly, Cigan and co-workers recently demonstrated that the one time creation of these macro channel(s) did not improve matrix accumulation in the core, and reported that this was due to the eventual blockade of the channel by newly formed tissue after a short period of culture (Bian, Angione et al. 2009, Cigan, Nims et al. 2014, Nims, Cigan et al. 2015). A follow up study from that same group reported that reopening the closed macro-channels midway through culture (by ‘re-punching’ the channels) refreshed nutrient transport and improved functional properties over the long term (Cigan, Durney et al.

2016). Collectively, these data indicate that prolonged provision of ready nutrient access to the center of large constructs will be essential for functional tissue formation in large constructs.

Based on the above challenges and limitations, our first objective in this study was to fabricate a tri-layered construct that recapitulates the cellular organization and depth-dependent functional properties of native articular cartilage, using the layered co-culture of zonal CHs and MSCs. Our second objective, acknowledging the nutrient limitations likely experienced by these larger constructs, was to enhance nutrient/waste transport to improve viability and matrix deposition by cells within the central core region. For this, we introduced a porous hollow fiber (HF) (Tharakan and Chau 1987) as a conduit to enable persistent diffusion of soluble factors into the central core (Potter, Butler et al. 1998, Chen, Fishbein et al. 2003, Kim, Bi et al. 2005). To avoid blockade of these channels, we also inserted cotton threads through the inner core of the HF to continuously wick media to the center of construct while maintaining an open channel for nutrient exchange. Our findings demonstrate the production of a tri-layered cell-based construct with depth-dependent morphology and functional properties, furthering our goal of generating biomimetic engineered cartilage to improve cartilage repair and long-term stability post-implantation.

7.2 Materials and Methods

7.2.1 Preparation of zonal chondrocytes (CHs) and mesenchymal stem cells (MSCs)

Chondrocytes and MSCs were isolated from juvenile bovine stifle joints (3 months old, Research 87, Bolyston, MA). Full-thickness cartilage plugs were excised from the femoral condyle and divided into three different layers (**Figure 7-1A**). The top-most 100μm thick layer at the articular surface was carefully divided and taken as the

superficial zone. The block from the bony surface to just above the tidemark was removed and discarded. The resulting “top” half was considered as middle zone and the “bottom” half as deep zone cartilage. Zonal chondrocytes (CHs) were isolated by collagenase digestion from these separated zonal cartilage tissues, and MSCs were isolated from bone marrow as in our previous studies (Mauck, Wang et al. 2003, Huang, Yeger-McKeever et al. 2008). These isolated zonal CHs and MSCs were separately maintained and expanded in basal media consisting of high glucose Dulbecco’s Modified Eagle Medium (DMEM; ThermoFisher, Grand Island, NY) supplemented with 10% fetal bovine serum (FBS; ThermoFisher, Grand Island, NY) and 1% penicillin/streptomycin/fungizone (PSF; ThermoFisher, Grand Island, NY). At passage 3, zonal CHs and MSCs were trypsinized and washed with phosphate buffered saline (PBS) (ThermoFisher, Grand Island, NY). To trace the distribution of each cell subpopulation, cells were labeled with CellTracker (Molecular Probes, Eugene, OR) prior to encapsulation (SZ = red, MZ = purple, DZ = green, MSC = blue). Later, cell viability was examined with Calcein-AM using the LIVE/DEAD Assay Kit (Molecular Probes, Eugene, OR) after 8 weeks of culture.

7.2.2 MeHA synthesis and cell encapsulation

Details on the synthesis of photocrosslinkabe hyaluronic acid (HA) macromer have previously described as in Burdick et al. (Burdick, Chung et al. 2005). Briefly, 1 % w/v sodium hyaluronate (65 kDa HA; Lifecore Biomedical, Chaska, MN) was reacted with methacrylic anhydride (Sigma, St. Louis, MO) on ice at pH 8.0 for 24 hours followed by dialysis to remove unreacted byproducts for 5 days. Following dialysis, the methacrylated HA (MeHA) solution was lyophilized and stored at −20°C. The lyophilized MeHA was dissolved at 1% w/v in PBS with 0.05% w/vol photoinitiator (Irgacure I2959, CibaGeigy, Tarrytown, NY). The CellTracker-labeled zonal CHs and MSCs were

encapsulated in 1% MeHA at a concentration of 60 million cells/mL and exposed to UV using a 365 nm BlakRay UV lamp (#UVL56, San Gabriel, CA). The range of the UV was 320–400 nm with a transmission maximum of 70% at 365 nm.

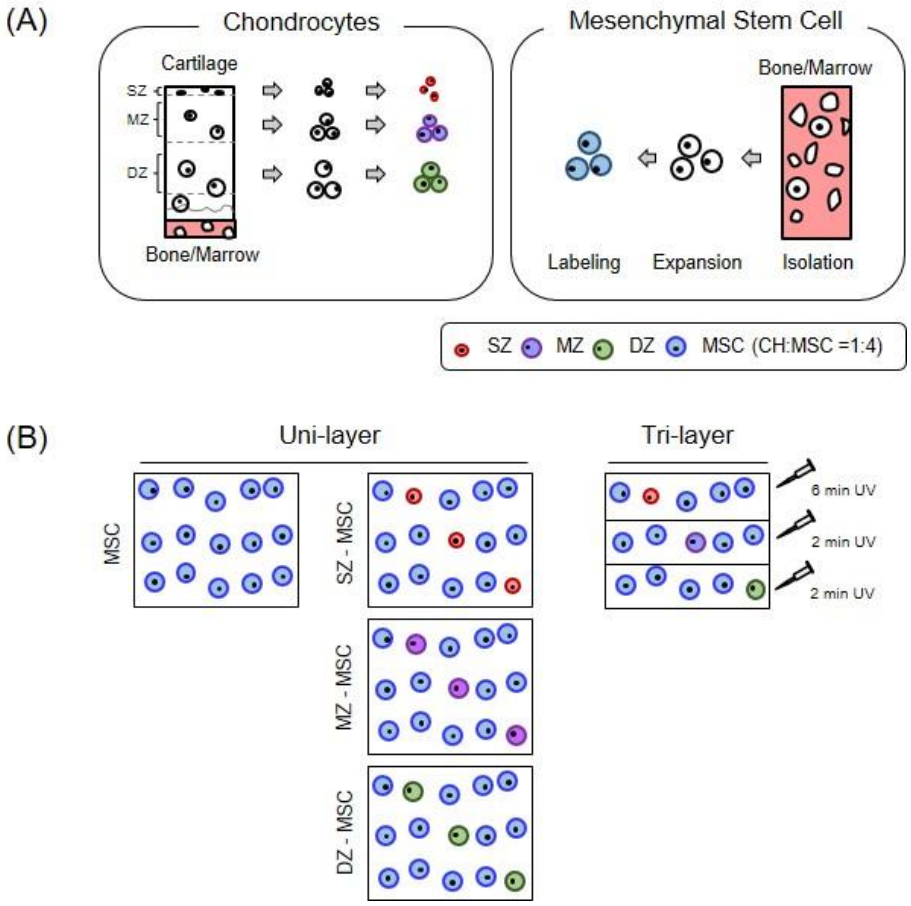

Figure 7-1: A Schematic of a tri-layered construct fabrication with zonal CH/MSC co-culture. (A) Zonal chondrocytes (SZ, MZ and DZ; Left) and MSCs (Right) were isolated from articular cartilage and bone marrow, respectively. Isolated cells were expanded in culture separately and labeled with CellTracker (SZ: Red, MZ: Purple, DZ: Green and MSC: Blue) to trace the distribution of cell subpopulations during long-term culture. (B) Fabrication procedure for single- and tri-layered constructs.

7.2.3 Fabrication of a tri-layered construct with zonal co-culture of CHs and MSCs

Previous studies have shown that freshly isolated zonal chondrocytes (CHs) retained their zonal characteristics in 3D cultures (Cheng, Conte et al. 2007, Ng, Ateshian et al. 2009). Our recent study showed passaged zonal CHs also restored their zonal characteristics when co-cultured with MSCs in HA hydrogels in the presence of TGF-β3 (Kim, Burdick et al. 2012). Based on these findings, we fabricated a tri-layered construct (Kim, Sharma et al. 2003) by partially polymerizing a zonal CH and MSC mixture in HA hydrogel (SZ-MSC, MZ-MSC and DZ-MSC, respectively) (**Figure 7-1B**). MSC alone or co-cultured cell populations were encapsulated in 1% w/v MeHA at 60 x 10^6 cell/mL at a ratio of 1: 4 (CH: MSC) for co-cultured group. Tri-layered constructs were created by exposing the first layer (20 µL; SZ-MSC mixture = 1:4) of MeHA solution to UV light for 2 minutes, followed by polymerization of the second layer (20 µL; MZ-MSC) for 2 minutes, and finally adding the third layer (20 µL; DZ-MSC) with completion of polymerization for another 6 minutes. Polymerization took place within a 1 mL syringe (Ø4.8 mm x 3.5 mm). All other groups (MSC alone, SZ-MSC, MZ-MSC and DZ-MSC; 60 µL/construct) were polymerized under continuous UV light for 10 minutes. Constructs were then transferred directly to a 12 well plate and cultured in chemically defined media (CM) (2 mL/construct) containing high glucose DMEM supplemented with 1% PSF, 0.1 µM dexamethasone, 50 µg/mL ascorbate 2-phosphate, 40 µg/mL L-proline, 100 µg/mL sodium pyruvate, 6.25 µg/mL insulin, 6.25 µg/mL transferrin, 6.25 ng/mL selenious acid, 1.25 mg/mL bovine serum albumin (BSA), and 5.35 µg/mL linoleic acid (Mackay, Beck et al. 1998, Yoo, Barthel et al. 1998) with TGF-β3 (CM+; 10 ng/mL, R&D Systems, Minneapolis, MN). Constructs were turned regularly to improve growth through the depth and media was replaced thrice weekly for the duration of study.

7.2.4 Enhanced nutrient transport by a porous hollow fiber (HF)

Constructs were cultured under static condition (**Fig 7-2A**) or regularly flipped (**Fig 7-2B**) during the culture period to maximize nutrient transport. However, even with flipping, early studies resulted in little matrix accumulation in the core region of the construct compared to peripheral region.

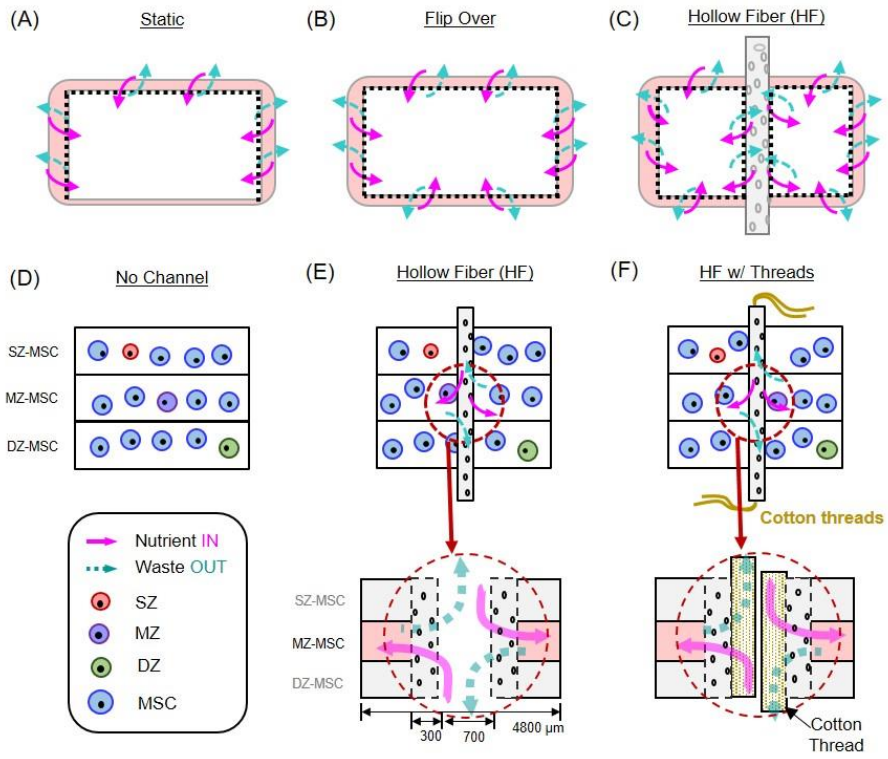

Figure 7-2: Schematics showing accessible surface area for nutrient/waste transport in gel-based constructs and novel strategies to enhance transport. (A-C) Nutrient transport paths under free swelling conditions; (A) Static culture, (B) Static culture where constructs are regularly flipped over (Flip over), (C) Static culture where transport is improved by ntroduction of hollow fiber (HF) channels. (D-F) HF (and HF w/cotton threads)-mediated strategies to improve nutrient transport; (D) No channel, (E) Hollow fiber (HF), (F) HF w/ cotton threads. Schematics of paths available for nutrient/waste transport by HF or HF/ cotton threads. (pink (solid) arrow = nutrient "in", blue (dashed) arrow = waste "out").

To address this limitation, we introduced a porous hollow fiber (HF) (FiberCell Systems Inc., Frederick, MD) through the core along the axial direction of construct after 3 days of culture (**Fig 7-2C**). The HF (polysulfone, OD = 1.3 mm, ID = 0.7mm, wall thickness = 300μm, pore size = 0.1μm) was activated by soaking in 70% ethanol for 24 hours to open the pores for nutrient and waste transport. The HF serves as a conduit, and was maintained in a hydrated state to keep the pores open after activation. Next, the HF was washed with sterile distilled water and was pre-cultured in CM+ at 37ºC/5% CO_2 for 24 hours. To ensure media delivery and to prevent clogging the channel with air bubbles, fresh media were injected through the inner core of the HF at each media change (**Fig 7-2E**). In addition, cotton threads pulled from a sterile gauze pad were inserted through the inner annulus of the HF to help wick media and to maintain an open channel pathway absent of tissue or air bubble obstruction (**Fig 7-2F**).

7.2.5 Analysis of bulk mechanical properties

To determine bulk mechanical properties, constructs were tested in unconfined compression using a custom-built device (Mauck, Yuan et al. 2006). Constructs were equilibrated under a static load of 2 grams for 5 minutes. Following this creep test, samples were subjected to 10% strain at 0.05%/s, calculated from the post creep thickness of the construct. This deformation phase was followed by a relaxation for 1000 seconds to allow the load to reach equilibrium. After stress-relaxation, dynamic testing was carried out by applying a superimposed 1% sinusoidal deformation at 1.0 Hz. Equilibrium and dynamic moduli were calculated from the stress–strain response during the test and the sample geometry. For the tri-layered constructs with HF and HF/threads, the surface area of HF was subtracted from total surface area in these calculations.

7.2.6 Analysis of local mechanical properties

Local mechanical properties (Schinagl, Gurskis et al. 1997) were measured using a custom-built compression device (Farrell, Comeau et al. 2012) coupled with an inverted microscope (Nikon Eclipse TE 2000-U, Nikon, Melville, NY). Subsequent to bulk compression testing, cylindrical constructs were cut in a half, and cell nuclei were stained with Hoechst 33342 (10 µL/mL; Molecular Probes, Eugene, OR) for 10 min. Stained constructs were placed in a PBS-filled chamber in the device, and the cross-section of the construct was oriented facing down (towards the microscope objective). Details to measure local properties were previously described as in (Schinagl, Gurskis et al. 1997, Farrell, Comeau et al. 2012). Briefly, the construct was uniaxially compressed while tracking displacement of nuclei on 2X magnification images captured at equilibrium (after 7 min relaxation) for compressive steps of 4% ranging from 0% to 20% strain. The load was recorded at each step once the construct had reached equilibrium. Stained nuclei served as fiducial markers to generate 'speckle' that was than tracked in the image series via digital image correlation using Vic-2D (Correlated Solutions, Columbia, SC). From these displacement fields, the local Lagrangian strain (E_{xx}) was calculated, where x is the axial direction of the hemi-cylindrical construct (depth from the S-M to D-Z region). Local strains were exported to MATLAB (The Math Works Inc., Natick, MA) and the average values were computed according to depth (defined as region 1 through 10 from the top to bottom of the construct). Local modulus was calculated using these resultant strain values and equilibrium boundary stresses. The reported local modulus was limited to the inner 70% (region 2 to region 8) of the construct thickness due to edge effects of the testing modality. To validate findings of depth dependency, we first tested bi-layered constructs with turned depth dependent material properties formed from 1% and 5% MeHA (2:1 ratio = 40 µL: 20 µL ratio, 20 million cells/mL in each sub-layer). These constructs were tested and analyzed as described above (**Fig 7-6A and B**).

7.2.7 Biochemical analysis

Subsequent to local mechanical testing, the construct wet weight (WW) was measured, followed by papain digestion (1 mL/construct, 0.56 U/mL in 0.1M sodium acetate, 10M cysteine hydrochloric acid, 0.05 M ethylenediaminetetraacetic acid, pH 6.0) at 60°C for 16 h. Glycosaminoglycan (GAG) content was determined using the 1, 9 dimethylmethylene blue (DMMB) dye binding assay (Farndale, Buttle et al. 1986) and collagen content using the orthohydroxyproline (OHP) assay, with a 1 : 7.14 (OHP : collagen) ratio, as previously described (Neuman and Logan 1950).

7.2.8 Histological analysis

Constructs were fixed in 4% paraformaldehyde (PFA) and embedded in paraffin. Sections (8 μm thick) were deparaffinized in a graded series of ethanol and stained with Alcian Blue (pH 1.0) for proteoglycans (PG) with nuclear fast red counterstain. Immunohistochemistry was carried out to visualize type II collagen and chondroitin sulfate (CS). Samples underwent antigen retrieval using hyaluranidase (HASE) from type IV bovine testes (Sigma-Aldrich, St. Louis, MO) for 1 hour and followed by Protease-K (DAKO, Glostrup, Denmark) digestion for 4 minutes at room temperature. Endogenous peroxidase activity was quenched by pretreating sections with 3% hydrogen peroxide. To block nonspecific staining, sections were incubated with 10% normal goat serum (Sigma-Aldrich, St. Louis, MO). Primary antibodies for type II collagen (II-II6B3; Developmental Studies Hybridoma Bank, Iowa City, IA), and chondroitin sulfate (C8035, Sigma-Aldrich, St. Louis, MO) were applied; antibody diluent solution (DAKO, Glostrup, Denmark) was used to dilute primary antibodies. After incubation with primary antibodies for overnight at 4ºC, sections were washed and treated with bioinylated goat anti-rabbit IgG secondary antibodies, followed by streptavidin horseradish peroxidase (HRP). Sections were reacted with DAB chromogen

reagent for 10 ~20 min (Millipore, Billerica, MA) and imaged on a polarizing light microscope (Leica DMLP, Leica Microsystems, Germany) equipped with a color charged-coupled device (CCD) digital camera.

7.2.9 Statistical analysis

Statistical analysis was performed using the SYSTAT software (v10.2, SYSTAT software Inc., San Jose, CA). Significance was determined by two-way ANOVA with Tukey's post hoc test ($p < 0.05$).

Table 7-1: Mechanical and biochemical properties of cell-laden HA constructs with long-term culture.

GROUP	Period (wk)	E_Y (kPa)	|G*| (MPa)	GAG (%WW)	Collagen (%WW)	DI (mm)
MSC	8	309 ± 89	2.1 ± 0.35	3.8 ± 0.23	2.2 ± 0.30	5.4 ± 0.11
	16	338 ± 51	2.5 ± 0.74	3.7 ± 0.42	7. 6 ± 1.45	5.5 ± 0.14
SZ-MSC	8	334 ± 88	1.9 ± 0.50	3.8 ± 0.45	1.9 ± 0.49	5.2 ± 0.09
	16	317 ± 47	2.0 ± 0.31	4.2 ± 1.04	3.3 ± 0.52	5.2 ± 0.14
MZ-MSC	8	377 ± 34	2.1 ± 0.19	4.3 ± 0.20	2.2 ± 0.23	5.4 ± 0.12
	16	481 ± 81	3.1 ± 0.42	4.8 ± 0.52	6.5 ± 0.94	5. 6 ± 0.21
DZ-MSC	8	370 ± 11	2.1 ± 0.14	4.5 ± 0.44	2.3 ± 0.19	5.3 ± 0.14
	16	428 ± 138	2.7 ± 0.50	4.5 ± 0.51	7.3 ± 1.58	5.7 ± 0.38
Tri-layer	8	522± 52	2.8 ± 0.33	5.0 ± 0.47	3.3 ± 1.11	5.3 ± 0.03
	16	537 ± 177	2.9 ± 0.85	4.4 ± 0.70	6.4 ± 2.14	5.3 ± 0.45

(Mean ± SD; N=3~4/group)

7.3 Results

7.3.1 Fabrication of tri-layered constructs with zonal CHs/MSCs co-cultured sublayers

Mechanical and biochemical properties of co-cultured (SZ-MSC, MZ-MSC and DZ-MSC) constructs depended on the zonal origin of chondrocytes: the least matrix production and lowest mechanics was seen in constructs from the SZ-MSC group (316kPa, 4.2%WW for GAG and 3.3%WW for collagen), and the highest mechanics/matrix

production was seen in MZ-MSC (480kPa, 4.8%WW GAG and 6.5%WW collagen) and DZ-MSC (427kPa, 4.5%WW GAG and 7.3%WW collagen) groups at 16 weeks. Overall bulk properties of the tri-layered construct reached 537kPa, 4.4%WW GAG and 6.4%WW, whereas MSC-only constructs reached only 338kPa, 3.7%WW GAG and 7.6%WW collagen at 16 weeks, respectively **(Table 7-1)**.

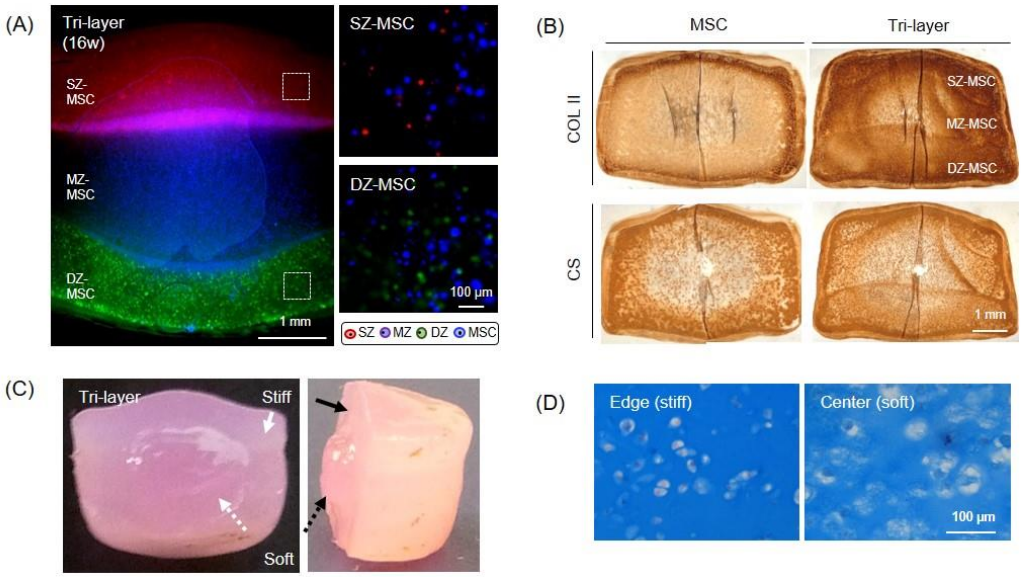

Figure 7-3: Development and maturation of a tri-layered construct. (A) A cross-sectional view of a tri-layered construct showing distinct zonal sub-layers visualized by CellTracker at 16 weeks (Left). (SZ: Red, MZ: Purple, DZ: Green, MSC: Blue; 2.5x; Scale bar = 1 mm). Co-cultures of SZ-MSC (Top right) and DZ-MSC (Bottom right) were evident in each sub-layer (20x; Scale bar = 100 μm). (B) Immunohistochemistry of type II collagen (Top) and chondroitin sulfate (Bottom) at 8 weeks (60 million cells/mL; CH:MSC = 1:4; Scale bar = 1 mm). (C) Heterogeneous matrix accumulation at 8 weeks in a tri-layered construct due to limited nutrient transport to the central region. The peripheral region (Solid arrow) showed more rigid matrix than the core (Dashed arrow) (Scale bar = 1 mm). (D) Alcian blue staining of peripheral (Left) and core (Right) region of the construct (20x, Scale bar = 100 μm).

MSCs and CHs remained viable over the 16 week culture period, and each cell population was well distributed within its appropriate layer (**Figure 7-3A**). Both tri-layered and MSC-only constructs showed dense type II collagen (COL II) and chondroitin sulfate (CS) deposition at 8 weeks (**Figure 7-3B**). While there was a robust matrix accumulation throughout the constructs, matrix accumulation was markedly limited in the core region. When observing the cross-section of these constructs, the peripheral region was much stiffer than the core, as evidenced by the core region swelling outward when the constructs were divided in a half (**Figure 7-3C**). Alcian blue staining confirmed greater PG deposition in the peripheral region compared to the core (**Figure 7-3D**). Further, the cells in the peripheral region retained a rounded morphology reminiscent of the native tissue, whereas the cells in the core region were enlarged with disorganized lacunae indicating a possible hypertrophic or unhealthy state.

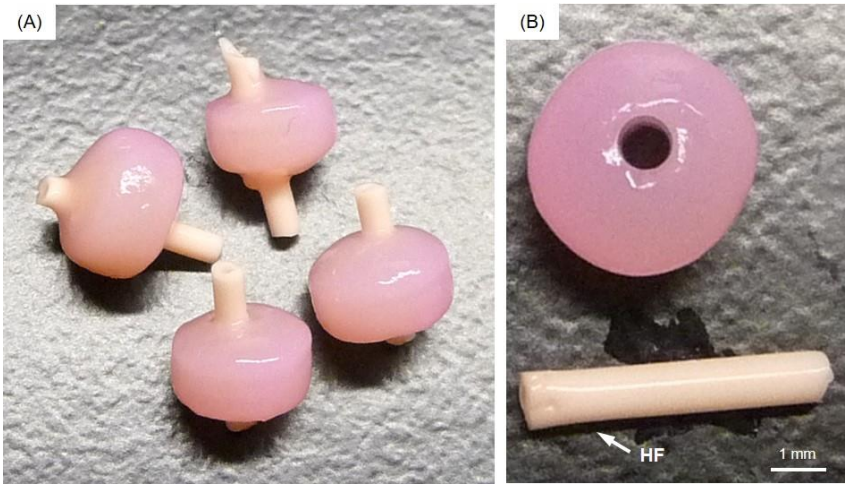

Figure 7-4: Gross appearance of tri-layered constructs with hollow fiber after 8 weeks of culture. The HF channel remained open during the culture period (A), and there was little to no interaction between the HF and the surrounding hydrogel (B) (Scale bar = 1 mm).

7.3.2 Enhancement of nutrient transport via the inclusion of a hollow fiber (HF)

To improve nutrient/waste transport in the core regions of these constructs, we introduced a porous hollow fiber (HF) with our without the addition of a cotton thread. HFs in the tri-layered constructs remained open during the culture periods (**Figure 7-4A**). There was little to no interaction between the HF and the hydrogel construct, as shown by a clear interface between the two upon removal of the HF (**Figure 7-4B**). To investigate the ability of the HFs (with or without thread) to promote nutrient/waste transport, particularly in the core region, we assessed three different conditions. These included constructs with no channel, with HF alone, and with HF w/cotton threads (**Figure 7-5**). Based on visual inspection, constructs from all groups grew well and achieved similar volumes (**Figure 7-5A**). However, the core regions of the constructs with no channel showed little matrix deposition compared to the peripheral regions. Conversely, those constructs with HF or HF w/cotton threads showed greater matrix accumulation, with the center comparable to the construct edge. The core region with HF w/cotton threads appeared fully matured and homogenous throughout the cross-section (**Figure 7-5B**). Each layer within constructs with HF and HF w/cotton threads remained flat, while those without a channel showed swelling of the MZ-MSC layer, resulting in deformations of the adjacent SZ-MSC and DZ-MSC layers. Mixed populations of CHs and MSCs were viable and well distributed within their appropriate layers in all groups (**Figure 7-5C**). Calcein-AM staining showed that the cells near the HF or HF w/cotton threads were more viable than those in the core region of constructs lacking a channel (**Figure 7-5D**). Furthermore, Alcian blue staining showed marked PG production in the core region for constructs with HF and HF w/cotton threads, and cells in these regions maintained a normal morphology, whereas in constructs with no channel, there was poor matrix accumulation in the core region with cells taking on an enlarged (hypertrophic) appearance (**Figure 7-5E**).

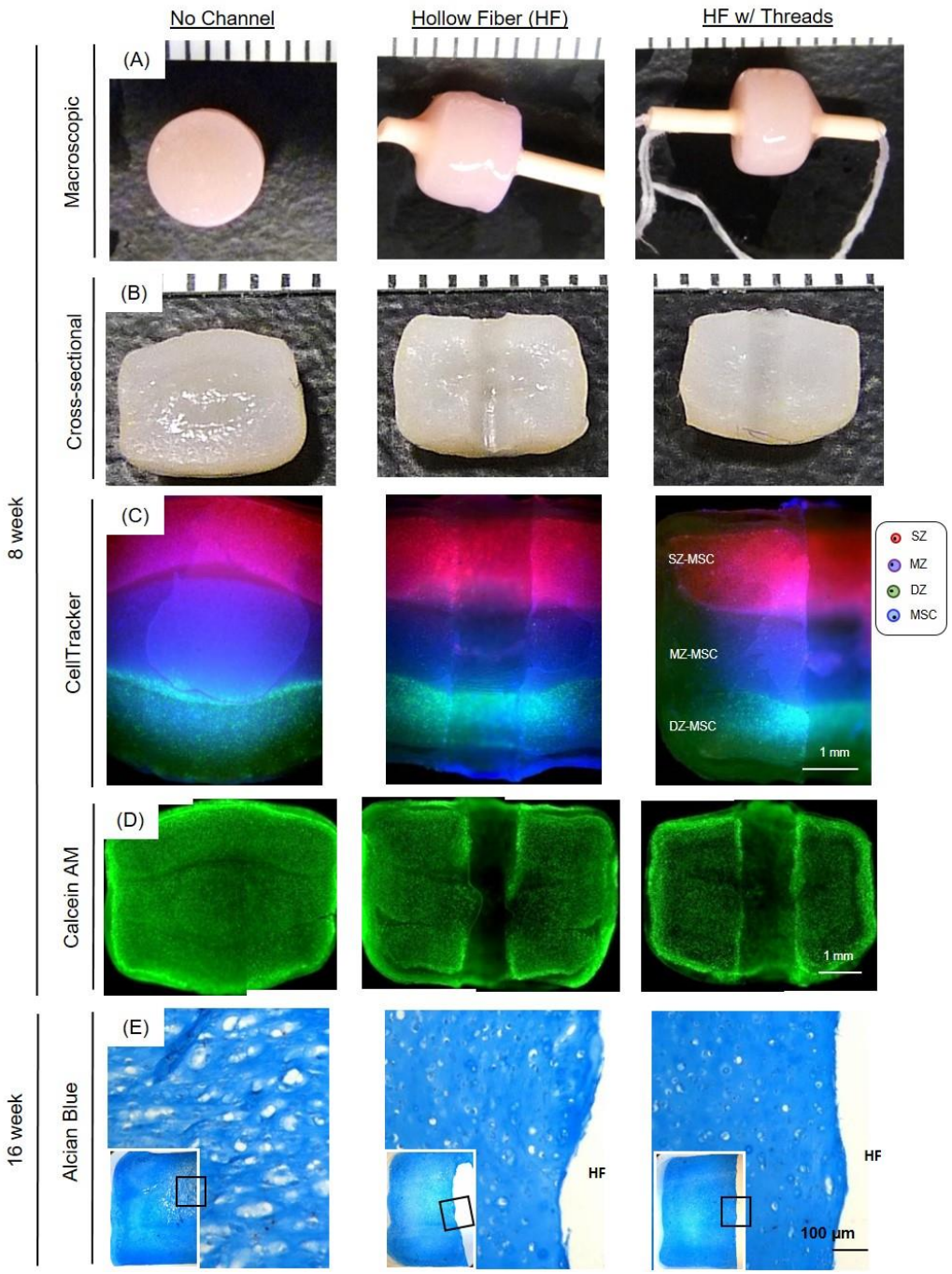

Figure 7-5: Maturation of tri-layered constructs with HFs. Groups are indicated as "No Channel" (Left column), "Hollow Fiber" (HF; Middle) and "HF w/threads" (Right), respectively. (A) Gross appearance of tri-layered constructs with 8 weeks of culture (Markers = 1 mm). (B) Cross-sectional view (Markers = 1 mm). (C) CellTracker-labeled zonal chondrocytes and MSCs co-cultured in a tri-layered construct (2.5x, Scale bar = 1

mm). (D) Calcein-AM staining of constructs at 8 weeks of culture (2.5x, Scale bar = 1 mm). (E) Alcian blue staining of constructs at 8 weeks of culture (10x and 2.5x (Inset), Scale bar = 100 μm). HF indicates original position of hollow fiber.

7.3.3 Functional properties of tri-layered constructs

Functional properties of tri-layered construct for all groups increased with time, with levels at the end of the study comparable to native cartilage tissue (shaded area) (**Figure 7-6C-E**). Bulk mechanical properties of no channel, HF, and HF w/cotton threads groups reached 630kPa (p=0.014), 600kPa, and 584kPa at 16 weeks, respectively (**Figure 7-6C**). Similarly, GAG and collagen contents (GAG/collagen) were 3.9%WW/4.5%WW, 4.0%WW/3.7%WW, and 4.4%WW/4.0%WW at 16 weeks, respectively (**Figure 7-6D and E**). While HF and HF w/thread increased matrix distribution in the core, it did not influence bulk properties. The local modulus of these tri-layered constructs exhibited depth-dependent increase from superficial region (SZ-MSC layer; ~0.3MPa) to deep region (DZ-MSC layer; ~1.4-2.3MPa) (**Figure 7-6F**). The properties of constructs with HF w/cotton threads (green) in the deep zone (DZ-MSC) nearly matched native levels (black/dashed line). Though the overall depth dependence mirrored native tissue, the properties in the central regions were still lower than that of the native tissue.

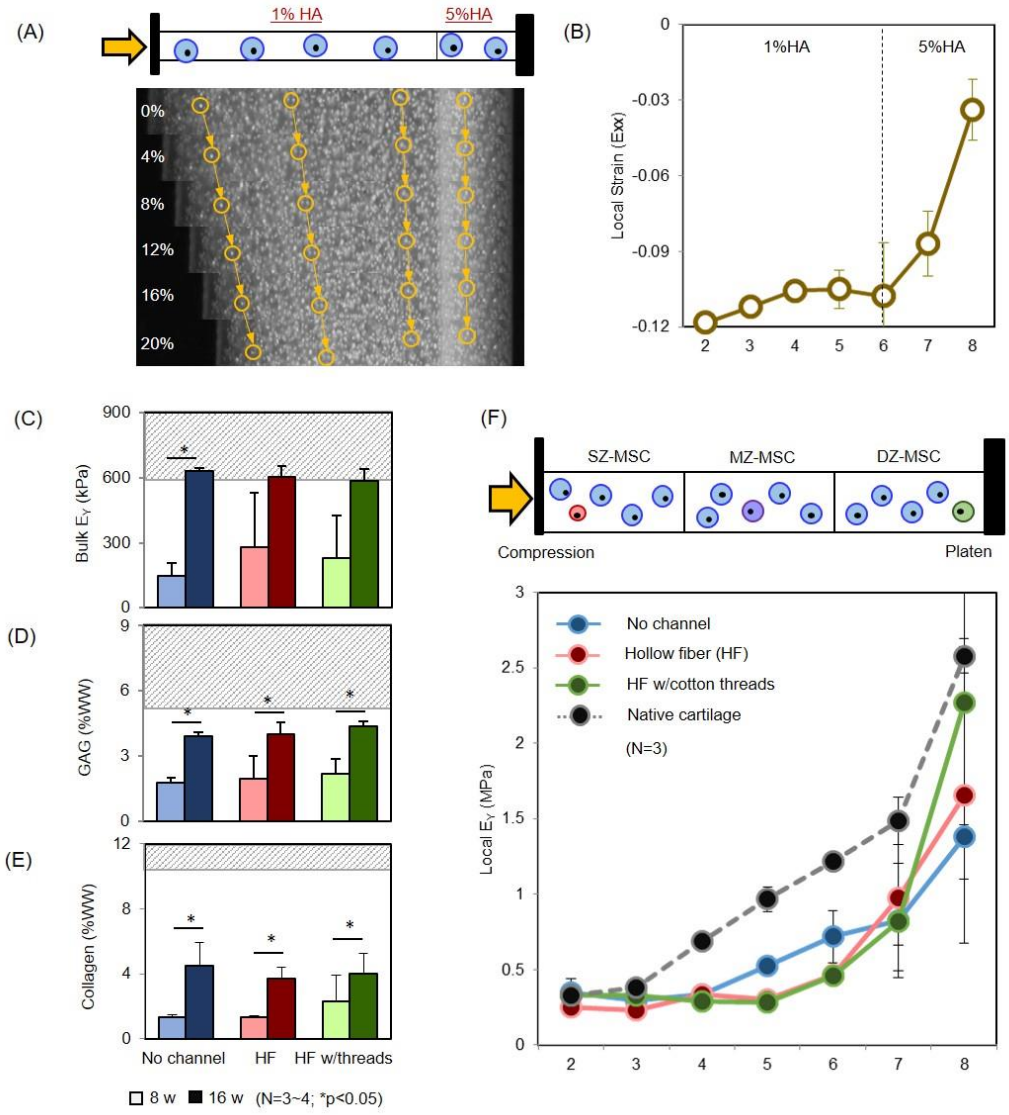

Figure 7-6: Depth-dependent properties of tri-layered construct with long-term culture. (A) MSC-laden bi-layered HA constructs (1 and 5% HA) stained with Hoechst were subjected to compression (0% ~ 20% strain applied) and nuclei were tracked to compute local properties. Yellow arrows and circles indicate nuclei traced from reference image (0% strain) on day 0. (B) Local strain (ε_{xx}, Day 0). (C-E) Bulk properties of tri-layered constructs: (C) E_Y (kPa), (D) GAG (%WW), (E) Collagen (%WW) (Dashed gray line = native cartilage; Lighter bars = 8 weeks, Darker bars = 16 weeks). (F) Local E_Y (kPa) for tri-layered constructs at 16 weeks (No channel = Blue, HF = Red, HF w/cotton threads = Green, Native cartilage = Black).

7.4 Discussion

In this study, we developed methods to co-culture zonal CHs with MSCs in 3D HA hydrogels, and fabricated a tri-layered construct (with mixed cell subpopulations in each layer) to mimic the zonal organization and depth-dependent properties of native cartilage. Constructs formed from superficial CHs and MSCs yields tissue with the lowest compressive properties and GAG content (320 kPa; 4.2% WW), while those formed from middle or deep zone CHs and MSCs had the highest bulk properties (>430 kPa; >4.5%). This indicates the passaged chondrocytes re-differentiated in the presence of TGF-β3 while retaining their zonal characteristics, even after multiple population doublings (Kim, Sharma et al. 2003, Darling and Athanasiou 2005, Hong and Reddi 2013). Importantly, the differences that emerged between cultures were apparent with CHs comprising only 20% of the starting cell population. This suggests that CH-MSC co-cultures of zonal origin might be harnessed to replicate native tissue form and function.

Building from this platform, single-layered constructs (with zonal co-culture) were combined into one tri-layered construct. Under this scenario, zonal CHs in each layer retained their distinct cellular matrix forming capacity and organization and remained viable over 16 weeks, as did the co-cultured MSCs. The fact that MSCs appeared remain viable and produced ECM may suggest that molecular factors secreted from CHs promote their function under these challenging conditions (Chen, Liang et al. 2012). Sustained ECM production by MSCs in this co-culture context could potentially reduce the need of CHs by up to 80%. Overall, we noted robust accumulation of type II collagen (COL II) and chondroitin sulfate (CS) throughout the cross-sectional area, though all constructs showed a core region in which little matrix was deposited. Cells in the peripheral regions maintained a small size and round shape with a distinct cell boundary

and nuclei, whereas those in the core appeared much larger. While both MSC-laden and mixed cell-laden constructs were maintained under the same culture conditions, the equilibrium modulus and GAG content of tri-layered constructs were 1.7 and 1.3 times greater than that of the MSC-laden constructs, respectively. This may be due to MSCs cultured alone being more sensitive to changes in their microenvironment (e.g., glucose level or oxidative stress) (Farrell, Fisher et al. 2014) compared to those mixed with CHs.

Despite these positive findings with tri-layered co-cultures, the need for improved nutrient transport was evident, as demonstrate by the differing matrix production in the central and peripheral regions. This transport challenge exists regardless of cell type, and has been reported by many others, particularly when engineering larger constructs (Buckley, Thorpe et al. 2009, O'Connell, Lima et al. 2012, Cigan, Nims et al. 2014, Nims, Cigan et al. 2015). Early efforts to overcome this issue have centered on the application of dynamic loading, decreasing construct thickness, or creating macro-channels. While channels appear promising during short term culture, we and others have shown that macro-channels can become filled with newly formed tissue early in culture (**Figure 7-7**). This can be addressed to some extent by 're-punching' the closed channels (Cigan, Nims et al. 2016), though this requires an additional handling step during culture. To overcome this limitation, in this study we included a porous HF or a HF strung with a cotton thread to maintain channel patency and improve nutrient/waste transport into the core of the construct. Introduction of the central HF or HF/thread preserved construct dimensions (limited swelling in each layer) and improved cell viability, particularly in the core region. Cells in the core region retained a normal morphology and produced abundant matrix, whereas cells in constructs lacking a channel were enlarged, with poor matrix production. However, while the HF and/or HF w/thread promoted more uniform matrix accumulation and maintained cell morphology, there was no effect on bulk

properties. This suggests that the bulk properties were mainly governed by properties of the periphery. That said, when we measured the local properties of the tri-layered constructs, we found that the deep zone of constructs with HF w/cotton thread nearly matched that of the native bovine cartilage deep zone (DZ-MSC) (Ng, Ateshian et al. 2009). Indeed, the ratio of local modulus from the top to bottom layer of the tri-layered construct (DZ:MSC / SZ:MSC) with no channel, with HF, and with HF w/thread was 4, 6.5 and 6.8, respectively. In native bovine cartilage, this ratio is 7.9 (DZ/SZ). While constructs overall began to mirror the depth dependence of native tissue, the properties of the central region (MZ-MSC layer) were still lower than that of the native tissue. This may in the future be addressed by adding additional nutrient channels (Cigan, Nims et al. 2016) and/or extending the culture duration.

Biomimetic design in engineering cartilage-like constructs is of importance not only for recapitulating native structure and function but also for enhancing integrative repair by modulating zone-to-zone integration and matching mechanical properties with the host tissue. By filling defects in a zonally consistent manner, one might promote better integration between the repair and host tissue under physiologic loading. That is, if the depth-dependent properties of the implant mirror the native tissue, this would harmonize deformations through the depth and diminish stress concentrations at the integrative surface. In this regard, the current design is still in need of fine tuning with respect to the thickness each layer, based on the generally defined 10% (superficial zone), 60% (middle) and 30% (deep zone) layers of native tissue. Further studies will be required to validate this concept using native cartilage and more precisely engineered depth-dependent engineered tissue constructs.

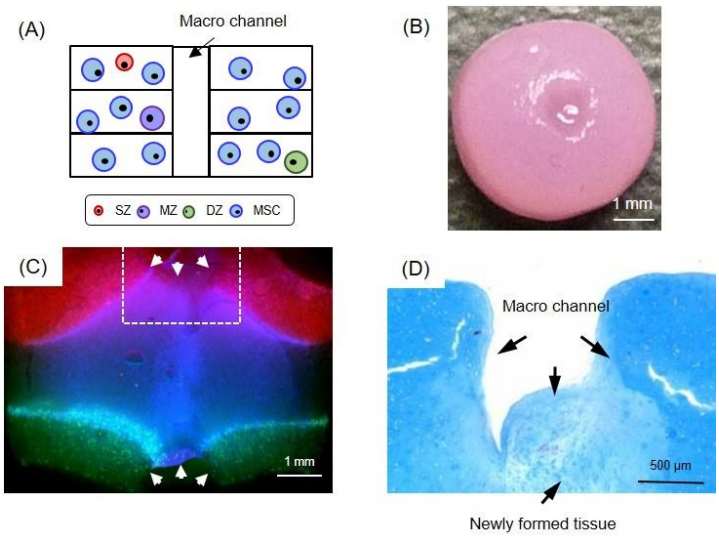

Figure 7-7: Tissue filling of macro-channels in tri-layered constructs. Macro-channels (Ø1mm) that were created on day 0 filled with matrix early in culture. (A) A schematic of creation of macro channel. (B) Gross appearance showing a closure of macro channel (Scale bar = 1 mm). (C) Cross-sectional view of a tri-layered construct showing new tissue deposition resulting in closure of the macro channel (Scale bar = 1 mm). (D) Zoomed-in view near the surface (Scale bar = 500 µm).

Taken together, our results demonstrate that a layer-by-layer fabrication scheme, including co-cultures of zone-specific articular CHs and MSCs, can reproduce the depth-dependent characteristics and mechanical properties of native cartilage while minimizing the need for large numbers of chondrocytes. Such a tri-layered construct may provide critical advantages for focal cartilage repair. These constructs hold promise for restoring a native tissue structure and function, and may be beneficial for zone-to-zone integration with adjacent host tissue and provide more appropriate strain transfer after implantation. Future work will investigate how individual cells within each layer communicate with one another and with adjacent layers, and will scale this technology to produce constructs of anatomic relevance for cartilage repair applications (Hung, Lima et al. 2003, Rowland, Colucci et al. 2016, Saxena, Kim et al. 2016).

CHAPTER 8: Fabrication of Micro-scale Chondrocyte-seeded 'Noodle-like' Constructs to Promotes Cartilage Repair with Microfracture

8.1 Introduction

Chondrocytes (CH) and mesenchymal stem cells (MSC) are a commonly used cell source for cartilage repair. CHs are stable and superior to MSCs in producing functional matrix, but are limited in number and lose their phenotype upon extensive passaging (Darling and Athanasiou 2005). Conversely, MSCs can be readily expanded and undergo chondrogenesis, but this capacity is attenuated with aging (Erickson, van Veen et al. 2011). This is in part why microfracture procedures, which enable MSC entry into a cartilage lesion from the underlying marrow, are contraindicated in older patients (Makris, Gomoll et al. 2015). To overcome this limitation, various studies have employed CH/MSC co-culture systems, and have shown that a small pool of healthy/young CHs can rejuvenate a larger pool of infirm/old MSCs when the two cell types are placed in close proximity to one another (de Windt, Saris et al. 2015). While an interesting finding, this co-culture effect is not altogether clinically relevant, as most studies are performed in larger, cylindrically shaped formats (Buschmann, Gluzband et al. 1992). These constructs not only have the disadvantage of heterogeneous matrix accumulation due to limitations in nutrient transport (making scale-up a challenge), but also would require the ex vivo expansion of both cell types (CH and MSCs), rather than just CHs (as is currently done for ACI procedures).

To overcome these obstacles, we developed a new micro-scaled tissue engineered construct that takes advantage of co-culture effects while at the same time having the potential for clinical use in the context of microfracture. The increase of surface area provided by micro-noodles was designed to enhance nutrient transport and intercellular

communication. We designed the CH-seeded micro-scale noodle-shaped construct (micro-noodle) in an injectable format, so that it could be readily implemented in the context of microfracture, allowing bone marrow derived MSCs entering the wound site to percolate into a micro-scaled CH-seeded gel fiber weave. Here, we report on the fabrication of these micro-noodles, investigate their chondro-inductive capacity in an environment mimicking microfracture (co-cultured with MSCs seeded in fibrin glue), and evaluate the stability and retention of micro-noodles after placement in defects in vivo using a large animal model of cartilage repair.

8.2 Materials and Methods

8.2.1 Isolation of chondrocytes (CHs) and MSCs

Chondrocytes (CHs) and MSCs were isolated from adult porcine stifle joints (18 months, Sinclair Bioresources). Cartilage segments were dissected from the femoral condyle, washed twice with phosphate buffered saline (PBS) contaning 2x PSF, minced, and digested with collagenase to isolate CHs. MSCs were isolated from bone marrow within the diaphysis near the metaphyseal region. Isolated CHs and MSCs were maintained and expanded in basal media consisting of high glucose Dulbecco's Modified Eagle Medium (DMEM; ThermoFisher, Grand Island, NY) supplemented with 10% fetal bovine serum (FBS; ThermoFisher, Grand Island, NY) and 1% penicillin/streptomycin/fungizone (PSF; ThermoFisher, Grand Island, NY) to passage 1 or 2.

8.2.2 Pellet culture of porcine CHs and MSCs

To determine the chondrogenic capacity of adult porcine CHs and MSCs, cells were cultured in pellet format. 250,000 CHs and MSCs were placed in a 96 well round-bottom polypropylene plate (Nunc, Paperville, IL) and centrifuged at 300xg for 5 minutes. The aggregated cell pellets were cultured for 2 and 4 weeks in 200 µL/pellet chemically

defined media (CM). CM was comprised of high glucose DMEM with 1x PSF; 0.1µM dexamethasone; 50 µg/mL ascorbate 2-phosphate; 40 µg/mL L-proline; 100 µg/mL sodium pyruvate; and 6.25 µg/mL insulin, 6.25 µg/mL transferrin, 6.25 ng/mL selenious acid, 1.25 mg/mL bovine serum albumin (BSA), and 5.35 µg/mL linoleic acid. CM was supplemented with 10 ng/mL TGF-ß3 (CM+, R&D Systems, Minneapolis, MN) to induce chondrogenesis, and media were changed thrice weekly.

8.2.3 Methacrylated hyaluronic acid (MeHA) synthesis

Methacrylated hyaluronic acid (MeHA) was synthesizied as previously reported by Burdick and colleagues (Burdick, Chung et al. 2005). Briefly, methacrylic anhydride (Sigma, St. Louis, MO) was added to 1% w/v sodium hyaluronate (65 kDa MW; Lifecore, Chaska, MN) dissolved in distilled water, and pH was adjusted at 8.0 with NaOH (Sigma, St. Louis, MO) on ice for 6 hours. This was followed by dialysis (6kDa MW cutoff; Spectrum Lab, Rancho Dominguez, CA) for one week with repeated changes of distilled water. The resulting MeHA solution was lyophilized and stored at -20°C until use.

8.2.4 Cell encapsulation

To form micro-noodles, lyophilized MeHA was dissolved at 1% w/v in PBS with 0.05% w/vol photoinitiator (Irgacure I2959, CibaGeigy, Tarrytown, NY). To trace the distribution of each cell population, cells were labeled with CellTracker (Molecular Probes, Eugene, OR) prior to encapsulation **(Figure 8-3A)**. These CellTracker-labeled ApCHs were encapsulated in 1% MeHA at a concentration of 20 or 60 million cells/mL. The cell solution was extruded into a micro-bore tube, exposed to UV using a 365 nm BlakRay UV lamp (#UVL56, San Gabriel, CA) for 10 minutes, and then extruded from the tube. The range of the UV was 320–400 nm, with a transmission maximum of 70% at 365 nm. Formed micro-noodles (Ø250µm) were cultured in CM+, and cell viability was

determined via Calcein-AM from the LIVE/DEAD Assay Kit (Molecular Probes, Eugene, OR).

8.2.5 Development of a micro-noodle system

A micro-bore tubing system was developed to generate micro-scaled noodle-like engineered constructs showing enhanced nutrient transport and intercellular communication via a dramatic increase in surface area compared to traditional fabrication methods and forms. To fabricate the micro-scaled noodle-shaped constructs (i.e., micro-noodles), a custom-built micro-bore tubing system was assembled, consisting of Tygon micro-bore tubing (Ø250μm, USP Corp, Lima, OH), a disposable syringe needle ($30G_{1/2}$), a three-way stopcock, and a disposable syringe (10 mL). A long piece of micro-bore tubing was washed with 70% EtOH through the inner core, rinsed with PBS and autoclaved using a dry cycle. These were then cut into shorter pieces (20cm-long) and autoclaved on a dry cycle. A disposable needle was then inserted through the inner annulus of the micro-bore tube, followed by assembly of the additional components **(Figure 8-3B)**. To verify the advantages to the use of micro-noodles, the surface areas of micro-noodle (Ø250μm) constructs compared to conventional cylindrical constructs (Ø4mm x 2.25mm) that are used in many studies, were calculated and compared based on the same volume of starting cell suspension/hydrogel **(Figure 8-4A)**.

8.2.6 Chondro-inductive effect of CH-laden micro-noodles on adult porcine MSCs in fibrin gel

To investigate the chondro-inductive effect of adult CHs in micro-noodles on adult MSCs that are expected in the microfracture environment, we developed an in vitro analog of this environment. That is, ApCH-laden micro-noodles (20 million cells/mL at 1% MeHA)

were pre-cultured in CM+ for 14 days and then mixed with AMSCs (ACH:AMSC ratio = 1:4) seeded in fibrin gel (Tisseel, Baxter) at a concentration of 20 million cells/mL. This co-culture formulation was cultured for an additional 14 days in CM+. CH-laden micro-noodles or AMSCs alone were embedded/seeded in fibrin gel as controls **(Figure 8-6A)**.

8.2.7 Detection of micro-noodles filled in the defects

To enable tracing of micro-noodles after implantation in vivo, MeHA was mixed with methacrylated rhodamine B (Polysciences, Inc., Warrington, PA) and/or radiodense zirconium (IV) oxide nanoparticles (Zirconia, Sigma-Aldrich, St. Louis, MO) (Martin, Milby et al. 2015). Micro-noodles loaded with methacrylated rhodamine B and/or zirconium nanoparticle were visualized on an inverted fluorescent (Nikon Eclipse TE 2000-U, Nikon, Melville, NY) or Nikon A1R confocal microscope (Nikon Instruments Inc., Melville, NY, USA) or were visualized by micro computed tomography (μCT; vivaCT 75, SCANCO Medical AG, Bruttisellen, Switzerland) as in (Fisher, Belkin et al. 2015, Fisher, Belkin et al. 2016), respectively.

8.2.8 Micro-noodle delivery to cartilage defects in an in vivo large animal model

All animal procedures were performed at the Philadelphia VA Medical Center with approval from the Institutional Animal Care and Use Committee and in accordance with policies set forth by the National Institutes of Health. Two adult Yucatan mini-pigs (18 months old, ~200lbs, Sinclair Bioresources) were utilized for these studies. Surgical protocols were as described in Fisher et al. (Fisher, Belkin et al. 2015, Kim, Pfeifer et al. 2015, Fisher, Belkin et al. 2016). Four defects were created in the trochlear groove of right hind limb in a unilateral procedure. Chondral defects were formed using a 4 mm biopsy punch to outline the defect boundary, followed by removal of cartilage tissue from the defect using a bone curette. After the complete removal of cartilage, microfracture

was performed, creating three perforations 1 mm deep to the subchondral bone in each defect using an awl. After microfracture, the cell/HA solution was extruded into the device and photo-polymerized, and then micro-noodles were extruded into the defect. After surgery, the arthrotomy was closed layer by layer and animals were recovered following standard post-surgical procedures for pain control. Animals were accommodated in a normal cage and free mobility for the duration of study. Animals were euthanized after 1 or 2 weeks, and the right hind limb was disarticulated at femoral head. The trochlear groove was grossly inspected, imaged, and individual cartilage defects including the underlying bone were isolated using a hand saw.

8.2.9 Verification of micro-noodle retention in chondral defects

Osteochondral units were fixed in 4% paraformaldehyde (PFA). To identify the presence of micro-noodles in the defect, one osteochondral unit was examined to detect micro-noodles based on fluorescently labeled dyes. Underlying trabecular bone adjacent to the cartilage was trimmed. The osteochondral unit was carefully cut in half, through the middle of the defect. The cross-sectional side was placed face down on a glass coverslip and imaged on a confocal microscope. Micro-noodles and delivered CHs were visualized in their respective fluorescent channels (red and purple).

8.2.10 Biochemical analysis

To assess micronoodle maturation, the wet weight of each micro-noodle was measured, followed by papain digestion (1mL/construct, 0.56U/mL in 0.1M sodium acetate, 10M cysteine hydrochloric acid, 0.05M ethylenediaminetetraacetic acid, pH 6.0) at 60°C for 16 hours. Sulfated glycosaminoglycan (s-GAG) content was assessed using 1,9-dimethylmethylene blue (DMMB) assay (Farndale, Buttle et al. 1986). Orthohydroxyproline (OHP) content was measured via reaction with chloramine T and

diaminobenzaldehyde. Collagen content was extrapolated from OHP using a 1:7.14 ratio of OHP (Neuman and Logan 1950).

8.2.11 Histological analysis

Constructs and osteochondral units were fixed in 4% paraformaldehyde (PFA) for 24 hours were decalcified (for osteochondral units) and embedded in paraffin. Sections (8 µm thick) were deparaffinized in a graded series of ethanol and stained with Alcian Blue (pH 1.0) for proteoglycans (PG). Immunohistochemistry was carried out to visualize type I and type II collagen and chondroitin sulfate (CS). Samples underwent antigen retrieval using hyaluranidase (HASE) from type IV bovine tests (Sigma-Aldrich, St. Louis, MO) for 1 hour and followed by Protease-K (DAKO, Glostrup, Denmark) for 4 minutes at room temperature. Endogenous peroxidase activity was quenched by pretreating sections with 3% hydrogen peroxide. To block nonspecific background staining, sections were incubated with 10% normal goat serum (Sigma-Aldrich, St. Louis, MO). Primary antibodies against type I collagen (MAB3391; Millipore, Billerica, MA), type II collagen (II-II6B3; Developmental Studies Hybridoma Bank, Iowa City, IA), and chondroitin sulfate (C8035, Sigma-Aldrich, St. Louis, MO) were used for detection. Antibody diluent solution (DAKO, Glostrup, Denmark) was used to dilute primary antibodies. After incubation with primary antibodies (overnight at 4ºC), sections were washed and treated with bioinylated goat anti-rabbit IgG secondary antibodies followed by streptavidin horseradish peroxidase (HRP). Sections were reacted with DAB chromogen reagent for 10-20 min (DAB150 IHC Select, Millipore, Billerica, MA). Native tissues (osteochondral plug and tendon) were used as negative or positive controls. Color images were captured at a magnification of 10X using an Eclipse 90i upright microscope (Nikon Corp).

8.2.12 Statistical Analysis

Statistical analysis was performed using the SYSTAT software (v10.2, SYSTAT software Inc., San Jose, CA). Significance was determined by two-way ANOVA with Tukey's post hoc test ($p<0.05$).

8.3 Results

8.3.1 Chondrogenic capacity of ApCHs and ApMSCs in pellet culture

Adult porcine MSC (ApMSC) pellets severely contracted through 4 weeks in CM+ while adult porcine chondrocyte (ApCH) pellets grew well and deposited an ECM with dense PG and collagen, as assessed by Alcian blue and Picrosirius red staining, respectively. ApMSCs produced dense collagen but little PG **(Figure 8-1A)**. Likewise, the GAG content in ApCHs was 3.3 and 6 times greater than ApMSCs at 2 and 4 weeks, respectively **(Figure 8-1B)**.

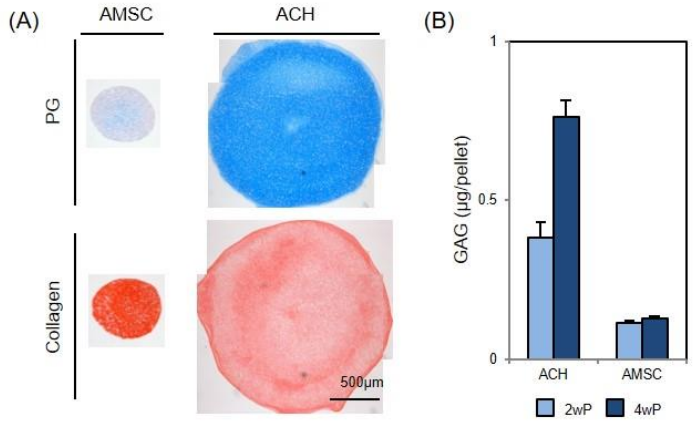

Figure 8-1: Chondrogenic capacity of ApCHs and ApMSCs in pellet culture.

(A) Alcian blue (Top) and Picrosirius red (Bottom) staining at 4 weeks, (B) GAG content (μg/construct). (Lighter bars = 2 weeks, Darker bars = 4 weeks; N = 3/group; $p<0.05$)

8.3.2 Micro-noodles increase surface area for nutrient exchange and intercellular communication

ApCHs remained viable within the micro-noodles **(Figure 8-2)** and deposited ECM. Cell-laden micro-noodles were initially straight **(Figure 8-3C)**, but curled into a random weave and opacified with culture duration **(Figure 8-5A)**. Cell-laden micro-noodles were initially straight **(Figure 8-3C)**, but curled into a random weave and opacified with culture duration **(Figure 8-5A)**. The actin cytoskeleton in ApCH-micro-noodles was cortical on day 0, but transitioned to a more fibrillar structure as cells divided and aggregated with one another by day 5 **(Figure 8-3D, inset)**.

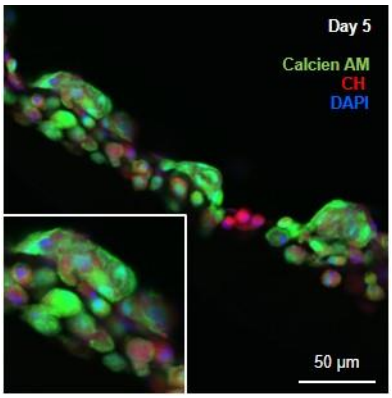

Figure 8-2: Viability of ApCH-laden micro-noodles at day 5. Live cells were visualized by Calcein-AM staining. (Green = Calcein-AM, Red = Chondrocytes, Blue = DAPI; Scale bar = 50 µm; Inset = Zoomed view; 10µm)

By design, the micro-noodles provided greater surface area in order to improve nutrient transport and intercellular communication. Given the same gel volume, the surface area of the micro-noodle was 8.5 times greater than a cylindrical construct. This difference in surface area accounted for up to 400 mm^2 **(Figure 8-4B and C)**.

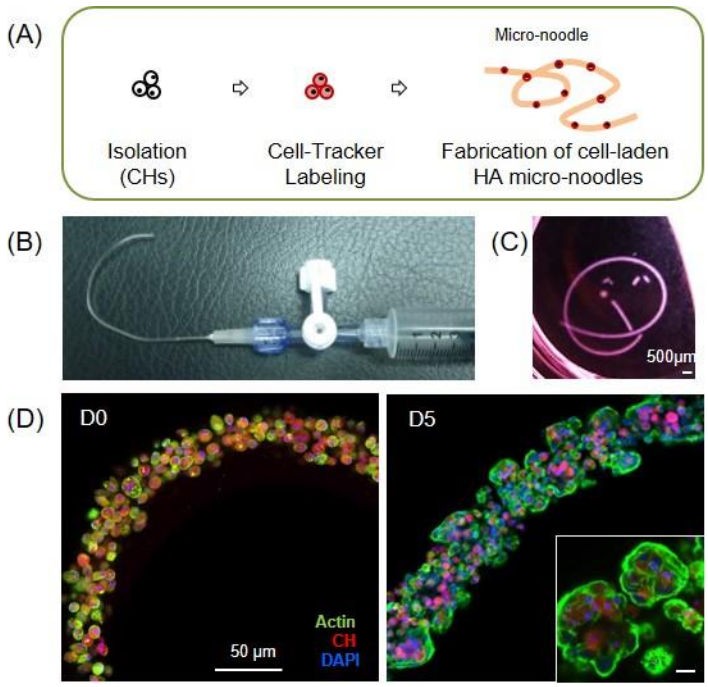

Figure 8-3: Fabrication of CH-laden micro-scale noodle-shaped construct. (A) Cell encapsulation and fabrication of micro-noodles, (B) Micro-bore tubing system, (C) gross image of micro-noodles on day 0 (Scale bar = 500μm), (D) visualization of micro-noodle by confocal microscopy on day 0 (Left) and day 5 (Right). (Green = actin, Blue = DAPI, Red = chondrocytes; Scale bar = 50 μm; Inset = Zoomed view; 10μm).

8.3.3 Chondrogenic maturation of ApCH-laden micro-noodles after long-term culture

Histological assessment showed that micro-noodles formed robust matrix that was homogeneously distributed throughout the diameter after 56 days in culture **(Figure 8-5)**. Immunohistochemistry of type II collagen showed dense staining with little evidence of type I collagen deposition. This indicates that ApCH form a cartilage like tissue within the micro-noodle format.

8.3.4 Influence of ApCH-laden micro-noodles on ApMSC chondrogenesis

Given our past findings that adult MSC function can be improved by co-culture with chondrocytes, we next developed an in vitro model of MSC colonization of a

microfracture treated defect. ApCH-laden micro-noodles were pre-cultured for 14 days in CM+ and then combined with ApMSCs in fibrin gel and cultured in CM+ for an additional 14 days. Staining on day 28 showed that the most intense matrix production by ApMSCs occurred at sites adjacent to the ApCH-laden micro-noodles. Fibrin construct seeded with only ApMSCs showed little matrix formation, and matrix occurred primarily in the periphery **(Figure 8-6C-E)**.

(A)

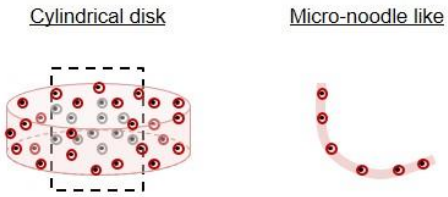

(B)

	Cylindrical construct	Micro-noodle
R (mm)	2	0.125
H (mm)	2.25	576
V (mm^3)	28.26	28.26
SA (mm^2)	53.38	**452.25**

(C)

Figure 8-4: Micro-noodles increase surface area to enhance nutrient transport and improve intercellular communication. (A) Schematic of cell-laden cylindrical constructs and micro-noodles (Red = healthy cells, Gray = apoptotic cells potentially due to the lack of nutrient transport). (B) Computation of surface area presented by micro-noodles and cylindrical constructs of a similar gel volume. Given the dimensions of cylindrical constructs (Ø4mm x 2.25mm), micro-noodles provide 8.5 times greater surface area and have 400 mm^2 greater surface area. (C) Gross appearance of cylindrical construct (Left) and micro-noodles (Right) on day 0 (Marking = 1mm).

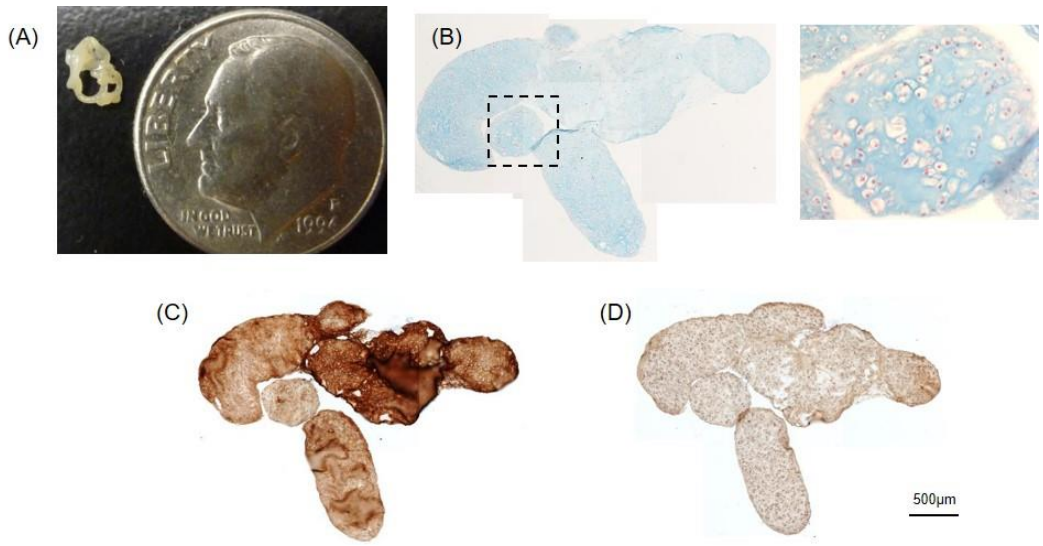

Figure 8-5: Histological assessment of CH-laden micro-noodles. (A) Gross image of micro-noodles after 8 weeks of culture. Histological analysis by (B) Alcian blue, (C) type II collagen, and (D) type I collagen staining (Scale bar = 500 µm).

Fibrin constructs with ApCH-laden micro-noodles co-cultured with ApMSCs showed dense PG, type II collagen and type I collagen deposition compared those cultured with ApMSC alone **(Figure 8-6C-E)**. PG produced by ApCH-laden micro-noodle alone constructs (lacking ApMSCs in the fibrin) remained within the boundary of micro-noodles and did not spread into the fibrin domain **(Figure 8-6B)**. Taken together, these findings suggest that the embedded ApCH-laden micro-noodles improve matrix production by co-cultured ApMSCs in this in vitro analog of a focal cartilage defect treated with microfracture.

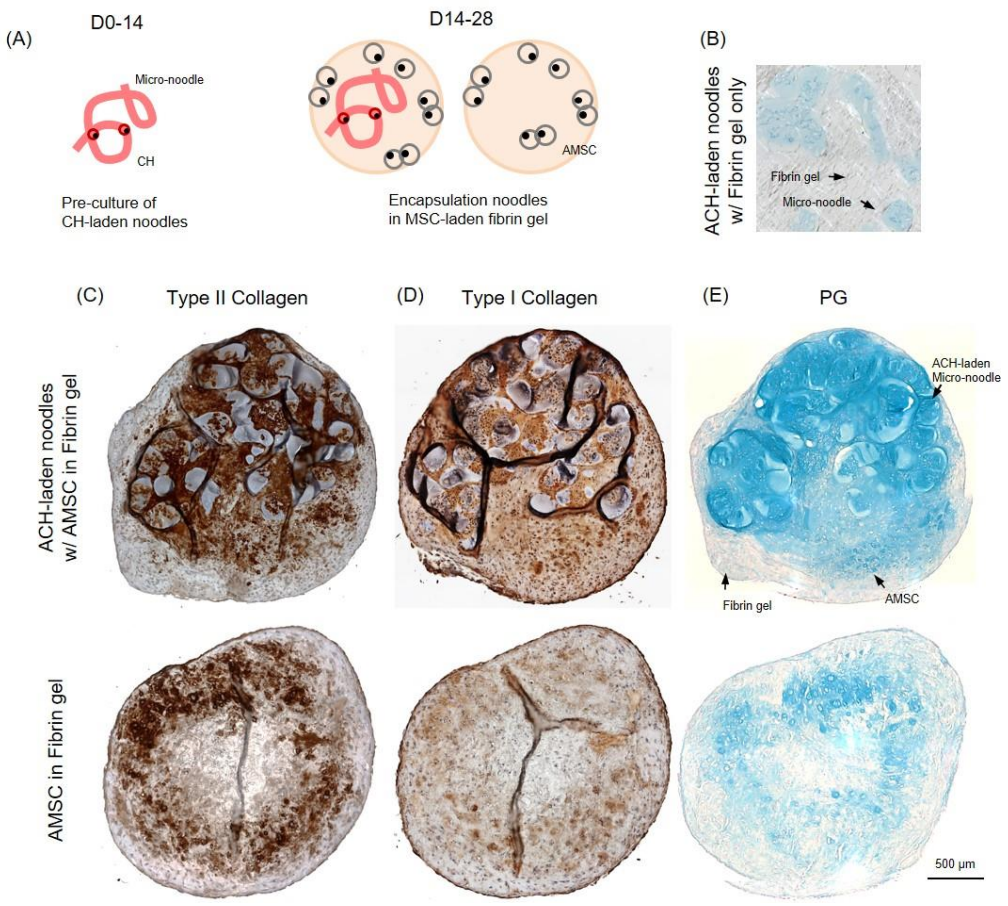

Figure 8-6: Influence of ApCH-laden micro-noodles on ApMSC chondrogenesis in fibrin gel. (A) Schematic of ApCH-laden micro-noodles and MSC/fibrin glue co-culture system. (B) Alcian blue staining: ApCH-laden micro-noodles only in fibrin gel. (C) Type II collagen staining: ApCH-laden micro-noodles co-cultured with ApMSC in fibrin gel (Top) and ApMSCs only in fibrin gel (Bottom). Type I collagen (D) and Alcian blue (E) staining of experimental groups (Scale bar = 500 µm).

8.3.5 Imaging of micro-noodles within chondral defects

To confirm the presence of micro-noodles in defects post implantation, we modified the materials to enable visualization using various imaging modalities (e.g., fluorescent/confocal microscopy or microCT). For this, HA macromer was reacted with a

fluorescent tag and/or combined with zirconium nanoparticles. To visualize delivered ApCH, cells were labeled with CellTracker prior to encapsulation in the micro-noodle. Results showed ApCH-laden micro-noodles visualized at a lower magnification in green (ApCHs) within red (micro-noodles) **(Figure 8-7A).** At higher magnification, using confocal microscopy, one can readily visualize cellular and subcellular components **(Figure 8-7B)**. Further, the combination of zirconium nanoparticles and methacrylated rhodamine B enabled visualization of micro-noodles by both microscopy and microCT **(Figure 8-7C)**. Visual inspection also showed that micro-noodles filled defects, with individual noodle structures randomly distributed through the defect space **(Figure 8-7D**). Micro-noodles within the cartilage defect were detected by fluorescent microscopy **(Figure 8-7E)** and microCT with 3D reconstruction **(Figure 8-7F).**

8.3.6 Detection of ApCH-laden micro-noodles in a large animal cartilage defect model

Using these methods, we next evaluated whether micro-noodles would remain in a focal cartilage defect after in vivo implantation and subsequent load-bearing use of the joint. ApCH-laden micro-noodles were injected into defects after microfracture was performed **(Figure 8-8A).** Visual inspection indicated that micro-noodles had remained within a chondral defect after one week post implantation **(Figure 8-8B)**. These micro-noodles clearly remained and covered the defect area, with some level of integration apparent with the adjacent cartilage **(Figure 8-8C)**. Confocal microscopy confirmed the presence of ApCH-laden micro-noodles in the defects as shown in red (delivered micro-noodles) and purple (delivered ApCHs). The fluorescent dyes that were used to label micro-noodles and ApCHs remained retained a strong signal intensity at this time point **(Figure 8-8D)**.

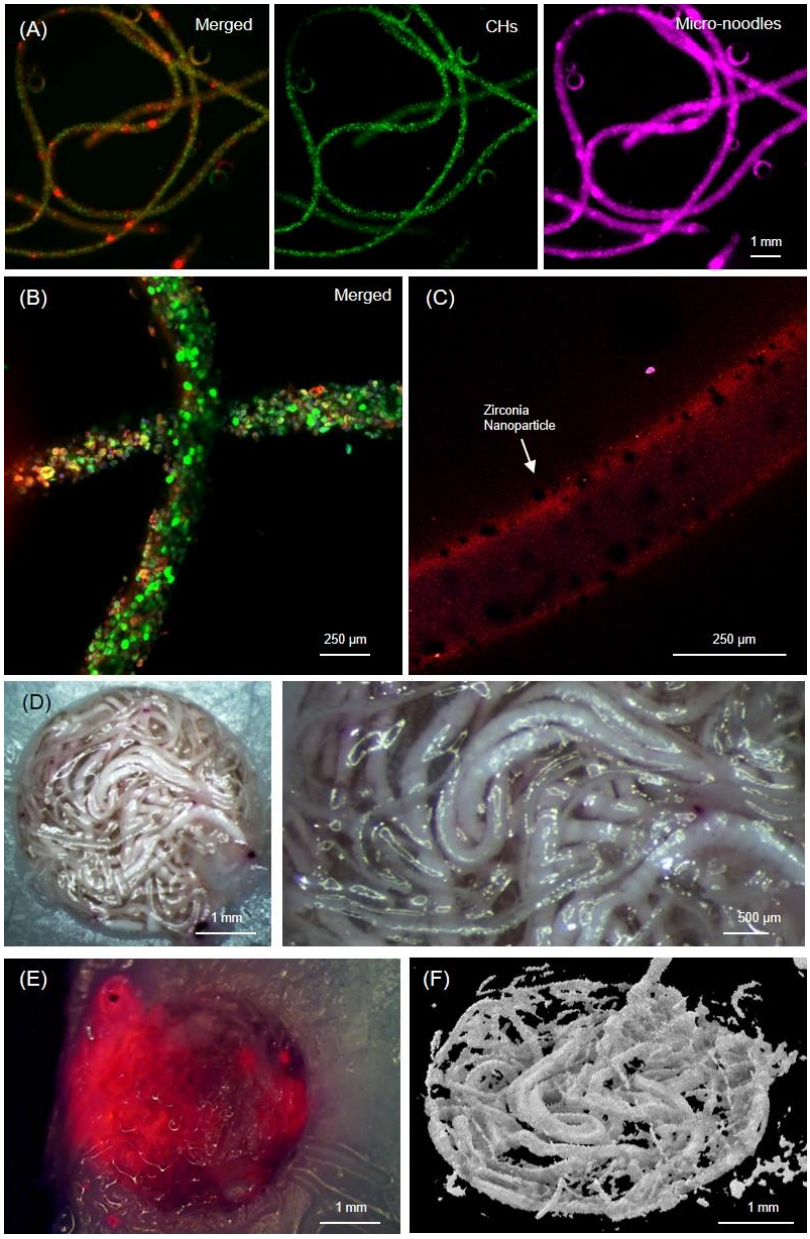

Figure 8-7: Detection of ApCH-laden micro-noodles in a focal cartilage defect. (A) To identify micro-noodles in defects after implantation, methacrylated rhodamine B was mixed with MeHA prior to polymerization. Merged image (Left) shows ApCHs (Green) and micro-noodles (Pink) (Scale bar = 1mm). (B) Micro-noodles imaged under confocal microscopy (Scale bar = 250 µm). (C) Micro-noodles mixed with zirconium nanoparticles for microCT, which appear as black speckles (Scale = 250 µm). (D) Osteochondral unit filled with zirconium nanoparticle-modified micro-noodles (Left) and zoomed view (Right) (Scale bar = 500 µm). (E) Micro-noodles detected by fluorescent microscopy (Scale = 1

mm). (F) MicroCT imaging of zirconium nanoparticle-seeded micro-noodles (Scale bar = 1mm).

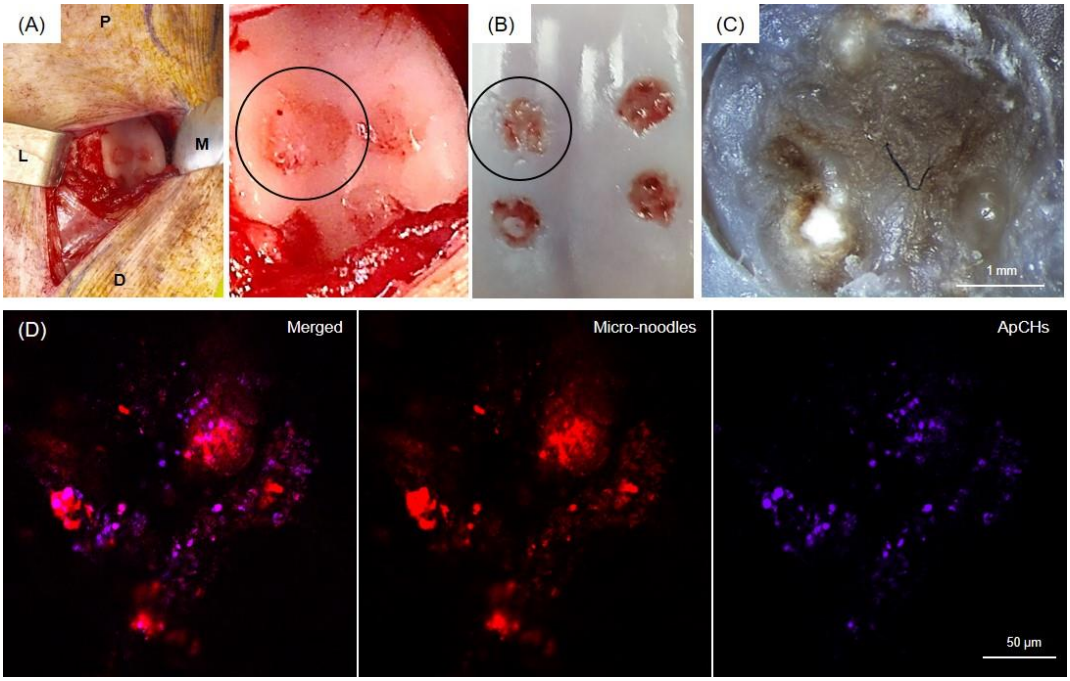

Figure 8-8: Retention of ApCH-laden micro-noodles in a large animal cartilage defect model. (A) Gross appearance of trochlear groove with defects filled with micro-noodles (Left) and zoomed in view of trochlear groove (Right). (B) Trochlear groove at one week post-surgery. (C) Zoomed view of defect filled with ApCH-laden micro-noodles at one week post-surgery. (D) Micro-noodles remained in the defect for one week post-surgery, as evidenced by presence of fluorescently labeled gel material and cells (Red = micro-noodles, Purple = ApCHs; Scale bar = 50 µm).

8.4 Discussion

In this study, we developed micro-scale CH-seeded noodle-shaped constructs that can be combined with current microfracture procedures. The small size of these constructs allowed for efficient nutrient transport and intercellular communication, resulting in

homogeneous matrix formation throughout the diameter and improved adult MSC chondrogenesis when these cells were co-cultured with CH-laden micro-noodles in vitro. The small size and flexibility of these micro-noodles also makes them suitable for filling various defect sizes and shapes. When first formed, CHs in micro-noodles appeared as distinct rounded cells (with cortical actin), but rapidly reorganized to form a thin and tough 3D structure that could be manipulated with forceps. Pre-cultured CH-seeded micro-noodles improved MSC chondrogenesis when these two elements were co-cultured in a fibrin gel, mimicking the environment of the cartilage defect post-microfracture. These micro-noodles could thus be incorporated within bone marrow/marrow concentrate and implanted to improve cartilage repair. Likewise, when the fluorescent dye-labeled CH-laden micro-noodles were directly injected into defects after microfracture was performed in an in vivo large animal model, micro-noodles remained in place over the first 1-2 weeks post-surgery, as was confirmed by confocal microscopy. Current studies are focused on further scaling down the diameter of these micro-noodles and optimizing their ease of use during surgical procedures. Together, these findings show that CH-laden micro-noodle constructs are a clinically relevant tool that can be used to capitalize on CH/MSC interactions to improve cartilage repair. This novel co-culture inspired repair strategy is now being evaluated to demonstrate functional cartilage regeneration in vivo over the long term.

CHAPTER 9: Summary and Future Directions

9.1 Summary

Cell-based cartilage tissue engineering strategies combined with biomaterials have achieved a fundamental goal in that they can now recapitulate the mechanical properties and biochemical content of native tissue with sophisticated in vitro culture methods. However, the persistent and remaining challenge and ultimate goal of tissue engineering is the successful translation of these engineering strategies to humans, who will experience a complete recovery of their intrinsic functions and biology. While great progress has been made towards this goal, the remaining gap seems quite large in reality. With the goal of contributing in linking this gap, placing one small stone in this pathway, we initially investigated the chondrogenic capacity of human MSCs **(Chapter 3)** and explored the optimal delivery methods of TGF-β3 and/or dexamethasone to promote functional outcomes of MSC-laden constructs **(Chapter 4 and 5)**. Likewise, we also queried the effect of molecular factors secreted from chondrocytes in restoring the functional chondrogenic potential of MSCs under co-culture condition **(Chapter 6)**. Based on the findings in Chapter 6, in terms of the characteristics of zonal chondrocytes, mechanisms of intercellular communication, and the functional outcomes as a result of co-culture, in **Chapter 7**, we developed engineered constructs that recapitulate native structure and functional properties while at the same time improving nutrient transport to enable growth of these large constructs. Finally, using the co-culture concept described in Chapter 6 and taking advantage of the importance of nutrient transport demonstrated in Chapter 7, we developed CH-seeded micro-scaled noodle-like constructs, 'micro-noodles', to deliver molecular factors secreted from CHs to endogenous MSCs recruited from underlying bone during the clinically utilized microfracture procedure, validated this micro-scale co-culture concept in a bone marrow-like condition in vitro, and eventually

evaluated the initial stability and retention of these micro-noodles in chondral defects in a large animal **(Chapter 8)**.

In Chapter 3, our findings showed marked differences in functional chondrogenesis of hMSCs in 3D culture, based on donor. Increasing cell density resulted in increased properties, but also promoted construct contraction for some donors. Increasing the macromer density generally stabilized construct dimensions, but limited the distribution of formed matrix. For donors that showed marked contraction in low weight percentage HA gels, inhibition of cell contractility stabilized construct dimensions and maintained cell distribution, but did not improve functional properties over the long term. Collectively, these findings suggest that the use of autologous MSCs may require tuning of cell density and gel mechanics on a donor-by-donor basis in order to provide for the most robust tissue formation for clinical application.

Results in Chapter 4 demonstrated that a brief exposure (7 days) to a very high level (100 ng/mL) of TGF-β3 was sufficient to both induce and maintain cartilage formation in these 3D constructs. Indeed, this short delivery resulted in constructs with mechanical and biochemical properties that exceeded that of continuous exposure to a lower level (10 ng/mL) of TGF-β3 over the entire 9-week time course. Of important note, the total TGF delivery in these two scenarios was roughly equivalent (200 vs. 180 ng), but the timing of delivery differed markedly. These data support the idea that acute exposure to a high dose of TGF will induce functional and long-term differentiation of stem cell populations, and furthers our efforts to improve cartilage repair *in vivo*.

In Chapter 5, constructs cultured in CM+ and DEX- conditions produced robust matrix, while those in ITS/BSA/LA- and Serum+ conditions produced little to no matrix. While

construct properties in DEX- conditions were greater than those in CM+ at 4 weeks, properties in CM+ and DEX- reversed by 8 weeks, with CM+ constructs being higher. While construct properties in DEX- were greater than those in CM+ at 4 weeks, the continued absence or removal of dexamethasone resulted in marked GAG loss by 8 weeks. Conversely, the continued presence or new addition of dexamethasone at 4 weeks further improved or maintained construct properties through 8 weeks. Finally, when constructs were converted to serum containing media after pre-culture in CM+ for 4 weeks, GAG loss was attenuated when cultured in Serum+ supplemented with dexamethasone (34% loss with dex vs. 80% loss without dex). These data suggest that dexamethasone influences the functional maturation of MSC-laden HA constructs, and may help to maintain properties during long-term culture, or with in vivo translation, by repressing pro-inflammatory signals that arise with time in culture or as a result of the implantation environment.

In Chapter 6, we showed the differential impact of zonal CHs on MSC chondrogenesis, demonstrated that juvenile CHs can promote functional growth by aged MSCs in co-culture, identified molecular pathways involved in this co-culture phenomenon, and demonstrated that extracellular vesicles (EVs) are a primary mechanism mediating the co-culture phenomenon. These findings will forward the development of new therapeutic agents and more effective delivery systems to promote functional cartilage tissue formation by adult autologous MSCs.

In Chapter 7, we were able to fabricate tri-layered constructs with depth-dependent organization and properties. To address the issue of scale up of these large constructs, we showed that the addition of HFs or HFs/threads improved matrix accumulation in the central core region. With HF/threads, the local modulus in the deep region of tri-layered

constructs nearly matched that of native tissue, though the properties in the central regions remained lower. These constructs reproduced the zonal organization and depth-dependent properties of native tissue, and demonstrated that a layer-by-layer fabrication scheme holds promise for the biomimetic repair of focal cartilage defects.

In this Chapter 8, we examined the chondrogenic capacity of adult porcine CHs and MSCs, reported on methods for the fabrication of micro-noodles, showed their chondro-inductive capacity in an environment mimicking microfracture (co-culture in an MSC-laden fibrin gel), and evaluated their delivery and retention in an in vivo large animal model of cartilage repair. Our findings demonstrated that CH-laden micro-noodle improved MSC chondrogenesis in vitro, and that micro-noodles remained in defects over 1-2 weeks in our large animal model. Taken together, these findings demonstrate the promise of this novel approach as a clinically relevant tool that can take advantage of CH/MSC interactions occurring during microfracture procedures to improve cartilage repair.

9.2 Limitations and Future Directions

9.2.1 Determination of molecular factors/pathways in co-culture

In Chapter 6, we demonstrated that molecular factors secreted from juvenile CHs rejuvenated the chondrogenic capacity of adult MSCs and altered their genomic profiles. However, specific upstream genes or pathways related to these genes were not fully investigated and validated. From this study, we identified and confirmed that the intercellular communication of co-culture occurred through clathrin-mediated endocytosis of extracellular vesicles (EVs), but we did not specifically identify their contents. EVs have been reported to transfer microRNAs, DNA, and various proteins, and recent studies have demonstrated the role of microRNAs in transferring genomic characteristics

from one cell type to another. Further work to isolate, identify the contents of, and delivery these EVs will be carried out in future studies.

9.2.2 Arthroscopic delivery of micro-noodles

In Chapter 8, we fabricated micro-noodles and demonstrated functional maturation of cell-laden micro-noodles and showed their impact when co-cultured with adult MSCs in vitro. We also proved the stability and retention of these micro-noodles after implantation in a large animal cartilage defect model. However, one limitation of the micro-bore tubing system is the high extrusion pressure required after photo-polymerization. To achieve better control in terms of delivering micro-noodles to the defects, the surface tension between the inner surface of the tubing and the polymerized micro-noodles needs be reduced. Also, given the design of the first generation delivery device, micro-noodles were delivered during an open knee surgery. However, because of their conformation and scale, micro-noodles can be delivered arthroscopically, with the appropriate delivery system. As minimally-invasive surgery provides greater benefits in terms of cost, patient happiness, and the time required for surgery/recovery, an ideal development would be the design of an arthroscopic delivery device to combine micro-noodles with microfracture (which itself can be performed arthroscopically). Efforts are underway now to design such a device **(Figure 9-1)**. Once complete, we will use this system to assess the impact of arthroscopic micro-noodle delivery on the long term quality of cartilage repair compared to arthroscopic microfracture alone. We will also, based on findings from Chapters 4-6, work to optimize the micro-noodles to produce robust matrix and exert a powerful co-culture effect within the synovial joint cavity, where cells are exposed to bone marrow and synovial fluid, through the controlled release of select agents, such as TGF-β3 and dexamethasone.

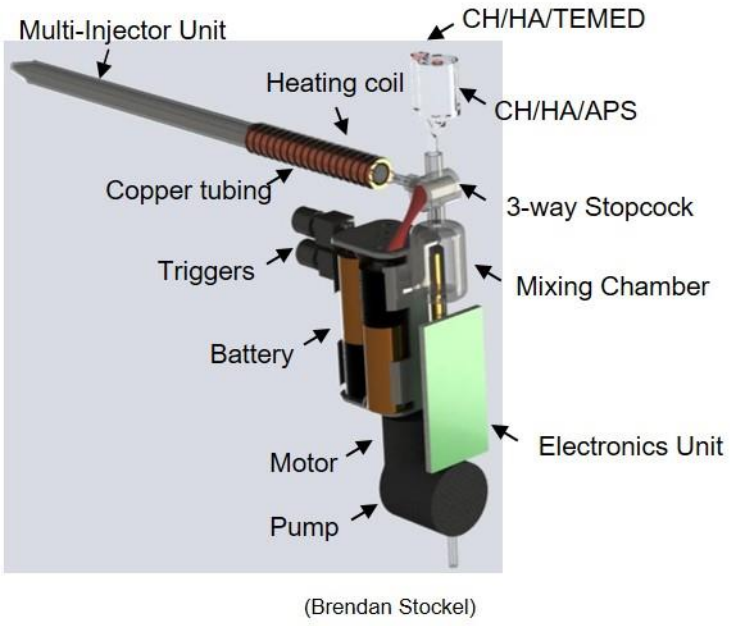

Figure 9-1: Schematic of arthroscopic micro-noodle delivery system

9.3 Conclusions

The ultimate goal of cartilage tissue engineering is not only to recapitulate the native structure, mechanical properties, and biochemical content of articular cartilage, but also to enable these engineered cartilage implants to function in the joint while maintaining the correct phenotype with physical and morphological integrity in the synovial joint. Ideally, delivery of a functional implant such as this would improve patient related outcomes (reducing pain) without causing pain or other side effects. While this seemed an unattainable goal a few decades ago, given the lack of knowledge of cartilage biology and lack of technological capacity, numerous novel findings have emerged that have gradually begun to fill the gap. The work contained in this thesis demonstrates that one can enhance the chondrogenic potential of adult MSCs not only by the proper delivery of growth factors and/or synthetic hormones, but also by taking advantage of naturally generated molecular factors secreted from chondrocytes. Further, based on the tunability of hyaluronic acid (HA) hydrogels and the zonal characteristics of chondrocytes

MSCs, we were able to recapitulate the depth-dependent mechanical properties and biochemical content of native tissue (with distinct zonal organization), using HA-based hydrogels while improving nutrient transport. Finally, based on our new understanding of co-culture mechanisms and limitations, we fabricated micro-noodles and showed their potential to harness the co-culture phenomenon in a clinical scenario (i.e., microfracture). Collectively, this work provides additional understanding of mesenchymal stem cell biology and advances and develops new technologies for engineering cartilage tissue that will ultimately speed the translation of novel regenerative therapies to address this widespread and debilitating condition.

BIBLIOGRAPHY

Acharya, C., A. Adesida, P. Zajac, M. Mumme, J. Riesle, I. Martin and A. Barbero (2012). "Enhanced chondrocyte proliferation and mesenchymal stromal cells chondrogenesis in coculture pellets mediate improved cartilage formation." J Cell Physiol **227**(1): 88-97.

Akizuki, S., V. C. Mow, F. Muller, J. C. Pita, D. S. Howell and D. H. Manicourt (1986). "Tensile properties of human knee joint cartilage: I. Influence of ionic conditions, weight bearing, and fibrillation on the tensile modulus." J Orthop Res **4**(4): 379-392.

Amano, M., M. Nakayama and K. Kaibuchi (2010). "Rho-kinase/ROCK: A key regulator of the cytoskeleton and cell polarity." Cytoskeleton (Hoboken) **67**(9): 545-554.

Ateshian, G. A. and C. T. Hung (2005). "Patellofemoral joint biomechanics and tissue engineering." Clin Orthop Relat Res **436**: 81-90.

Ateshian, G. A., L. J. Soslowsky and V. C. Mow (1991). "Quantitation of articular surface topography and cartilage thickness in knee joints using stereophotogrammetry." J Biomech **24**(8): 761-776.

Aung, A., G. Gupta, G. Majid and S. Varghese (2011). "Osteoarthritic chondrocyte-secreted morphogens induce chondrogenic differentiation of human mesenchymal stem cells." Arthritis Rheum **63**(1): 148-158.

Aydelotte, M. B., R. R. Greenhill and K. E. Kuettner (1988). "Differences between sub-populations of cultured bovine articular chondrocytes. II. Proteoglycan metabolism." Connect Tissue Res **18**(3): 223-234.

Aydelotte, M. B. and K. E. Kuettner (1988). "Differences between sub-populations of cultured bovine articular chondrocytes. I. Morphology and cartilage matrix production." Connect Tissue Res **18**(3): 205-222.

Bajpayee, A. G., M. A. Quadir, P. T. Hammond and A. J. Grodzinsky (2016). "Charge based intra-cartilage delivery of single dose dexamethasone using Avidin nano-carriers suppresses cytokine-induced catabolism long term." Osteoarthritis Cartilage **24**(1): 71-81.

Bajpayee, A. G., C. R. Wong, M. G. Bawendi, E. H. Frank and A. J. Grodzinsky (2014). "Avidin as a model for charge driven transport into cartilage and drug delivery for treating early stage post-traumatic osteoarthritis." Biomaterials **35**(1): 538-549.

Bassilana, F., A. Carlson, J. A. DaSilva, B. Grosshans, S. Vidal, V. Beck, B. Wilmeringwetter, L. A. Llamas, T. B. Showalter, P. Rigollier, A. Bourret, A. Ramamurthy, X. Wu, F. Harbinski, S. Plonsky, L. Lee, H. Ruffner, P. Grandi, M. Schirle, J. Jenkins, A. W. Sailer, T. Bouwmeester, J. A. Porter, V. Myer, P. M. Finan, J. A. Tallarico, J. F. Kelleher, 3rd, K. Seuwen, R. K. Jain and S. J. Luchansky (2014). "Target identification for a Hedgehog pathway inhibitor reveals the receptor GPR39." Nat Chem Biol **10**(5): 343-349.

Bayliss, M. T., D. Osborne, S. Woodhouse and C. Davidson (1999). "Sulfation of chondroitin sulfate in human articular cartilage. The effect of age, topographical position, and zone of cartilage on tissue composition." J Biol Chem **274**(22): 15892-15900.

Berezhkovskii, A. M., C. Sample and S. Y. Shvartsman (2011). "Formation of morphogen gradients: Local accumulation time." Phys Rev E Stat Nonlin Soft Matter Phys **83**(5 Pt 1): 051906.

Bhosale, A. M. and J. B. Richardson (2008). "Articular cartilage: structure, injuries and review of management." Br Med Bull **87**: 77-95.

Bian, L., S. L. Angione, K. W. Ng, E. G. Lima, D. Y. Williams, D. Q. Mao, G. A. Ateshian and C. T. Hung (2009). "Influence of decreasing nutrient path length on the development of engineered cartilage." Osteoarthritis Cartilage **17**(5): 677-685.

Bian, L., M. Guvendiren, R. L. Mauck and J. A. Burdick (2013). "Hydrogels that mimic developmentally relevant matrix and N-cadherin interactions enhance MSC chondrogenesis." Proc Natl Acad Sci U S A **110**(25): 10117-10122.

Bian, L., D. Y. Zhai, R. L. Mauck and J. A. Burdick (2011). "Coculture of human mesenchymal stem cells and articular chondrocytes reduces hypertrophy and enhances functional properties of engineered cartilage." Tissue Eng Part A **17**(7-8): 1137-1145.

Bian, L., D. Y. Zhai, E. Tous, R. Rai, R. L. Mauck and J. A. Burdick (2011). "Enhanced MSC chondrogenesis following delivery of TGF-beta3 from alginate microspheres within hyaluronic acid hydrogels in vitro and in vivo." Biomaterials **32**(27): 6425-6434.

Bian, L., D. Y. Zhai, E. Tous, R. Rai, R. L. Mauck and J. A. Burdick (2011). "Enhanced MSC chondrogenesis following delivery of TGF-ß3 from alginate microspheres within hyaluronic acid hydrogels in vitro and in vivo." Biomaterials **32**(27): 6425-6434.

Blunk, T., A. L. Sieminski, K. J. Gooch, D. J. Courter, A. P. Hollander, A. M. Nahir, R. Langer, G. Vunjak-Novakovic and L. E. Freed (2002). "Differential effects of growth factors on tissue-engineered cartilage." Tissue Eng **8**(1): 73-84.

Boskey, A. L. and N. Pleshko Camacho (2007). "FT-IR imaging of native and tissue-engineered bone and cartilage." Biomaterials **28**(15): 2465-2478.

Bosserhoff, A. K. and R. Buettner (2003). "Establishing the protein MIA (melanoma inhibitory activity) as a marker for chondrocyte differentiation." Biomaterials **24**(19): 3229-3234.

Bosserhoff, A. K., S. Kondo, M. Moser, U. H. Dietz, N. G. Copeland, D. J. Gilbert, N. A. Jenkins, R. Buettner and L. J. Sandell (1997). "Mouse CD-RAP/MIA gene: structure, chromosomal localization, and expression in cartilage and chondrosarcoma." Dev Dyn **208**(4): 516-525.

Broom, N. D. and D. L. Marra (1986). "Ultrastructural evidence for fibril-to-fibril associations in articular cartilage and their functional implication." J Anat **146**: 185-200.

Buckley, C. T., S. D. Thorpe and D. J. Kelly (2009). "Engineering of large cartilaginous tissues through the use of microchanneled hydrogels and rotational culture." Tissue Eng Part A **15**(11): 3213-3220.

Buckley, C. T., S. D. Thorpe, F. J. O'Brien, A. J. Robinson and D. J. Kelly (2009). "The effect of concentration, thermal history and cell seeding density on the initial mechanical properties of agarose hydrogels." J Mech Behav Biomed Mater **2**(5): 512-521.

Buckwalter, J. A. and H. J. Mankin (1998). "Articular cartilage: tissue design and chondrocyte-matrix interactions." Instr Course Lect **47**: 477-486.

Buckwalter, J. A., H. J. Mankin and A. J. Grodzinsky (2005). "Articular cartilage and osteoarthritis." Instr Course Lect **54**: 465-480.

Buckwalter, J. A., J. Martin and H. J. Mankin (2000). "Synovial joint degeneration and the syndrome of osteoarthritis." Instr Course Lect **49**: 481-489.

Burdick, J. A., C. Chung, X. Jia, M. A. Randolph and R. Langer (2005). "Controlled degradation and mechanical behavior of photopolymerized hyaluronic acid networks." Biomacromolecules **6**(1): 386-391.

Buschmann, M. D., Y. A. Gluzband, A. J. Grodzinsky and E. B. Hunziker (1995). "Mechanical compresson modulates matrix biosynthesis in chondrocyte/agarose culture." J Cell Sci **108**(Pt 4): 745-758.

Buschmann, M. D., Y. A. Gluzband, A. J. Grodzinsky, J. H. Kimura and E. B. Hunziker (1992). "Chondrocytes in agarose culture synthesize a mechanically functional extracellular matrix." J Orthop Res **10**(6): 745-758.

Byers, B. A., R. L. Mauck, I. E. Chiang and R. S. Tuan (2008). "Transient exposure to transforming growth factor beta 3 under serum-free conditions enhances the biomechanical and biochemical maturation of tissue-engineered cartilage." Tissue Eng Part A **14**(11): 1821-1834.

Camacho, N. P., P. West, P. A. Torzilli and R. Mendelsohn (2001). "FTIR microscopic imaging of collagen and proteoglycan in bovine cartilage." Biopolymers **62**(1): 1-8.

Caplan, A. I. (1991). "Mesenchymal stem cells." J Orthop Res **9**(5): 641-650.

Carney, S. L. and H. Muir (1988). "The structure and function of cartilage proteoglycans." Physiol Rev **68**(3): 858-910.

Caterson, E. J., L. J. Nesti, W. J. Li, K. G. Danielson, T. J. Albert, A. R. Vaccaro and R. S. Tuan (2001). "Three-dimensional cartilage formation by bone marrow-derived cells seeded in polylactide/alginate amalgam." J Biomed Mater Res **57**(3): 394-403.

Chen, C. T., K. W. Fishbein, P. A. Torzilli, A. Hilger, R. G. Spencer and W. E. Horton, Jr. (2003). "Matrix fixed-charge density as determined by magnetic resonance microscopy of bioreactor-derived hyaline cartilage correlates with biochemical and biomechanical properties." Arthritis Rheum **48**(4): 1047-1056.

Chen, S. S., Y. H. Falcovitz, R. Schneiderman, A. Maroudas and R. L. Sah (2001). "Depth-dependent compressive properties of normal aged human femoral head articular cartilage: relationship to fixed charge density." Osteoarthritis Cartilage **9**(6): 561-569.

Chen, X., H. Liang, J. Zhang, K. Zen and C. Y. Zhang (2012). "Secreted microRNAs: a new form of intercellular communication." Trends Cell Biol **22**(3): 125-132.

Chen, Y. G. (2009). "Endocytic regulation of TGF-beta signaling." Cell Res **19**(1): 58-70.

Cheng, C., E. Conte, N. Pleshko-Camacho and C. Hidaka (2007). "Differences in matrix accumulation and hypertrophy in superficial and deep zone chondrocytes are controlled by bone morphogenetic protein." Matrix Biol **26**(7): 541-553.

Cheng, X., J. L. Chen, Z. L. Ma, Z. L. Zhang, S. Lv, D. M. Mai, J. J. Liu, M. Chuai, K. K. Lee, C. Wan and X. Yang (2014). "Biphasic influence of dexamethasone exposure on embryonic vertebrate skeleton development." Toxicol Appl Pharmacol **281**(1): 19-29.

Chung, C., M. Beecham, R. L. Mauck and J. A. Burdick (2009). "The influence of degradation characteristics of hyaluronic acid hydrogels on in vitro neocartilage formation by mesenchymal stem cells." Biomaterials **30**(26): 4287-4296.

Chung, C. and J. A. Burdick (2009). "Influence of three-dimensional hyaluronic acid microenvironments on mesenchymal stem cell chondrogenesis." Tissue Eng **15**(2): 243-254.

Chung, C. and J. A. Burdick (2009). "Influence of three-dimensional hyaluronic acid microenvironments on mesenchymal stem cell chondrogenesis." Tissue Eng Part A **15**(2): 243-254.

Cigan, A. D., K. M. Durney, R. J. Nims, G. Vunjak-Novakovic, C. T. Hung and G. A. Ateshian (2016). "Nutrient Channels Aid the Growth of Articular Surface-Sized Engineered Cartilage Constructs." Tissue Eng Part A **22**(17-18): 1063-1074.

Cigan, A. D., R. J. Nims, M. B. Albro, G. Vunjak-Novakovic, C. T. Hung and G. A. Ateshian (2014). "Nutrient channels and stirring enhanced the composition and stiffness of large cartilage constructs." J Biomech **47**(16): 3847-3854.

Cigan, A. D., R. J. Nims, G. Vunjak-Novakovic, C. T. Hung and G. A. Ateshian (2016). "Optimizing nutrient channel spacing and revisiting TGF-beta in large engineered cartilage constructs." J Biomech **49**(10): 2089-2094.

Cosgrove, B. D., K. L. Mui, T. P. Driscoll, S. R. Caliari, K. D. Mehta, R. K. Assoian, J. A. Burdick and R. L. Mauck (2016). "N-cadherin adhesive interactions modulate matrix mechanosensing and fate commitment of mesenchymal stem cells." Nat Mater **15**(12): 1297-1306.

Cravero, J. D., C. S. Carlson, H. J. Im, R. R. Yammani, D. Long and R. F. Loeser (2009). "Increased expression of the Akt/PKB inhibitor TRB3 in osteoarthritic chondrocytes inhibits insulin-like growth factor 1-mediated cell survival and proteoglycan synthesis." Arthritis Rheum **60**(2): 492-500.

Darling, E. M. and K. A. Athanasiou (2005). "Rapid phenotypic changes in passaged articular chondrocyte subpopulations." J Orthop Res **23**(2): 425-432.

Darling, E. M. and K. A. Athanasiou (2005). "Retaining zonal chondrocyte phenotype by means of novel growth environments." Tissue Eng **11**(3-4): 395-403.

de Windt, T. S., D. B. Saris, I. C. Slaper-Cortenbach, M. H. van Rijen, D. Gawlitta, L. B. Creemers, R. A. de Weger, W. J. Dhert and L. A. Vonk (2015). "Direct Cell-Cell Contact with Chondrocytes Is a Key Mechanism in Multipotent Mesenchymal Stromal Cell-Mediated Chondrogenesis." Tissue Eng Part A **21**(19-20): 2536-2547.

Di Guglielmo, G. M., C. Le Roy, A. F. Goodfellow and J. L. Wrana (2003). "Distinct endocytic pathways regulate TGF-beta receptor signalling and turnover." Nat Cell Biol **5**(5): 410-421.

Diao, H. J., C. W. Yeung, C. H. Yan, G. C. Chan and B. P. Chan (2013). "Bidirectional and mutually beneficial interactions between human mesenchymal stem cells and osteoarthritic chondrocytes in micromass co-cultures." Regen Med **8**(3): 257-269.

Dore, S., J. P. Pelletier, J. A. DiBattista, G. Tardif, P. Brazeau and J. Martel-Pelletier (1994). "Human osteoarthritic chondrocytes possess an increased number of insulin-like growth factor 1 binding sites but are unresponsive to its stimulation. Possible role of IGF-1-binding proteins." Arthritis Rheum **37**(2): 253-263.

Eckstein, F., A. Gavazzeni, H. Sittek, M. Haubner, A. Losch, S. Milz, K. H. Englmeier, E. Schulte, R. Putz and M. Reiser (1996). "Determination of knee joint cartilage thickness using three-dimensional magnetic resonance chondro-crassometry (3D MR-CCM)." Magn Reson Med **36**(2): 256-265.

Erickson, I. E., A. H. Huang, C. Chung, R. T. Li, J. A. Burdick and R. L. Mauck (2009). "Differential maturation and structure-function relationships in mesenchymal stem cell- and chondrocyte-seeded hydrogels." Tissue Eng Part A **15**(5): 1041-1052.

Erickson, I. E., A. H. Huang, S. Sengupta, S. Kestle, J. A. Burdick and R. L. Mauck (2009). "Macromer density influences mesenchymal stem cell chondrogenesis and maturation in photocrosslinked hyaluronic acid hydrogels." Osteoarthritis Cartilage **17**(12): 1639-1648.

Erickson, I. E., A. H. Huang, S. Senqupta, S. Kestle, J. A. Burdick and R. L. Mauck (2009). "Macromer density influences mesenchymal stem cell chondrogenesis and maturation in photocrosslinked hyaluronic acid hydrogel." Osteoarthitis Cartilage **17**(12): 1639-1648.

Erickson, I. E., S. R. Kestle, K. H. Zellars, J. A. Burdick and R. L. Mauck (2011). "High Density MSC-Seeded Hyaluronic Acid Constructs Produce Engineered Cartilage with Near-Native Properties." The 57th Annual Meeting of the Orthopaedic Research Society, Long Beach, CA, January 13-16.

Erickson, I. E., S. R. Kestle, K. H. Zellars, M. J. Farrell, M. Kim, J. A. Burdick and R. L. Mauck (2012). "High mesenchymal stem cell seeding densities in hyaluronic acid hydrogels produce engineered cartilage with native tissue properties." Acta Biomater **8**(8): 3027-3034.

Erickson, I. E., S. C. van Veen, S. Sengupta, S. R. Kestle and R. L. Mauck (2011). "Cartilage matrix formation by bovine mesenchymal stem cells in three-dimensional culture is age-dependent." Clin Orthop Relat Res **469**(10): 2744-2753.

Erickson, I. E., S. C. van Veen, S. Senqupta, S. R. Kestle and R. L. Mauck (2011). "Cartilage Matrix Formation by Bovine Mesenchymal Stem Cells in Three-dimensional Culture Is Age-dependent." Clin Orthop Relat Res.

Eyre, D. (2002). "Collagen of articular cartilage." Arthritis Res **4**(1): 30-35.

Fakhari, A. and C. Berkland (2013). "Applications and emerging trends of hyaluronic acid in tissue engineering, as a dermal filler and in osteoarthritis treatment." Acta Biomater **9**(7): 7081-7092.

Farndale, R. W., D. J. Buttle and A. J. Barrett (1986). "Improved quantitation and discrimination of sulphated glycosaminoglycans by use of dimethylmethylene blue." Biochim Biophys Acta **883**(2): 173-177.

Farnum, C. E., J. Turgai and N. J. Wilsman (1990). "Visualization of living terminal hypertrophic chondrocytes of growth plate cartilage in situ by differential interference contrast microscopy and time-lapse cinematography." J Orthop Res **8**(5): 750-763.

Farrell, M. J., E. Comeau, N. Neururkar, A. H. Huang and R. L. Mauck (2011). "Depth-Dependent Mechanical Properties of MSC-laden Engineered Cartilage Constructs." The 57th Annual Meeting of the Orthopaedic Research Society, Long Beach, CA, January 13-16.

Farrell, M. J., E. S. Comeau and R. L. Mauck (2012). "Mesenchymal stem cells produce functional cartilage matrix in three-dimensional culture in regions of optimal nutrient supply." Eur Cell Mater **23**: 425-440.

Farrell, M. J., M. B. Fisher, A. H. Huang, J. I. Shin, K. M. Farrell and R. L. Mauck (2014). "Functional properties of bone marrow-derived MSC-based engineered cartilage are unstable with very long-term in vitro culture." J Biomech **47**(9): 2173-2182.

Fischer, J., A. Dickhut, M. Rickert and W. Richter (2010). "Human articular chondrocytes secrete parathyroid hormone-related protein and inhibit hypertrophy of mesenchymal stem cells in coculture during chondrogenesis." Arthritis Rheum **62**(9): 2696-2706.

Fisher, M. B., N. S. Belkin, A. H. Milby, E. A. Henning, M. Bostrom, M. Kim, C. Pfeifer, G. Meloni, G. R. Dodge, J. A. Burdick, T. P. Schaer, D. R. Steinberg and R. L. Mauck (2015). "Cartilage repair and subchondral bone remodeling in response to focal lesions in a mini-pig model: implications for tissue engineering." Tissue Eng Part A **21**(3-4): 850-860.

Fisher, M. B., N. S. Belkin, A. H. Milby, E. A. Henning, N. Soegaard, M. Kim, C. Pfeifer, V. Saxena, G. R. Dodge, J. A. Burdick, T. P. Schaer, D. R. Steinberg and R. L. Mauck

(2016). "Effects of Mesenchymal Stem Cell and Growth Factor Delivery on Cartilage Repair in a Mini-Pig Model." Cartilage **7**(2): 174-184.

Florine, E. M., R. E. Miller, R. M. Porter, C. H. Evans, B. Kurz and A. J. Grodzinsky (2013). "Effects of Dexamethasone on Mesenchymal Stromal Cell Chondrogenesis and Aggrecanase Activity: Comparison of Agarose and Self-Assembling Peptide Scaffolds." Cartilage **4**(1): 63-74.

Goldring, M. B. (2012). "Articular cartilage degradation in osteoarthritis." HSS J **8**(1): 7-9.

Goldring, M. B. and K. B. Marcu (2012). "Epigenomic and microRNA-mediated regulation in cartilage development, homeostasis, and osteoarthritis." Trends Mol Med **18**(2): 109-118.

Gstraunthaler, G. (2003). "Alternatives to the use of fetal bovine serum: serum-free cell culture." ALTEX **20**(4): 275-281.

Gurdon, J. B. and P. Y. Bourillot (2001). "Morphogen gradient interpretation." Nature **413**: 797-803.

Gyorgy, B., T. G. Szabo, M. Pasztoi, Z. Pal, P. Misjak, B. Aradi, V. Laszlo, E. Pallinger, E. Pap, A. Kittel, G. Nagy, A. Falus and E. I. Buzas (2011). "Membrane vesicles, current state-of-the-art: emerging role of extracellular vesicles." Cell Mol Life Sci **68**(16): 2667-2688.

He, B., J. P. Wu, H. H. Chen, T. B. Kirk and J. Xu (2013). "Elastin fibers display a versatile microfibril network in articular cartilage depending on the mechanical microenvironments." J Orthop Res **31**(9): 1345-1353.

Hettrich, C. M., D. Crawford and S. A. Rodeo (2008). "Cartilage repair: third-generation cell-based technologies-basic science, surgical techniques, clinical outcomes." Sports Med Arthrosc **16**(4): 230-235.

Heywood, H. K., D. L. Bader and D. A. Lee (2006). "Glucose concentration and medium volume influence cell viability and glycosaminoglycan synthesis in chondrocyte-seeded alginate constructs." Tissue Eng **12**(12): 3478-3496.

Hong, E. and A. H. Reddi (2013). "Dedifferentiation and redifferentiation of articular chondrocytes from surface and middle zones: changes in microRNAs-221/-222, -140, and -143/145 expression." Tissue Eng Part A **19**(7-8): 1015-1022.

Huang, A. H., M. J. Farrell and R. L. Mauck (2010). "Mechanics and mechanobiology of mesenchymal stem cell-based engineered cartilage." J Biomech **43**(1): 128-136.

Huang, A. H., A. Stein and R. L. Mauck (2010). "Evaluation of the complex transcriptional topography of mesenchymal stem cell chondrogenesis for cartilage tissue engineering." Tissue Eng Part A **16**(9): 2699-2708.

Huang, A. H., A. Stein, R. S. Tuan and R. L. Mauck (2009). "Transient exposure to transforming growth factor beta 3 improves the mechanical properties of mesenchymal stem cell-laden cartilage constructs in a density-dependent manner." Tissue Eng Part A **15**(11): 3461-3472.

Huang, A. H., M. Yeger-McKeever, A. Stein and R. L. Mauck (2008). "Tensile properties of engineered cartilage formed from chondrocyte- and MSC-laden hydrogels." Osteoarthritis Cartilage **16**(9): 1074-1082.

Huang, B. J., J. C. Hu and K. A. Athanasiou (2016). "Cell-based tissue engineering strategies used in the clinical repair of articular cartilage." Biomaterials **98**: 1-22.

Huber, M., S. Trattnig and F. Lintner (2000). "Anatomy, biochemistry, and physiology of articular cartilage." Invest Radiol **35**(10): 573-580.

Huber, M., S. Trattnig and F. Lintner (2000). "Anatomy, biochemistry, and physiology of articular cartilage. </pubmed/11041151>." Invest Radiol **35**(10): 573-580.

Hung, C. T., E. G. Lima, R. L. Mauck, E. Takai, M. A. LeRoux, H. H. Lu, R. G. Stark, X. E. Guo and G. A. Ateshian (2003). "Anatomically shaped osteochondral constructs for articular cartilage repair." J Biomech **36**(12): 1853-1864.

Hung, C. T., R. L. Mauck, C. C. Wang, E. G. Lima and G. A. Ateshian (2004). "A paradigm for functional tissue engineering of articular cartilage via applied physiologic deformational loading." Ann Biomed Eng **32**(1): 35-49.

Ibanes, M. and J. C. Izpisua Belmonte (2008). "Theoretical and experimental approaches to understand morphogen gradients." Mol Syst Biol **4**(176): 1.

Ionescu, L. C., G. C. Lee, B. J. Sennett, J. A. Burdick and R. L. Mauck (2010). "An anisotropic nanofiber/microsphere composite with controlled release of biomolecules for fibrous tissue engineering." Biomaterials **31**(14): 4113-4120.

Jackson, D. W., T. M. Simon and H. M. Aberman (2001). "Symptomatic articular cartilage degeneration: the impact in the new millennium." Clin Orthop Relat Res(391 Suppl): S14-25.

Jakobsen, R. B., E. Ostrup, X. Zhang, T. S. Mikkelsen and J. E. Brinchmann (2014). "Analysis of the effects of five factors relevant to in vitro chondrogenesis of human mesenchymal stem cells using factorial design and high throughput mRNA-profiling." PLoS One **9**(5): e96615.

James, C. G., C. T. Appleton, V. Ulici, T. M. Underhill and F. Beier (2005). "Microarray analyses of gene expression during chondrocyte differentiation identifies novel regulators of hypertrophy." Mol Biol Cell **16**(11): 5316-5333.

Jiang, J., N. L. Leong, J. C. Mung, C. Hidaka and H. H. Lu (2008). "Interaction between zonal populations of articular chondrocytes suppresses chondrocyte mineralization and this process is mediated by PTHrP." Osteoarthritis Cartilage **16**(1): 70-82.

Johnstone, B., T. M. Hering, A. I. Caplan, V. M. Goldberg and J. U. Yoo (1998). "In vitro chondrogenesis of bone marrow-derived mesenchymal progenitor cells." Exp Cell Res **238**(1): 265-272.

Jung, H., J. S. Park, J. Yeom, N. Selvapalam, K. M. Park, K. Oh, J. A. Yang, K. H. Park, S. K. Hahn and K. Kim (2014). "3D tissue engineered supramolecular hydrogels for controlled chondrogenesis of human mesenchymal stem cells." Biomacromolecules **15**(3): 707-714.

Kelly, T. A., K. W. Ng, C. C. Wang, G. A. Ateshian and C. T. Hung (2006). "Spatial and temporal development of chondrocyte-seeded agarose constructs in free-swelling and dynamically loaded cultures." J Biomech **39**(8): 1489-1497.

Khetan, S., C. Chung and J. A. Burdick (2009). "Tuning hydrogel properties for applications in tissue engineering." Conf Proc IEEE Eng Med Biol Soc **2009**: 2094-2096.

Kim, I. L., C. G. Pfeifer, M. B. Fisher, V. Saxena, G. R. Meloni, M. Y. Kwon, M. Kim, D. R. Steinberg, R. L. Mauck and J. A. Burdick (2015). "Fibrous Scaffolds with Varied Fiber Chemistry and Growth Factor Delivery Promote Repair in a Porcine Cartilage Defect Model." Tissue Eng Part A **21**(21-22): 2680-2690.

Kim, M., X. Bi, W. E. Horton, R. G. Spencer and N. P. Camacho (2005). "Fourier transform infrared imaging spectroscopic analysis of tissue engineered cartilage: histologic and biochemical correlations." J Biomed Opt **10**(3): 0311051-0311056.

Kim, M., X. Bi, W. E. Horton, R. G. Spencer and N. P. Camacho (2005). "Fourier transform infrared imaging spectroscopic analysis of tissue engineered cartilage: histologic and biochemical correlations." J Biomed Opt **10**(3): 031105.

Kim, M., J. A. Burdick and R. L. Mauck (2012). "Influence of chondrocyte zone on co-culture with mesenchymal stem cells in HA hydrogels for cartilage tissue engineering." Proceedings of the ASME 2012 Summer Bioengineering Conference, June 20-23, Farjardo, Puerto Rico, USA.

Kim, M., I. E. Erickson, M. Choudhury, N. Pleshko and R. L. Mauck (2012). "Transient exposure to TGF-beta3 improves the functional chondrogenesis of MSC-laden hyaluronic acid hydrogels." J Mech Behav Biomed Mater **11**: 92-101.

Kim, M., L. F. Foo, C. Uggen, S. Lyman, J. T. Ryaby, D. P. Moynihan, D. A. Grande, H. G. Potter and N. Pleshko (2010). "Evaluation of early osteochondral defect repair in a rabbit model utilizing fourier transform-infrared imaging spectroscopy, magnetic resonance imaging, and quantitative T2 mapping." Tissue Eng Part C Methods **16**(3): 355-364.

Kim, T. K., B. Sharma, C. G. Williams, M. A. Ruffner, A. Malik, E. G. McFarland and J. H. Elisseeff (2003). "Experimental model for cartilage tissue engineering to regenerate the zonal organization of articular cartilage." Osteoarthritis Cartilage **11**(9): 653-664.

Kisiday, J. D., J. H. Lee, P. N. Siparsky, D. D. Frisbie, C. R. Flannery, J. D. Sandy and A. J. Grodzinsky (2009). "Catabolic responses of chondrocyte-seeded peptide hydrogel to dynamic compression." Ann Biomed Eng **37**(7): 1368-1375.

Klein, T. J., J. Malda, R. L. Sah and D. W. Hutmacher (2009). "Tissue engineering of articular cartilage with biomimetic zones." Tissue Eng Part B Rev **15**(2): 143-157.

Klein, T. J., S. C. Rizzi, J. C. Reichert, N. Georgi, J. Malda, W. Schuurman, R. W. Crawford and D. W. Hutmacher (2009). "Strategies for zonal cartilage repair using hydrogels." Macromol Biosci **9**(11): 1049-1058.

Klein, T. J., B. L. Schumacher, T. A. Schmidt, K. W. Li, M. S. Voegtline, K. Masuda, E. J. Thonar and R. L. Sah (2003). "Tissue engineering of stratified articular cartilage from chondrocyte subpopulations." Osteoarthritis Cartilage **11**(8): 595-602.

Knudson, W. and R. F. Loeser (2002). "CD44 and integrin matrix receptors participate in cartilage homeostasis." Cell Mol Life Sci **59**(1): 36-44.

Knutsen, G., L. Engebretsen, T. C. Ludvigsen, J. O. Drogset, T. Grontvedt, E. Solheim, T. Strand, S. Roberts, V. Isaksen and O. Johansen (2004). "Autologous chondrocyte

implantation compared with microfracture in the knee. A randomized trial." J Bone Joint Surg Am **86-A**(3): 455-464.

Kopesky, P. W., S. Byun, E. J. Vanderploeg, J. D. Kisiday, D. D. Frisbie and A. J. Grodzinsky (2014). "Sustained delivery of bioactive TGF-beta1 from self-assembling peptide hydrogels induces chondrogenesis of encapsulated bone marrow stromal cells." J Biomed Mater Res A **102**(5): 1275-1285.

Korhonen, R. K., M. S. Laasanen, J. Toyras, R. Lappalainen, H. J. Helminen and J. S. Jurvelin (2003). "Fibril reinforced poroelastic model predicts specifically mechanical behavior of normal, proteoglycan depleted and collagen degraded articular cartilage." J Biomech **36**(9): 1373-1379.

Kosaka, N., H. Iguchi, Y. Yoshioka, F. Takeshita, Y. Matsuki and T. Ochiya (2010). "Secretory mechanisms and intercellular transfer of microRNAs in living cells." J Biol Chem **285**(23): 17442-17452.

Kretlow, J. D., Y. Q. Jin, W. Liu, W. J. Zhang, T. H. Hong, G. Zhou, L. S. Baggett, A. G. Mikos and Y. Cao (2008). "Donor age and cell passage affects differentiation potential of murine bone marrow-derived stem cells." BMC Cell Biol **9**: 60.

Lai, J. H., G. Kajiyama, R. L. Smith, W. Maloney and F. Yang (2013). "Stem cells catalyze cartilage formation by neonatal articular chondrocytes in 3D biomimetic hydrogels." Sci Rep **3**: 3553.

Langer, R. and J. P. Vacanti (1993). "Tissue engineering." Science **260**(5110): 920-926.

Lee, S. H. and H. Shin (2007). "Matrices and scaffolds for delivery of bioactive molecules in bone and cartilage tissue engineering." Adv Drug Deliv Rev **59**(4-5): 339-359.

Levorson, E. J., M. Santoro, F. K. Kasper and A. G. Mikos (2014). "Direct and indirect co-culture of chondrocytes and mesenchymal stem cells for the generation of polymer/extracellular matrix hybrid constructs." Acta Biomater **10**(5): 1824-1835.

Lima, E. G., L. Bian, R. L. Mauck, B. A. Byers, R. S. Tuan, G. A. Ateshian and C. T. Hung (2006). "The effect of applied compressive loading on tissue-engineered cartilage constructs cultured with TGF-beta3." Conf Proc IEEE Eng Med Biol Soc **1**: 779-782.

Lima, E. G., L. Bian, K. W. Ng, R. L. Mauck, B. A. Byers, R. S. Tuan, G. A. Ateshian and C. T. Hung (2007). "The beneficial effect of delayed compressive loading on tissue-engineered cartilage constructs cultured with TGF-beta3." Osteoarthitis Cartilage **15**(9): 1025-1033.

Lima, E. G., K. M. Durney, S. R. Sirsi, A. B. Nover, G. A. Ateshian, M. A. Borden and C. T. Hung (2012). "Microbubbles as biocompatible porogens for hydrogel scaffolds." Acta Biomater **8**(12): 4334-4341.

Lv, Q. (2016). "Glucocorticoid combined with hyaluronic acid enhance glucocorticoid receptor activity through inhibiting p-38MAPK signal pathway activation in treating acute lung injury in rats." Eur Rev Med Pharmacol Sci **20**(18): 3920-3929.

Mackay, A. M., S. C. Beck, J. M. Murphy, F. P. Barry, C. O. Chichester and M. F. Pittenger (1998). "Chondrogenic differentiation of cultured human mesenchymal stem cells from marrow." Tissue Eng **4**(4): 415-428.

Makris, E. A., A. H. Gomoll, K. N. Malizos, J. C. Hu and K. A. Athanasiou (2015). "Repair and tissue engineering techniques for articular cartilage." Nat Rev Rheumatol **11**(1): 21-34.

Malda, J., J. Boere, C. H. van de Lest, P. van Weeren and M. H. Wauben (2016). "Extracellular vesicles - new tool for joint repair and regeneration." Nat Rev Rheumatol **12**(4): 243-249.

Mansfield, J., J. Yu, D. Attenburrow, J. Moger, U. Tirlapur, J. Urban, Z. Cui and P. Winlove (2009). "The elastin network: its relationship with collagen and cells in articular cartilage as visualized by multiphoton microscopy." J Anat **215**(6): 682-691.

Maroudas, A. and P. Bullough (1968). "Permeability of articular cartilage." Nature **219**(5160): 1260-1261.

Maroudas, A., P. Bullough, S. A. Swanson and M. A. Freeman (1968). "The permeability of articular cartilage." J Bone Joint Surg Br **50**(1): 166-177.

Martel-Pelletier, J. (1998). "Pathophysiology of osteoarthritis." Osteoarthitis Cartilage **6**(6): 374-376.

Martel-Pelletier, J. (1998). "Pathophysiology of osteoarthritis." Osteoarthritis Cartilage **6**(6): 374-376.

Martin, J. T., A. H. Milby, K. Ikuta, S. Poudel, C. G. Pfeifer, D. M. Elliott, H. E. Smith and R. L. Mauck (2015). "A radiopaque electrospun scaffold for engineering fibrous musculoskeletal tissues: Scaffold characterization and in vivo applications." Acta Biomater **26**: 97-104.

Mauck, R. L., M. A. Soltz, C. C. Wang, D. D. Wong, P. H. Chao, W. Valhmu, C. T. Hung and G. A. Ateshian (2000). "Functional tissue engineering of articular cartilage through dynamic loading of chondrocyte-seeded agarose gels." J Biomech Eng **122**(3): 252-260.

Mauck, R. L., M. A. Soltz, C. C. Wang, D. D. Wong, P. H. Chao, W. B. Valhmu, C. T. Hung and G. A. Ateshian (2000). "Functional tissue engineering of articular cartilage through dynamic loading of chondrocyte-seeded agarose gels." J Biomech Eng **122**(3): 252-260.

Mauck, R. L., C. C. Wang, E. S. Oswald, G. A. Ateshian and C. T. Hung (2003). "The role of cell seeding density and nutrient supply for articular cartilage tissue engineering with deformational loading." Osteoarthritis Cartilage **11**(12): 879-890.

Mauck, R. L., C. C. Wang, E. S. Oswald, G. A. Ateshian and C. T. Hung (2003). "The role of cell seeding density and nutrient supply for articular cartilage tissue engineering with deformational loading." Osteoarthritis Cartilage **11**(12): 879-890.

Mauck, R. L., X. Yuan and R. S. Tuan (2006). "Chondrogenic differentiation and functional maturation of bovine mesenchymal stem cells in long-term agarose culture." Osteoarthritis Cartilage **14**(2): 179-189.

Meretoja, V. V., R. L. Dahlin, F. K. Kasper and A. G. Mikos (2012). "Enhanced chondrogenesis in co-cultures with articular chondrocytes and mesenchymal stem cells." Biomaterials **33**(27): 6362-6369.

Meyer, E. G., C. T. Buckley, S. D. Thorpe and D. J. Kelly (2010). "Low oxygen tension is a more potent promoter of chondrogenic differentiation than dynamic compression." J Biomech **43**(13): 2516-2523.

Meyerrose, T., S. Olson, S. Pontow, S. Kalomoiris, Y. Jung, G. Annett, G. Bauer and J. Nolta (2010). "Mesenchymal stem cells for the sustained in vivo delivery of bioactive factors." Adv Drug Deliv Rev **62**(12): 1167-1174.

Morris, J. G., W. S. Cripe, H. L. Chapman, Jr., D. F. Walker, J. B. Armstrong, J. D. Alexander, Jr., R. Miranda, A. Sanchez, Jr., B. Sanchez, J. R. Blair-West and et al. (1984). "Selenium deficiency in cattle associated with Heinz bodies and anemia." Science **223**(4635): 491-493.

Moutos, F. T., L. E. Freed and F. Guilak (2007). "A biomimetic three-dimensional woven composite scaffold for functional tissue engineering of cartilage." Nat Mater **6**(2): 162-167.

Mow, V. C., C. C. Wang and C. T. Hung (1999). "The extracellular matrix, interstitial fluid and ions as a mechanical signal transducer in articular cartilage." Osteoarthritis Cartilage **7**(1): 41-58.

Mueller, M. B. and R. S. Tuan (2008). "Functional characterization of hypertrophy in chondrogenesis of human mesenchymal stem cells." Arthritis Rheum **58**(5): 1377-1388.

Muir, H. (1970). "The intracellular matrix in the environment of connective tissue cells." Clin Sci **38**(2): 8P.

Muralidharan-Chari, V., J. W. Clancy, A. Sedgwick and C. D'Souza-Schorey (2010). "Microvesicles: mediators of extracellular communication during cancer progression." J Cell Sci **123**(Pt 10): 1603-1611.

Murphy, J. M., K. Dixon, S. Beck, D. Fabian, A. Feldman and F. Barry (2002). "Reduced chondrogenic and adipogenic activity of mesenchymal stem cells from patients with advanced osteoarthritis." Arthritis Rheum **46**(3): 704-713.

Na, K., S. Kim, D. G. Woo, B. K. Sun, H. N. Yang, H. M. Chung and K. H. Park (2007). "Combination material delivery of dexamethasone and growth factor in hydrogel blended with hyaluronic acid constructs for neocartilage formation." J Biomed Mater Res A **83**(3): 779-786.

Na, K., J. H. Park, S. W. Kim, B. K. Sun, D. G. Woo, H. M. Chung and K. H. Park (2006). "Delivery of dexamethasone, ascorbate, and growth factor (TGF beta-3) in thermo-reversible hydrogel constructs embedded with rabbit chondrocytes." Biomaterials **27**(35): 5951-5957.

Nakagawa, Y., T. Muneta, K. Otabe, N. Ozeki, M. Mizuno, M. Udo, R. Saito, K. Yanagisawa, S. Ichinose, H. Koga, K. Tsuji and I. Sekiya (2016). "Cartilage Derived from Bone Marrow Mesenchymal Stem Cells Expresses Lubricin In Vitro and In Vivo." PLoS One **11**(2): e0148777.

Nazempour, A. and B. J. Van Wie (2016). "Chondrocytes, Mesenchymal Stem Cells, and Their Combination in Articular Cartilage Regenerative Medicine." Ann Biomed Eng **44**(5): 1325-1354.

Neuman, R. E. and M. A. Logan (1950). "The determination of hydroxyproline." J Biol Chem **184**(1): 299-306.

Ng, K. W., G. A. Ateshian and C. T. Hung (2009). "Zonal chondrocytes seeded in a layered agarose hydrogel create engineered cartilage with depth-dependent cellular and mechanical inhomogeneity." Tissue Eng Part A **15**(9): 2315-2324.

Nguyen, L. H., A. K. Kudva, N. S. Saxena and K. Roy (2011). "Engineering articular cartilage with spatially-varying matrix composition and mechanical properties from a single stem cell population using a multi-layered hydrogel." Biomaterials **32**(29): 6946-6952.

Nieminen, M. T., J. Toyras, J. Rieppo, J. M. Hakumaki, J. Silvennoinen, H. J. Helminen and J. S. Jurvelin (2000). "Quantitative MR microscopy of enzymatically degraded articular cartilage." Magn Reson Med **43**(5): 676-681.

Nims, R. J., A. D. Cigan, M. B. Albro, G. Vunjak-Novakovic, C. T. Hung and G. A. Ateshian (2015). "Matrix Production in Large Engineered Cartilage Constructs Is Enhanced by Nutrient Channels and Excess Media Supply." Tissue Eng Part C Methods **21**(7): 747-757.

Nuttelman, C. R., M. C. Tripodi and K. S. Anseth (2006). "Dexamethasone-functionalized gels induce osteogenic differentiation of encapsulated hMSCs." J Biomed Mater Res A **76**(1): 183-195.

O'Connell, G. D., E. G. Lima, L. Bian, N. O. Chahine, M. B. Albro, J. L. Cook, G. A. Ateshian and C. T. Hung (2012). "Toward engineering a biological joint replacement." J Knee Surg **25**(3): 187-196.

Park, J. S., K. Na, D. G. Woo, H. N. Yang and K. H. Park (2009). "Determination of dual delivery for stem cell differentiation using dexamethasone and TGF-beta3 in/on polymeric microspheres." Biomaterials **30**(27): 4796-4805.

Park, S., C. T. Hung and G. A. Ateshian (2004). "Mechanical response of bovine articular cartilage under dynamic unconfined compression loading at physiological stress levels." Osteoarthitis Cartilage **12**(1): 65-73.

Park, S., C. T. Hung and G. A. Ateshian (2004). "Mechanical response of bovine articular cartilage under dynamic unconfined compression loading at physiological stress levels." Osteoarthritis Cartilage **12**(1): 65-73.

Payne, K. A., D. M. Didiano and C. R. Chu (2010). "Donor sex and age influence the chondrogenic potential of human femoral bone marrow stem cells." Osteoarthritis Cartilage **18**(5): 705-713.

Pittenger, M. F., A. M. Mackay, S. C. Beck, R. K. Jaiswal, R. Douglas, J. D. Mosca, M. A. Moorman, D. W. Simonetti, S. Craig and D. R. Marshak (1999). "Multilineage potential of adult human mesenchymal stem cells." Science **284**(5411): 143-147.

Pittenger, M. F. and B. J. Martin (2004). "Mesenchymal stem cells and their potential as cardiac therapeutics." Circ Res **95**(1): 9-20.

Poole, A. R., T. Kojima, T. Yasuda, F. Mwale, M. Kobayashi and S. Laverty (2001). "Composition and structure of articular cartilage: a template for tissue repair." Clin Orthop Relat Res(391 Suppl): S26-33.

Potter, K., J. J. Butler, C. Adams, K. W. Fishbein, E. W. McFarland, W. E. Horton and R. G. Spencer (1998). "Cartilage formation in a hollow fiber bioreactor studied by proton magnetic resonance microscopy." Matrix Biol **17**(7): 513-523.

Pritzker, K. P., S. Gay, S. A. Jimenez, K. Ostergaard, J. P. Pelletier, P. A. Revell, D. Salter and W. B. van den Berg (2006). "Osteoarthritis cartilage histopathology: grading and staging." Osteoarthritis Cartilage **14**(1): 13-29.

Raj, A., S. A. Rifkin, E. Andersen and A. van Oudenaarden (2010). "Variability in gene expression underlies incomplete penetrance." Nature **463**(7283): 913-918.

Raposo, G. and W. Stoorvogel (2013). "Extracellular vesicles: exosomes, microvesicles, and friends." J Cell Biol **200**(4): 373-383.

Rebeyrol, C., V. Saint-Criq, L. Guillot, L. Riffault, H. Corvol, K. Chadelat, D. W. Ray, A. Clement, O. Tabary and P. Le Rouzic (2012). "Glucocorticoids reduce inflammation in cystic fibrosis bronchial epithelial cells." Cell Signal **24**(5): 1093-1099.

Regard, J. B., D. Malhotra, J. Gvozdenovic-Jeremic, M. Josey, M. Chen, L. S. Weinstein, J. Lu, E. M. Shore, F. S. Kaplan and Y. Yang (2013). "Activation of Hedgehog signaling by loss of GNAS causes heterotopic ossification." Nat Med **19**(11): 1505-1512.

Rhee, D. K., J. Marcelino, M. Baker, Y. Gong, P. Smits, V. Lefebvre, G. D. Jay, M. Stewart, H. Wang, M. L. Warman and J. D. Carpten (2005). "The secreted glycoprotein lubricin protects cartilage surfaces and inhibits synovial cell overgrowth." J Clin Invest **115**(3): 622-631.

Richardson, S. M., R. V. Walker, S. Parker, N. P. Rhodes, J. A. Hunt, A. J. Freemont and J. A. Hoyland (2006). "Intervertebral disc cell-mediated mesenchymal stem cell differentiation." Stem Cells **24**(3): 707-716.

Rieppo, J., J. Toyras, M. T. Nieminen, V. Kovanen, M. M. Hyttinen, R. K. Korhonen, J. S. Jurvelin and H. J. Helminen (2003). "Structure-function relationships in enzymatically modified articular cartilage." Cells Tissues Organs **175**(3): 121-132.

Roach, B. L., A. Kelmendi-Doko, E. C. Balutis, K. G. Marra, G. A. Ateshian and C. T. Hung (2016). "Dexamethasone Release from Within Engineered Cartilage as a Chondroprotective Strategy Against Interleukin-1alpha." Tissue Eng Part A **22**(7-8): 621-632.

Rowland, C. R., L. A. Colucci and F. Guilak (2016). "Fabrication of anatomically-shaped cartilage constructs using decellularized cartilage-derived matrix scaffolds." Biomaterials **91**: 57-72.

Roy, R., A. L. Boskey and L. J. Bonassar (2008). "Non-enzymatic glycation of chondrocyte-seeded collagen gels for cartilage tissue engineering." J Orthop Res **26**(11): 1434-1439.

Ruta, D. J., A. D. Villarreal and D. R. Richardson (2016). "Orthopedic Surgical Options for Joint Cartilage Repair and Restoration." Phys Med Rehabil Clin N Am **27**(4): 1019-1042.

Sabatino, M. A., R. Santoro, S. Gueven, C. Jaquiery, D. J. Wendt, I. Martin, M. Moretti and A. Barbero (2015). "Cartilage graft engineering by co-culturing primary human articular chondrocytes with human bone marrow stromal cells." J Tissue Eng Regen Med **9**(12): 1394-1403.

Sahoo, S., C. Chung, S. Khetan and J. A. Burdick (2008). "Hydrolytically degradable hyaluronic acid hydrogels with controlled temporal structures." Biomacromolecules **9**(4): 1088-1092.

Salinas, C. N., B. B. Cole, A. M. Kasko and K. S. Anseth (2007). "Chondrogenic differentiation potential of human mesenchymal stem cells photoencapsulated within poly(ethylene glycol)-arginine-glycine-aspartic acid-serine thiol-methacrylate mixed-mode networks." Tissue Eng **13**(5): 1025-1034.

Saxena, V., M. Kim, N. M. Keah, A. L. Neuwirth, B. D. Stoeckl, K. Bickard, D. J. Restle, R. Salowe, M. Y. Wang, D. R. Steinberg and R. L. Mauck (2016). "Anatomic Mesenchymal Stem Cell-Based Engineered Cartilage Constructs for Biologic Total Joint Replacement." Tissue Eng Part A **22**(3-4): 386-395.

Schinagl, R. M., D. Gurskis, A. C. Chen and R. L. Sah (1997). "Depth-dependent confined compression modulus of full-thickness bovine articular cartilage." J Orthop Res **15**(4): 499-506.

Schmid, R., K. Meyer, R. Spang, B. Schittek and A. K. Bosserhoff (2013). "YBX1 is a modulator of MIA/CD-RAP-dependent chondrogenesis." PLoS One **8**(12): e82166.

Schmidt, T. A., N. S. Gastelum, Q. T. Nguyen, B. L. Schumacher and R. L. Sah (2007). "Boundary lubrication of articular cartilage: role of synovial fluid constituents." Arthritis Rheum **56**(3): 882-891.

Schubert, T., J. Schlegel, R. Schmid, A. Opolka, S. Grassel, M. Humphries and A. K. Bosserhoff (2010). "Modulation of cartilage differentiation by melanoma inhibiting

activity/cartilage-derived retinoic acid-sensitive protein (MIA/CD-RAP)." Exp Mol Med **42**(3): 166-174.

Schuurman, W., T. J. Klein, W. J. Dhert, P. R. van Weeren, D. W. Hutmacher and J. Malda (2015). "Cartilage regeneration using zonal chondrocyte subpopulations: a promising approach or an overcomplicated strategy?" J Tissue Eng Regen Med **9**(6): 669-678.

Sharma, B., C. G. Williams, T. K. Kim, D. Sun, A. Malik, M. Khan, K. Leong and J. H. Elisseeff (2007). "Designing zonal organization into tissue-engineered cartilage." Tissue Eng **13**(2): 405-414.

Shintani, N. and E. B. Hunziker (2011). "Differential effects of dexamethasone on the chondrogenesis of mesenchymal stromal cells: influence of microenvironment, tissue origin and growth factor." Eur Cell Mater **22**: 302-319; discussion 319-320.

Soltz, M. A. and G. A. Ateshian (1998). "Experimental verification and theoretical prediction of cartilage interstitial fluid pressurization at an impermeable contact interface in confined compression." J Biomech **31**(10): 927-934.

Sophia Fox, A. J., A. Bedi and S. A. Rodeo (2009). "The basic science of articular cartilage: structure, composition, and function." Sports Health **1**(6): 461-468.

Stegemann, H. and K. Stalder (1967). "Determination of hydroxyproline." Clin Chim Acta **18**(2): 267-273.

Strassburg, S., N. W. Hodson, P. I. Hill, S. M. Richardson and J. A. Hoyland (2012). "Bi-directional exchange of membrane components occurs during co-culture of mesenchymal stem cells and nucleus pulposus cells." PLoS One **7**(3): e33739.

Studer, R. K. (2004). "Nitric oxide decreases IGF-1 receptor function in vitro; glutathione depletion enhances this effect in vivo." Osteoarthritis Cartilage **12**(11): 863-869.

Studer, R. K., E. Levicoff, H. Georgescu, L. Miller, D. Jaffurs and C. H. Evans (2000). "Nitric oxide inhibits chondrocyte response to IGF-I: inhibition of IGF-IRbeta tyrosine phosphorylation." Am J Physiol Cell Physiol **279**(4): C961-969.

Tangtrongsup, S. and J. D. Kisiday (2016). "Effects of Dexamethasone Concentration and Timing of Exposure on Chondrogenesis of Equine Bone Marrow-Derived Mesenchymal Stem Cells." Cartilage **7**(1): 92-103.

Tharakan, J. P. and P. C. Chau (1987). "Modeling and analysis of radial flow mammalian cell culture." Biotechnol Bioeng **29**(6): 657-671.

Theocharis, A. D., M. E. Tsara, N. Papageorgakopoulou, D. H. Vynios and D. A. Theocharis (2001). "Characterization of glycosaminoglycans from human normal and scoliotic nasal cartilage with particular reference to dermatan sulfate." Biochim Biophys Acta **1528**(2-3): 81-88.

Ueda, H., T. Baba, H. Toriumi and S. Ohno (2001). "Anionic sites in articular cartilage revealed by polyethyleneimine staining." Micron **32**(4): 439-446.

Valadi, H., K. Ekstrom, A. Bossios, M. Sjostrand, J. J. Lee and J. O. Lotvall (2007). "Exosome-mediated transfer of mRNAs and microRNAs is a novel mechanism of genetic exchange between cells." Nat Cell Biol **9**(6): 654-659.

Vaughan, B. L., Jr., P. A. Galie, J. P. Stegemann and J. B. Grotberg (2013). "A poroelastic model describing nutrient transport and cell stresses within a cyclically strained collagen hydrogel." Biophys J **105**(9): 2188-2198.

Wolpert, L. (1969). "Positional information and the spatial pattern of cellular differentiation." J Theor Biol **25**(1): 1-47.

Woods, A., G. Wang and F. Beier (2005). "RhoA/ROCK signaling regulates Sox9 expression and actin organization during chondrogenesis." J Biol Chem **280**(12): 11626-11634.

Wu, L., X. Cai, S. Zhang, M. Karperien and Y. Lin (2013). "Regeneration of articular cartilage by adipose tissue derived mesenchymal stem cells: perspectives from stem cell biology and molecular medicine." J Cell Physiol **228**(5): 938-944.

Wu, L., J. N. Post and M. Karperien (2015). "Engineering cartilage tissue by pellet coculture of chondrocytes and mesenchymal stromal cells." Methods Mol Biol **1226**: 31-41.

Wu, L., H. J. Prins, M. N. Helder, C. A. van Blitterswijk and M. Karperien (2012). "Trophic effects of mesenchymal stem cells in chondrocyte co-cultures are independent of culture conditions and cell sources." Tissue Eng Part A **18**(15-16): 1542-1551.

Xu, L., Q. Wang, F. Xu, Z. Ye, Y. Zhou and W. S. Tan (2013). "Mesenchymal stem cells downregulate articular chondrocyte differentiation in noncontact coculture systems: implications in cartilage tissue regeneration." Stem Cells Dev **22**(11): 1657-1669.

Yamane, I., O. Murakami and M. Kato (1975). "Role of bovine albumin in a serum-free suspension cell culture medium." Proc Soc Exp Biol Med **149**(2): 439-442.

Yang, K. G., D. B. Saris, R. E. Geuze, M. H. van Rijen, Y. J. van der Helm, A. J. Verbout, L. B. Creemers and W. J. Dhert (2006). "Altered in vitro chondrogenic properties of chondrocytes harvested from unaffected cartilage in osteoarthritic joints." Osteoarthritis Cartilage **14**(6): 561-570.

Yang, Y. H., A. J. Lee and G. A. Barabino (2012). "Coculture-driven mesenchymal stem cell-differentiated articular chondrocyte-like cells support neocartilage development." Stem Cells Transl Med **1**(11): 843-854.

Yoo, J. U., T. S. Barthel, K. Nishimura, L. Solchaga, A. I. Caplan, V. M. Goldberg and B. Johnstone (1998). "The chondrogenic potential of human bone-marrow-derived mesenchymal progenitor cells." J Bone Joint Surg Am **80**(12): 1745-1757.

Zhang, F., K. Su, Y. Fang, S. Sandhya and D. A. Wang (2015). "A mixed co-culture of mesenchymal stem cells and transgenic chondrocytes in alginate hydrogel for cartilage tissue engineering." J Tissue Eng Regen Med **9**(1): 77-84.